SHRINKAGE CRACKING OF REINFORCED CONCRETE SLABS EXPOSED TO FIRE

A Thesis

Submitted to the College of Engineering of the University of Babylon in Partial Fulfillment of the Requirements for the Degree of Master of Science in Civil Engineering

By

MOHAMMED MANSOUR KADHUM

Supervised by

ASST. PROF. DR. MAHDI S. ESSA
ASST. PROF. MR. SAMIR A. AL-MASHHEDI

July ٢٠٠٣ **Jumada ١ ١٤٢٤**

تشققات الانكماش للسقوف الخرسانيه الممعرضه للحريق

رسالة

مقدمة إلى كلية الهندسة في جامعة بابل

كجزء من متطلبات نيل درجة الماجستير

في علوم الهندسة المدنية

من قبل

محمد منصور كاظم الخفاجي

إشراف

أ.م.د. مهدي صالح عيسى
أ.م. سامر عبد الامير المشهدي

جمادى الاولى ١٤٢٣ اب ٣٢٠٠

ABSTRACT

This investigation is conducted to study the cracking behavior due to the restrained drying shrinkage of the reinforced concrete slabs then subjected to direct fire flame. These slabs were externally restrained by different end restraints. Cracking was detected when these slabs were subjected to fire flames and shrinkage after burning.

In this study reduced scale slab models (which are believed to resemble as much as possible field conditions) were used. Slab movements, crack spacing, crack width and crack lengths were measured before and after exposure to fire flame.

The reinforced concrete slabs were exposed to drying shrinkage for a period of two months. Then, they were exposed to direct fire fame temperature of (٦٠٠^{o}C) for ١.٥ hour period of exposure at the same day, without any imposed loads during burning. Then, the slabs were cooled to the laboratory temperature before burning (٢٣^{o}C) .A comparison of the slabs behavior before and after exposure to fire flames was made.

From the results obtained before and after burning, it was observed that there is a variation in the crack widths along the slab length. At edge level there is a certain crack width, which increases towards the center of the slab until the level of (٢٠-٥٠٪) and (١٥-٣٨٪), of crack length before and after exposure to fire flame respectively where the maximum crack width usually occurs. Beyond which the crack width decreases to zero at a certain length depending on some factors including the position of the crack from the centerline of the slab. This behavior implies the cracks that appeared from the restrained ends of three and four end restrained slabs. Whereas, the cracks which appeared form the free ends of two and three end

restrained slabs possess maximum width at the edge level and decreases to zero towards the center of the slab.

In the present investigation the behavior of cracks and deflection in these slabs during and after burning was obtained.

Based on the results of this work, it can be noticed that the maximum crack widths were (٠.٢٤, ٠.٢٥٥ and ٠.٢٧٥) mm for two, three and four end restrained slabs respectively at the age of ٦٠ days before burning. While the maximum crack widths for free, two end, three end and four end restrained slabs during burning and after burning at the age of ٦٠ days were (٠.٢٥, ٠.٧٥, ٠.٧٢٥ and ٠.٧١) mm and (٠.٠٧, ٠.٦٧٥, ٠.٧ and ٠.٧٥) mm respectively. The deflection at mid span of the reinforced concrete slabs was measured during and after exposure to fire flames. It was noticed that the maximum deflection recorded was during burning (١.٩٨)mm for free slab ,whereas, the minimum deflection during burning recorded was (٠.٨٥)mm for four end restrained slab. After a period of ٦٠ days from burning the maximum and minimum deflections were (٠.٦٥ and ٠.٦)mm respectively. Therefore, it is obvious from the test results that the mid-span deflection of free end slab was greater by ٥٧٪ than that of the four end restrained slab.

The results of the finite element analysis and field measurements were found to confirm the results obtained from the experimental tests. Hence, the finite element method was found to give a reasonable description of the observed cracking behavior.

Simplified formulas were modified and suggested for calculating the minimum and maximum crack spacing and maximum crack width at any position along the slab length.

الخلاصة

هذا البحث تم أجراؤه لدراسة سلوك تشققات الانكماش الحاصلة في السقوف الخرسانية المسلحة والمقيدة والتي تم تعريضها بعد ذلك إلى لهب النار المباشر. هذه السقوف تم تقييدها بحالات تقيد مختلفة من النهايات. التشقق أيضآ تم التحري عنه عندما جرى تعريض هذه السقوف إلى لهب النار المباشر.

في هذه الدراسة تم استخدام نماذج بحث مصغرة يعتقد إنها توفر ظروفا مشابهة للظروف الطبيعية الموقعية .لقد تم خلال البحث أخذ قراءات حركات السقوف، المسافة بين التشققات ، عرض التشققات وأطوالها قبل وبعد فترة تعريضها إلى لهب النار.

تم تعريض السقوف الخرسانية المسلحة إلى انكماش الجفاف لمدة شهرين. وبعد ذلك تم تعريضها إلى لهب النار المباشر بدرجة حرارة (٦٠٠) درجة مئوية لمدة ساعة ونصف في نفس اليوم بدون أن يتم تسليط أية أحمال عرضية أثناء عملية الحرق. بعد ذلك تم تبريد نماذج السقوف إلى درجة حرارة المختبر والتي كانت (٢٣) درجة مئوية قبل الحرق. تم عمل مقارنة لسلوك هذه السقوف قبل وبعد تعريضها إلى لهب النار.

من النتائج المستحصلة قبل وبعد عملية الحرق تم ملاحظة وجود اختلاف في عرض التشققات الموجودة على طول السقف. في مستوى الحافة يوجد عرض معين يتزايد باتجاه مركز السقف حتى يصل إلى اكبر قيمة له عند مسافة تتراوح بين (٢٠-٥٠%) و (١٥-٣٨%) من طول الشق قبل وبعد الحريق بالتتابع والذي فيه يحصل اكبر عرض للشق عادة. وبعد ذلك يأخذ هذا الشق بالتناقص حتى يضمحل ويتلاشى عند طول معين اعتمادا على عوامل معينة تشمل موقع الشق عن خط المركز للسقف. هذا السلوك يشمل التشققات التي ظهرت في الحافات المقيدة للسقوف الخرسانية المقيدة من ثلاث جهات أو أربع جهات. بينما التشققات التي ظهرت من الحافات الحرة في السقوف المقيدة من جهتين أو ثلاث جهات تمتلك أقصى عرض للشق عند مستوى الحافة ثم تصل وتضمحل باتجاه مركز السقف .

واعتمادا على نتائج هذا البحث يمكن الاستنتاج بأن أقصى عرض للتشققات بعمر ٦٠ يوما قبل تعرضها للحرق كان (٠.٢٤ ، ٠.٢٥٥ ، ٠.٢٧٥) ملم لنماذج السقوف الخرسانية المقيدة من جهتين ، من ثلاث جهات ومن أربع جهات على التوالي . بينما كان عرض التشققات للسقف الحر والمقيد من جهتين والمقيد من ثلاث جهات والمقيد من أربع جهات بعد فترة ساعة ونصف من تعرضها للهب النار المباشر كانت (٠.٢٥ ، ٠.٧٥ ، ٠.٧٢٥ ، ٠.٧١) ملم على التوالي في حين عرضها بعد مدة ٦٠ يوما بعد الحرق كانت (٠.٠٧ ، ٠.٦٧٥ ، ٠.٧ ، ٠.٧٥) ملم على التوالي. تم قياس الانحراف في وسط السقوف الخرسانية أثناء وبعد تعريضها إلى لهب النار. تم ملاحظة إن أعلى انحراف تم تسجيله هو ١.٩٨ ملم وكان لحالة السقف الحر، بينما أوطأ انحراف تم تسجيله فقد كان ٠.٨٥ ملم لحالة السقف المقيد من الجهات الاربعه . بعد ٦٠ يوما من الحرق كان أعلى واقل انحراف مسجل هو (٠.٦٥ و ٠.٦) ملم على التوالي. لذلك من الواضح من خلال النتائج المختبرية إن الانحراف لحالة السقف الحر كان أكبر بمقدار ٠.٥٧ من الانحراف في حالة السقف المقيد من أربع جهات.

النتائج التي تم استحصالها بواسطة طريقة تحليل العناصر المحددة وكذلك النتائج المستحصلة من المشاهدة الحقلية أيدت النتائج العملية. لذلك يمكن القول بأن طريقة العناصر المحددة تعطي وصفا معقولا لسلوك التشققات الذي تم ملاحظته.

تم تحوير والتوصية باعتماد معادلات مبسطة لغرض حساب المسافات الدنيا والقصوى بين الشقوق وكذلك حساب أقصى عرض لتلك الشقوق في أي موقع على طول السقف وذلك باستخدام النتائج التي تم استحصالها من خلال البحث.

CERTIFICATE

We certify that the thesis titled **"*Shrinkage Cracking of Reinforced Concrete Slabs Exposed to Fire*",** was prepared by **"*Mohammed Mansour Kadhum*",** under our supervision at Babylon University in fulfillment of partial requirements for the degree of Master of Science in Civil Engineering.

Signature:

Name**: Assist Prof. Dr.Mahdi S. Essa**

Date: / / ٢٠٠٣

Signature:

Name: **Assist Prof. Mr. Samir A. AL-Mashhedi**

Date: / /٢٠٠٣

CHAPTER ONE

INTRODUCTION

١.١ General

Concrete is universally used as a construction material because it can be molded into any shape man desires and it provides at reasonable cost a material that can be designed to ensure high compressive strength.

Cracking of concrete is perhaps its major disadvantage which results mainly from its low tensile strength and low tensile strain capacity, where concrete is considered as a brittle material and lacks ductility.

In general, concrete cracks when there are tensile stresses exceeding in magnitude its tensile strength.

Concrete would change volume without inducing stresses if it is free to move. This case rarely occurs in practice, since concrete is always restrained to some degree. Thus, cracking will take place due to the combination of the tendency of concrete to contract and the restraint which prevents it from doing so.

The tendency of concrete toward cracking will depend on the magnitude of volume change movement, restraint and the properties of the concrete itself, i.e., strength, extensibility and creep (relaxation).

The concrete building construction could be exposed to the effect of fire. Human safety is one of the considerations in the design of residential, public and industrial buildings.

The effect of fire on structural members depends on different factors such as: the amount, nature, and distribution of fire loading, ventilation and compartment size.

One of these structural members is a reinforced concrete slab. This type of structural member may be subjected to high temperatures during fire, which will cause change in properties of its constituents namely concrete and steel, therefore, in reinforced concrete structural design of buildings it may be necessary to design not only for the dead and live loads, but also for fire resistance [١].

Fire could bring a chemical reaction, essentially decomposition of $Ca(OH)_2$ will cause a decrease in concrete compressive strength, which follows the development of heat. Most huge fires start from small ones, and during their development the rate at which heat is produced exceeds the rate at which it is dissipated.

The fire resistance of reinforced concrete slabs is expressed in terms of fire endurance as determined by standard fire tests. The fire endurance of the slab is then expressed as the time duration necessary to induce failure. ASTM E-١١٩ standard method for floor slab fire tests specifies that a fire test will be considered as successful if:

a- The slab does not allow the passage of flames or gases hot enough to ignite oven-dried cotton, and

b- The rise in temperature of the unexposed surface is less than ١٢٠ ^oC (٢٥٠ ^oF). For steel reinforcement, these standards specify that steel temperature should not exceed ٥٤٠ ^oC (١٠٠٠ ^oF) within the rated fire endurance.

In the structural design of buildings, in addition to the normal gravity and lateral loads, it is in many cases necessary to design the structure to safely resist exposure to fire. However, it is usually necessary to guard against structural collapse for a given period of time [٢].

١.٢ Objective of This Work

Many authors studied restrained shrinkage. They used several types of molds and ways for restraining. However, very little work was done on shrinkage cracking of reinforced concrete slabs with different cases of restraint that are exposed to fire flame.

In order to simulate this problem to practical site conditions, reduced scale slab models were cast and they were as close as possible to practical under laboratory circumstances.

The main goals of this study are;

١- The main parameter studied was the effect of different restrained cases of reinforced concrete slabs on the cracking behavior (crack width, crack spacing and crack length) of these models. A comparison was made between the experimentally obtained data with the theoretical results of the finite element approach for each case of restraint.

٢- Studying the fire effect on cracking tendency and pattern in reinforced concrete slabs with different restrained cases before and after exposure to fire flame.

٣- Investigating the fire endurance of reinforced concrete slabs subjected to different end restraint conditions.

٤- Studying the fire flame effect on the deflection of the reinforced concrete slabs.

١.٣ Research Layout

The research work presented in this thesis is given through seven chapters:

Chapter One provides a general introduction.

Chapter Two, “Review of Literature”, introduces a definition of the shrinkage and types of shrinkage, and the main factors influencing it. Also, the forms of restraint and their effects on cracking were reviewed. As well as reviews literature including the effect of fire endurance on the behavior of reinforced concrete slabs.

Chapter Three, “Experimental work”, a description of the experimental slab models which were made to observe cracking is being presented. Materials, mixing and casting procedures, and procedure of measurements carried out in this study are discussed.

Chapter Four, includes theoretical analysis using “Finite Element Modeling of Reinforced Concrete Structures”.

Chapter Five includes “Experimental Results and Analysis”, based on the results obtained, a formula for the relationship between maximum crack width to be expected in the slabs and maximum crack spacing, free shrinkage strain, creep strain and elastic tensile strain capacity of concrete is presented in Chapter Five. The validity if this formula and formulas of previous researchers are examined with reference to the results of the tests performed on the slab models in the above-mentioned experimental research, and on actual slabs. It is found that there is a good agreement between the present formulas results and both experimental and actual slab models measurements.

In Chapter Six, “Analysis Results and Discussion”, A comparison between of the experimental and theoretical results are presented in this chapter.

Finally, Chapter Seven is devoted to the general conclusions and suggestions for further research.

CHAPTER TWO

LITERATURE REVIEW

٢.١ Shrinkage of Concrete

Shrinkage is a time dependent phenomenon. It is mainly due to the drying out of cement gel. The process of drying depends on the rate of diffusion of moisture to the surface of the concrete where it evaporates. Therefore, shrinkage develops with time at high rate initially and slows down with concrete again.

٢.٢ Types of Concrete Shrinkage

There are different types of concrete shrinkage, which can be summarized as below.

٢.٢.١ Plastic Shrinkage

Plastic shrinkage is a reduction of volume in fresh concrete when placed in forms due to settlement of solids and bleeding of clear water at the top surface which is followed by its evaporation [٣].

The magnitude of plastic shrinkage is affected by the amount of water lost from surface of concrete, which is influenced by many factors related to the concrete properties or the ambient conditions like: concrete temperature, ambient temperature, relative humidity, and wind velocity. The properties of the material in contact with concrete surface also affect the amount of water loss from concrete.

According to ACI Committee ٣٠٥[٤], if evaporation is more than ١ kg/m^{٢}/hr plastic shrinkage cracks may occur.

٢.٢.٢ Carbonation Shrinkage

The presence of carbon dioxide ($CO_{٢}$) and moisture in air can produce carbonic acid which reacts with hydrated lime in cement to produce $CaCO_{٣}$.

$$Ca(OH)_2 + CO_2 \rightarrow CaCO_3 + H_2O \qquad .....(٢\text{-}١)$$

The actual rate of carbonation depends on the permeability of concrete, moisture and the $CO_{٢}$ content and relative humidity of the ambient medium. Therefore concrete with high w/c ratio and inadequately cured will be more prone to carbonation.

٢.٢.٣ Drying shrinkage

This type of shrinkage is the most important type of concrete shrinkage with respect to cracking of hardened concrete. It is defined as the volumetric contraction, which is attributed to the withdrawal of water from concrete stored in unsaturated air. Thus when concrete is exposed to dry condition, moisture slowly diffuses from the interior mass to the surface where it is lost by evaporation.

According to *Power* and *Brownyard* [٥] there are three types of water occurring in cement paste which are:

١- Non-evaporable water [fixed water].
٢- Gel water. } Free water
٣- Capillary water. }

The non-evaporable water is very difficult to evaporate under the normal conditions.

Gel water is difficult to evaporate, its evaporation may take ٢٠ years, and this is the principal cause of drying shrinkage.

Capillary water is easy to evaporate but its effect on shrinkage is limited by the paste structure.

According to *Hobbs* [٦], due to progressive loss of water from cement paste, capillary tension that develops in the residual water induces compressive stresses in concrete resulting in concrete shrinkage.

٢.٢.٤ Autogenous Shrinkage

The autogenous shrinkage of concrete is a result of chemical reaction of Portland cement and water, since the sum of dry cement and mixing water is greater than that of hydrated products plus the remaining free water. This type is considered small for the usual concrete mixes. For practical purposes, the typical value is normally taken equal to ٤٠ microstrains [٧].

Autogenous shrinkage tends to increase at higher temperatures, with a higher cement content, and possibly with finer cements, and with cements which have a higher C_3A and C_4AF content [٨].

٢.٣ Factors Affecting Shrinkage of Concrete

There are many factors influencing shrinkage of concrete but the main factors are summarized as follows:

٢.٣.١ Influence of Aggregate

The aggregate appears clearly to have a great influence on shrinkage of concrete. It occupies about (٦٥-٧٥)% of total concrete volume and restrain the shrinkage of cement paste.

Carlson et. al. [٩] reported that the aggregates dilute and reinforce the cement paste against contraction, thus reduce its magnitude to (١/٤ to ١/٦) its original value depending on the type and amount of aggregate used.

ACI Committee ٢٢٤ [١٠] explained that the ability of aggregate to restrain shrinkage of cement paste depends on compressibility and shrinkage of aggregate, extensibility of cement paste and bond between cement paste and aggregate.

٢.٣.٢ Cement Type and Fineness

In general the increase of cement content increases the shrinkage and therefore the cracking tendency, but at the same time the increase in cement content increases the strength of concrete and the tensile strain capacity.

Torrent [١١] and *Troxell et. al.* [١٢] concluded that shrinkage of low heat cement (type IV) is greater than that of (type I). This is believed to be due to high C_2S content in (type IV) cement, which exhibits high shrinkage.

Carlson [١٣] pointed out that fineness of cement has probably two opposing influences on shrinkage of concrete. Finer cement hydrates more extensively and thus produces a denser gel, which has a lesser shrinkage. While the gel of the finer cement is stronger and therefore it has a higher effect against restraint of aggregate and this increases shrinkage.

٢.٣.٣ Water to Cement Ratio

One of the most important factors in shrinkage is w/c ratio of the mix because its increase tends to increase shrinkage and, at the same time, to reduce the strength of the concrete.

Brooks [١٤] demonstrated that shrinkage of hydrated cement paste is directly proportional to w/c ratio.

Carlson [٩] reported that a decrease of water content of concrete by ١٥ percent causes a decrease in shrinkage of about ٣٠ percent, as similar trend was given by the ACI Committee ٢٢٤ [١٠] for ١٠ percent reduction of water content, the one year drying shrinkage decreased by ١٥ percent.

٢.٣.٤ Effect of Curing, Exposure Conditions and Size of Member

Duration of moist curing of concrete does not seem to have much effect on drying shrinkage, especially for curing times of less than a month [١٥]. *Neville* [١٦] reported that the effect of curing on magnitude of shrinkage is small and that well cured concrete shrinks more rapidly.

When concrete is exposed to a hot and dry climate as much as half the total shrinkage may occur in the first month after casting [١٧]. *Troxell et al.* [١٢] reported that drying shrinkage of concrete in an atmosphere of ٧٠ percents relative humidity is about one-third lower than if the concrete was exposed to ٥٠ percent relative humidity.

The rate and magnitude of shrinkage of small laboratory specimens is believed to be much greater than that of field concrete members (slabs, walls … etc). *Hansen* and *Mattock* [١٨] concluded through extensive tests, that the volume/surface area ratio of the concrete member is a suitable parameter when estimating its shrinkage and creep deformations. Increasing the volume / surface area decreases the shrinkage.

٢.٣.٥ Relative Humidity

The standard condition assumes that the ambient relative humidity during drying is ٤٠ percent. If the ambient relative humidity is greater than ٤٠ percent, the ultimate shrinkage is reduced.

According to *Troxell et. al.* [٣] the drying shrinkage of concrete in atmosphere of ٧٠ percent R.H. is about one-third lower than in ٥٠ percent R.H.

٢.٣.٦ Temperature

It is well known that increasing concrete temperature after casting increases the evaporation of the water therefore shrinkage increases.

٢.٤ Shrinkage Induced Cracking

Shrinkage may cause cracking of concrete. If the shrinkage takes place without any restraint, the concrete would not crack. However, in practice the concrete is always under some degree of restraint either externally or internally. The combination of shrinkage and restraint develops tensile stresses. When the induced strain exceeds the tensile strain capacity of the concrete, cracking takes place. Alternatively, when the developed stress exceeds the tensile strength of concrete, cracking occurs as shown in Figure (٢-١).

The magnitude of tensile stress developed during drying of the concrete is influenced by a combination of factors such as:

i- the amount of shrinkage,
ii- the degree of restraint,
iii- the modulus of elasticity of the concrete, and
iv- the creep or relaxation of the concrete.

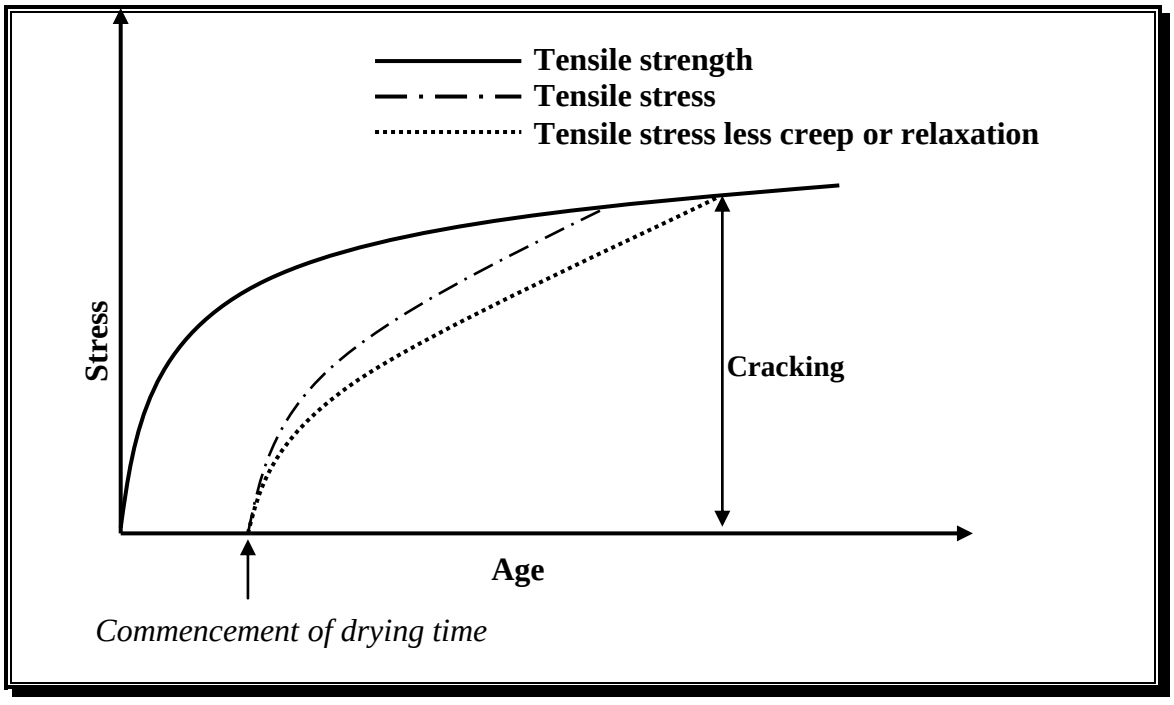

Figure (٢-١): Sketch of Crack Development (Stress Wise) [٢٢].

Thus, the amount of shrinkage is only one factor governing cracking. For prevention of shrinkage cracking, low modulus of elasticity and high

creep characteristics of the concrete are desirable since they reduce the magnitude of tensile stresses [١٠].

The need to control crack spacing and width in reinforced concrete structures arises from aesthetic reasons, water tightness requirements, concrete durability, structural safety, and preservation of steel reinforcement considerations [١٩].

٢.٤.١ Plastic Shrinkage Cracking

Plastic shrinkage cracks are the most dangerous cracks. They occur when concrete is still in the plastic state and subjected to fast loss of large amount of water per unit area. The width of plastic shrinkage cracks may reach ٦ mm, therefore, can result in serious problems.

According to ACI ٣٠٥R-٩١ [٢٠] the risk of plastic shrinkage cracking is identical for the following combinations of temperature and relative humidity: ٤١^{o}C and ٩٠ percent, ٣٥^{o}C and ٧٠ percent, ٢٤^{o}C and ٣٠ percent. Typical plastic shrinkage cracks are parallel to one another, spaced ٠.٣-١.٠ m apart, and have considerable depth.

Plastic shrinkage cracking is some times confused with another type of cracking called plastic settlement cracking. The plastic settlement cracking occurs on the surface of fresh concrete and caused by differential settlement of fresh concrete due to some obstruction to settlement, such as large particles of aggregate or reinforcing bars.

Plastic shrinkage cracking can develop also when a large horizontal area of concrete makes contraction in the horizontal direction more difficult than vertically, deep cracks of an irregular pattern are then formed [٢١]. Such cracks can properly be called pre-setting cracks.

٢.٤.٢ Restrained Shrinkage Cracking

The term “restraint” is defined by ACI Committee ٢٠٧ [٢٣], as “to hold back from action; check; suppress; curb; to limit; restrict”. Restraint

acts to limit the change in dimensions and produces strain, with corresponding stress in concrete member. Numerically, the strain is equal to the product of the degree of restraint existing at the point in question and the change in unit length which could occur if the concrete was not restrained.

The degree of restraint depends largely on relative dimensions, strength, creep or relaxation, modulus of elasticity of concrete and the restraining object. In practice, the degree of restraint of any concrete section within the member depends largely on its location and the type of restraint [٢٤].

The possible restraints of concrete members are internal restraint, external end-restraint, and base-restraint. In practice, concrete is usually under some type of restraint, internally or externally.

The source of internal restraint is steel reinforcement, aggregate, and exists in members with nonuniform volume change in a cross section. This occurs for example, with slabs, walls, or masses with interior temperatures greater than surface temperatures.

In addition to internal restraints caused by aggregate and reinforcement, some restraint arises also from non-uniform shrinkage within the concrete member itself. Moisture loss takes place at the surface so that a moisture gradient is established in the concrete section, which is subjected to differential shrinkage. This shrinkage is compensated by strain due to internal stresses, tensile near the surface and compressive in the core [٢٥].

The external restraint occurs from the ends or the base of concrete or stem from other parts of the structure. Most researchers did not take into consideration difference between end restraint or base restraint. Test methods commonly used for measuring shrinkage cracking of concrete are:

bar test, plate test, and the ring type specimens for restraint shrinkage cracking test. All of these methods have several drawbacks, in particular, the difficulty of providing a constant restraint. *Al-Rawi* [٢٦] used I-shaped molds having a channel section to study shrinkage crack spacing and crack width.

Figure (٢-٢) shows distribution of restrained movement expressed as degree of restraint (R) at the center – lines of concrete walls restrained completely at the base with different values of L/H ratios.

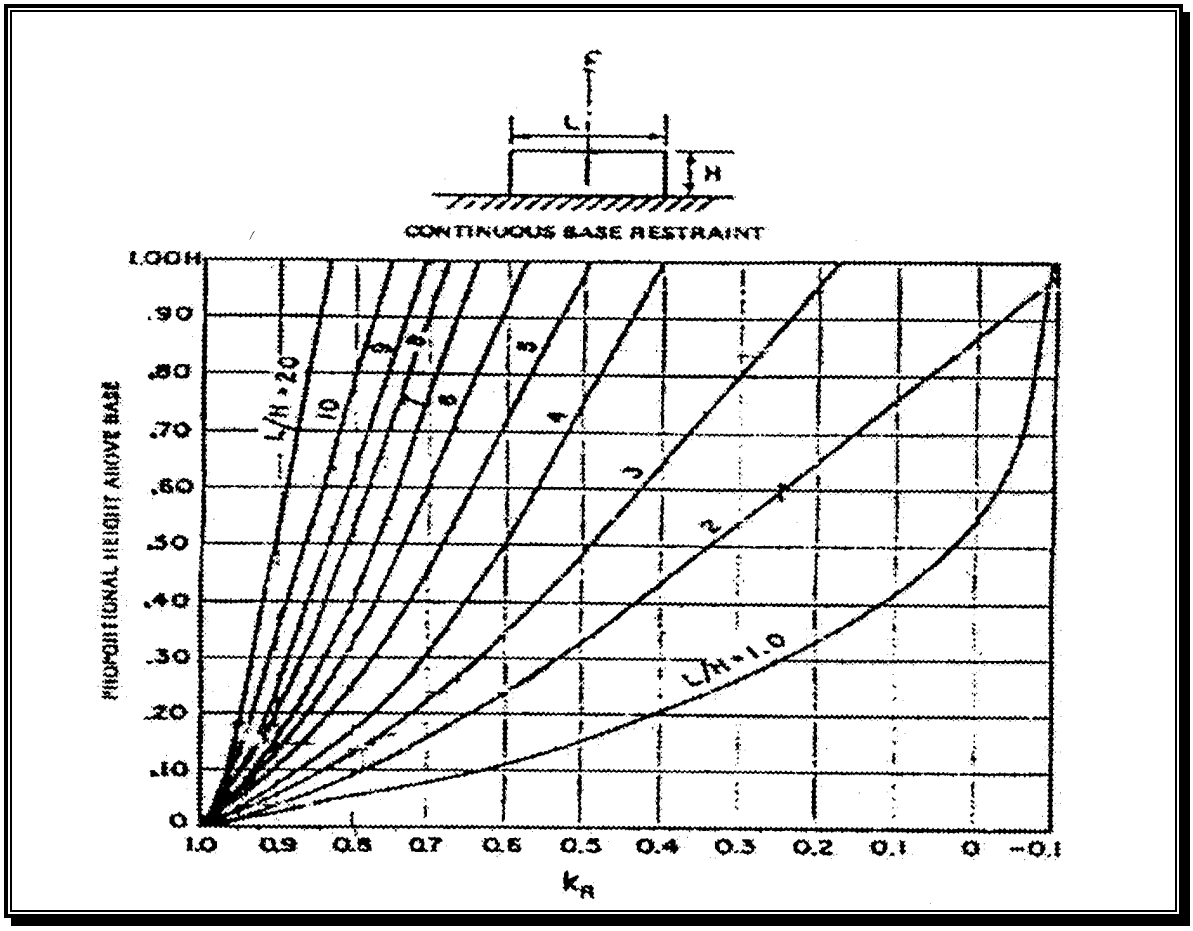

Figure (٢-٢): Degree of tensile restraint at center section [٢٥].

A- End-Restrained Shrinkage Cracking

Since the restraining edges exist only at the member ends, the restraint in such members will be uniform; accordingly, a uniform state of tensile strain will develop in the member as it shrinks or contracts.

Cracking of the member will therefore begin to propagate at the weakest section existing at any position within the member length [١٩].

In fact crack location depends mainly on the position of the weakest concrete section. As discussed previously, for a fully developed crack pattern, the spacing between cracks must be between S_{min} (bond slip distance) and S_{max} (twice the bond slip distance). As can be seen from Figure (٢-٣).

$$(D_b =) S_{\min} < S < S_{\max} (= 2 D_b)$$

where (D_b) is the bond slip distance.

Evans and *Hughes* [٢٨] derived the equation

$$S_{\min} = \frac{1}{4} \frac{d}{\rho} \frac{f_{tu}}{f_b} \qquad \text{(For rounded bars)} \qquad .....(٢-٢)$$

where;

d : bar diameter,

ρ : steel ratio,

f_{tu} : tensile strength of concrete, and

f_b : average bond strength between steel and concrete.

Evans and *Hughes* assumed that f_{tu}/f_b ratio can be taken as ٠.٦٧, ٠.٨ and ١.٠ for ribbed, indented and plain round bars respectively.

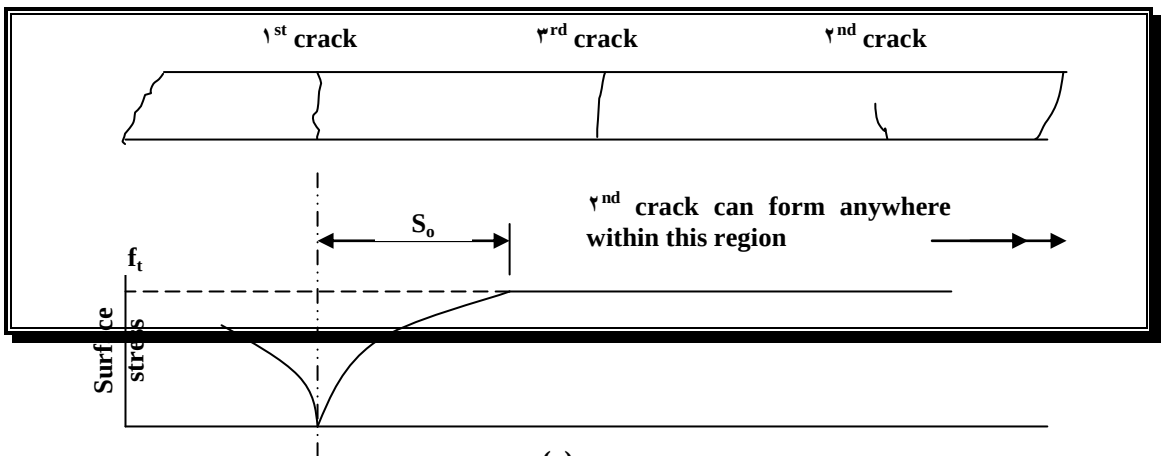

Figure (٢-٣): Concrete stress conditions during the development of cracking [٢٧].

Al-Rawi [٢٦] presented the following formula for the minimum crack spacing based on experimentally measured bond slip distance, using a new model which was believed to resemble field conditions:

$$S_{\min} = 0.85K\frac{d}{\rho} \qquad \text{.....(٢-٣)}$$

where (K) is a constant depending on the type of reinforcement

$$K = \begin{cases} 0.8 & \textit{for indented deformed bars} \\ 0.67 & \textit{for ribbed deformed bars} \end{cases}$$

(d) is the bar diameter and ρ is steel ratio. And S_{max} was taken as twice the above value for S_{min}.

The initial crack width formed can be calculated by the simple law of triangle area

$$w_i = \frac{S_{\max}.e_{ult}}{2} \qquad \text{.....(٢-٤)}$$

where;

w_i : initial crack width, and

e_{ult} : elastic tensile strain capacity of concrete.

The width of fully developed crack due to drying shrinkage and heat of hydration in restrained slabs and walls may be obtained [٢٩].

$$W_{\max} = S_{\max}\left[\varepsilon_{cs} + \varepsilon_{te} - \left(100\times10^{-6}\right)\right] \quad .....(٢\text{-}٥)$$

where;

w_{max} : maximum crack width,

S_{max} : maximum crack spacing,

ε_{cs} : shrinkage strain, and

ε_{te} : total thermal contraction after peak temperature due to heat of hydration.

The value of w_{max} can be calculated as suggested by [٢٩] (taking into consideration cooling to ambient from the peak hydration and the seasonal variations):

$$w_{\max} = S_{\max}.\frac{\alpha}{2}.\left(T_1 + T_2\right) \quad .....(٢\text{-}٦)$$

where;

$T_١$: fall in temperature between hydration peak and ambient, and

$T_٢$: fall in temperature due to seasonal variations.

Evans and *Hughes* [٢٨] expressed the maximum crack width as the product of maximum crack spacing by the average free shrinkage strain minus the average residual surface strain between cracks (taken as half the elastic tensile strain capacity of concrete):

$$w_{\max} = S_{\max}\left(e_{sh} - \frac{e_{ult}}{2}\right) \quad .....(٢\text{-}٧)$$

Al-Rawi [٢٦] obtained the following equation to estimate the maximum final crack width in end restrained concrete members, Figure (٢-٤).

$$w_{\max} = S_{\max}\left[e_{shr} - (creep_1 + loss\ of\ restra\text{int}) - \left(e_{ult} + \frac{creep_2}{2}\right)\right] \quad .....(٢\text{-}٨)$$

where;

$creep_1$: creep prior to cracking, and

$creep_2$: creep after cracking.

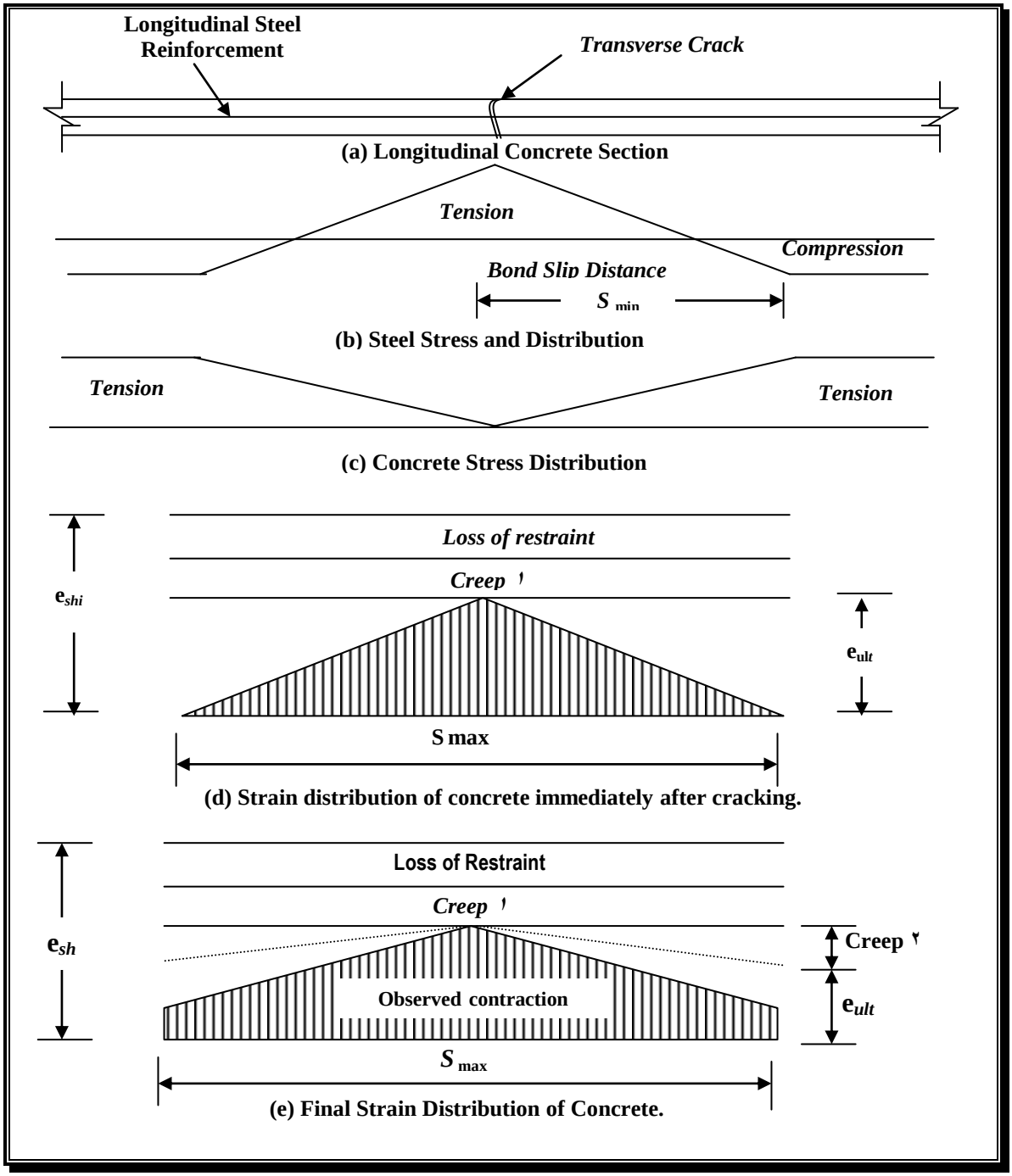

Figure (٢-٤):Sketch of stress and strain distribution in steel and concrete for deformed bars.**[٢٦]**

ACI-Committee ٢٠٨ [٢٦] presented an expression for crack width taking the effect of variation in restraint in the wall before cracking only into consideration:

$$w_{\max} = 1.5 S_{ave} \left(R_b \alpha_c T_e - f_{ct} / E_c \right) \quad \text{.....(٢-٩)}$$

where;

S_{ave} : average crack spacing.

α_c : coefficient of thermal expansion of concrete.

T_e :effective temperature change including an equivalent temperature change to compensate for drying shrinkage.

F_{ct} : tensile strength of concrete.

E_c : modulus of elasticity of concrete.

The committee suggested that the lower half of the wall, (near the base) requires maximum reinforcement and the upper half of the wall, requires minimum reinforcement. Again, this idea conflicts with facts that can be seen in practice. Figure (٢-٥) represents the cracking sequence that is proposed by the committee.

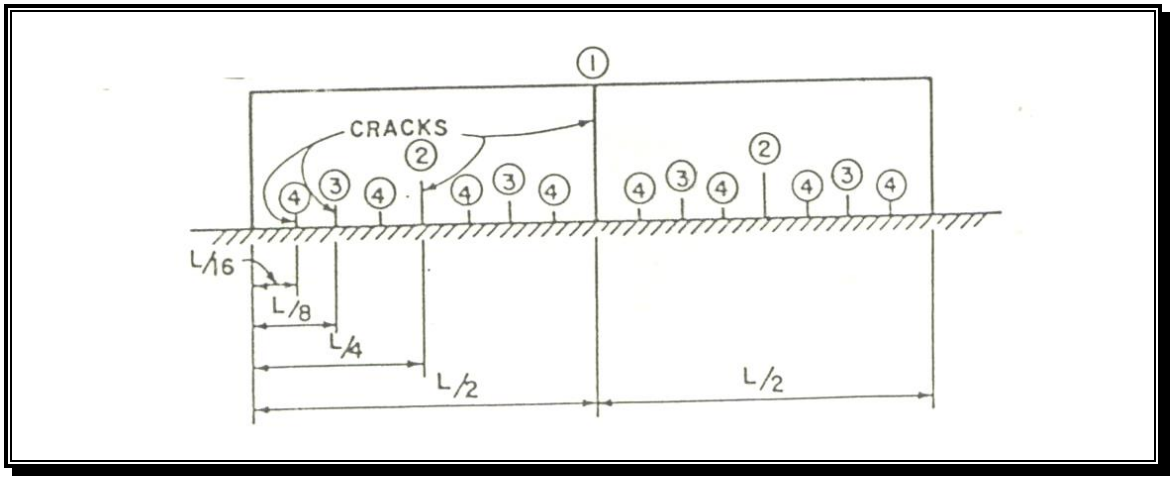

Figure (٢-٥): Sequence of crack propagation.**[٢٣]**

B- <u>Base Restrained Shrinkage Cracking</u>

A concrete wall cast on a continuous concrete base is a typical example for base restrained concrete members. The restraint in the walls is not uniform throughout the wall height, but varies from point to point within the wall. The magnitude of restraint depends on: length/height ratio of the wall, wall and base dimensions, degree of fixity between the wall

and the base, position of the point, and amount and distribution of reinforcement.

Al-Rawi [١٩] investigated the combining effects of the base restraint and the reinforcing steel in distributing volume change cracking. He suggested the following equations for prediction of minimum crack spacing (S_{min}) and maximum crack width (w_{max}) in base – restrained concrete members:

$$S_{\min} = \frac{K_1 d H}{\rho H + K_1 d} \qquad \text{.....(٢-١٠)}$$

where;

$K_١$: factor equals ٠.٥٧ for deformed bars, ٠.٦٨ for indented bars, and ٠.٨٥ for plain bars,

d : bar diameter,

ρ : steel reinforcement ratio, and

H : wall height.

$$w_{\max} = S_{\max}\left[K\left(R_b - 0.8R_a\right)e_{sh} - e_{ult}/2\right] \qquad \text{.....(٢-١١)}$$

K=١-c'

where;

R_a : degree of restraint after cracking,

R_b : degree of restraint before cracking,

S_{max} : maximum crack spacing,

e_{sh} : free shrinkage, and

e_{ult} : elastic tensile strain capacity of concrete.

Assuming the sum of the creep strain before cracking C_b and the average value of the creep strain after cracking C_a to be c' (constant) of the total net shrinkage, where c' equals ٠.٤ for reinforced concrete walls and ٠.٢٥ for plain concrete walls.

The B.S. ٥٣٣٧ [٢٩] gives the following equation for the prediction of maximum crack width:

$$w_{\max} = S_{\max}\left[e_{th}/2 + e_{sh} - e_{ult}/2\right] \quad .....(٢\text{-}١٢)$$

Using the equation above, results in a uniform predicted crack width along the wall height. *Harrison* [٣٠] modified this equation by introducing the effect of the degree of restraint before cracking at the wall center line. Thus, Equation (٢-١٢) will become:

$$w_{\max} = S_{\max}\left[0.5R_b\left(e_{th} + e_{sh}\right) - e_{ult/2}\right] \quad .....(٢\text{-}١٣)$$

where R_b is the degree of restraint before cracking.

Since R_b is maximum at the wall base, and decreases toward the wall top, therefore according to *Harrisons* formula the crack width will be the maximum at the base and minimum at the wall top. Harrison considered the creep to be about ٥٠٪ of the total volume change (e_{th}+e_{sh}).

٢.٥ Factors which Affect Cracking Resistance

٢.٥.١ Creep or Relaxation of Concrete

Creep is generally defined as the continued deformation of concrete under sustained stress [١٠]. According to *Neville* [١٦], if the restraints are such that a stressed concrete specimen is subjected to a constant strain, creep will be expressed as a progressive decrease in stress with time known as (relaxation).

The basic effect of creep on cracking tendency of concrete is to delay or prevent the cracking of concrete through delaying the shrinkage strain propagation and preventing the stage at which tensile strain capacity is exceeded.

Many factors which affect creep such as; relative humidity, w/c ratio, mix proportion, age of concrete, ambient temperature, influence shrinkage in a similar manner. Hence, their influence on cracking tendency is very little.

٢.٥.٢ Tensile Strain Capacity of Concrete

Control of shrinkage cracking of concrete depends partly upon the maximum strain which the concrete can sustain in tension before cracking occurs (strain capacity). The tensile strain capacity includes both the elastic strain capacity and the creep strain, which, develops during tensile strain build up by restrained shrinkage, which is time dependent.

Mann [٣١] reported a value for ultimate strain capacity is approximately ١٠٠ microstrain at a variety of ages and strength. Other researchers quoted experimental values of strain capacity ranging between (١٠٠-٢٠٠) microstrain, however higher values can be used safely before cracking and this was confirmed by *Al-Rawi* [٢٢]. *Hughes* and *Ghunaim* [٣٢] reported that tensile that tensile strain capacity increases with increase of concrete age. *Hoobs* [٣٣] concluded that the strain capacity will be improved with age and strength of concrete. An increase in strain capacity from (٨٠-١٠٠) microstrain to (١٢٥-١٦٠) microstrain was obtained with increase in age from ٧ to ١٨٠ days.

The values presented in previous literature are about (١٠٠-٢٠٠) microstrain [٣١]. Higher values, however, have been reported more recently by *Al-Rawi* [٢٢].

٢.٦ Cracking Age

It is the time required for the shrinkage induced strains to build up and exceed the tensile strain capacity of concrete. The age of first crack and the cracking sequence is dependent on the same factors that influence the cracking tendency of concrete (i.e. degree of restraint, shrinkage, creep, tensile strain capacity … etc). Thus, cracking age, as stated by *Al-Rawi* [٢٢] could be used as an index to assess the possibility of cracking of various mixes.

Al-Rawi [٢٢] reported that the cracking time depends on both shrinkage and tensile strain capacity. It increases with decrease in w/c ratio (mix preparations being unchanged), with increase in normal curing time and amount of crushed coarse aggregate.

٢.٧ Effect of Fire

٢.٧.١ Introduction

Behavior of reinforced concrete under fire has been studied by many investigators. The effect of temperature on the reinforced concrete properties and the calculation of the resulting stress, deformations and strains has been subjected to considerable research in recent years. A number of research dealt with the effect of fire on reinforced concrete members. It is clearly stated that both concrete and steel are affected by exposure to fire.

This review is concerned with the properties of concrete and reinforcing steel at temperatures higher than the normal range, which may occur through accidents by fire in conventional buildings.

٢.٧.٢ The effect of Fire on the Concrete

Harada et al. [٣٤] showed that the strength of concrete generally decreases with the increase in temperature, although below ١٠٠^{o}C exceptions to this rule have been found. Also, they found experimentally that the residual bond strength of concrete with steel reinforcement was ٤٤٪ of reference strength at a temperature range of ١٠٠ to ٣٠٠^{o}C but dropped rapidly to ١٠٪ at ٤٥٠^{o}C. This effect was more remarkable than the effect of temperature on the compressive strength where the residual strength was ٦٠٪ at ٤٥٠^{o}C.

High temperature [٣٥] induces a loss of strength, both in (compression and tension) and in concrete stiffness (Young's modulus),

and an increase in the elastic deformability, creep and shrinkage by altering the chemical – physical composition of the cement paste transmigration and vaporization of the free water, loss of the combined and adsorbed water, dissociation of the calcium hydroxide at about ٤٠٠ ^{o}C, shift from α-quartz to β-quartz in the crystalline silicon dioxide at ٥٧٥^{o}C. These processes occur not only at the micro-structural level [within the hydrated binder, i.e. within the cement paste], but also at the mesolevel for instance, in the medium and large aggregate particles, which may exhibit a sever splitting because of the loss of zeolitically – bonded water [٣٦, ٣٧].

In the temperature range ٣٠٠^{o}C to ٥٠٠^{o}C, the total porosity of the cement paste increased rapidly due to formation of microcracks [٣٨]. This behavior is attributed to the dehydration of some cement paste compounds. Additional significant increase in porosity beyond ٥٠٠^{o}C was stated to be caused by two chemical processes [٣٨]: liberation of water from the dissociation of $Ca(OH)_{٢}$ in the range ٤٥٠^{o}C-٥٥٠^{o}C and liberation of $CO_{٢}$ as a result of $CaCO_{٣}$ decomposition above ٦٠٠^{o}C.

Umran [٣٩] investigated the fire flame exposure effect on some mechanical properties of concrete. The specimens were subjected to fire flame ranging between (٢٥-٧٠٠^{o}C). Three temperature levels of (٤٠٠, ٥٠٠ and ٧٠٠ ^{o}C) were chosen with four different exposure duration of ٠.٥, ١, ١.٥ and ٢ hours without any imposed loads during heating. The specimens were heated and cooled under the same regime and tested after exposure to fire flame at ages (٣٠, ٦٠ and ٩٠ days). Compressive strength of ١٥٠ mm cubes and flexural strength of (١٠٠x١٠٠x٤٠٠ mm) prisms were measured. Ultrasonic pulse velocity (U.P.V) and dynamic modulus of elasticity (Ed) were tested also. He found that the residual compressive strength ranged between (٧٠-٨٥٪) at ٤٠٠ ^{o}C, (٥٩-٧٨٪) at ٥٠٠ ^{o}C and (٤٣-٦٢٪) at ٧٠٠ ^{o}C. The flexural strength was found to be more sensitive to fire flame exposure than the compressive strength. The residual flexural strength was in the

range of (٦٧-٧٨٪) at ٤٠٠ ^{o}C, (٤٠-٦٧٪) at ٥٠٠ ^{o}C and (٢٠-٤٥٪) at ٧٠٠ ^{o}C. He also found that ultrasonic pulse velocity (U.P.V) and dynamic modulus of elasticity (Ed) were more sensitive to fire flame than compressive strength. He also noticed that exposure time after one hour has a significant effect on residual compressive strength of concrete.

٢.٧.٢ The Effect of Fire on Reinforcing Steel

Edwared, and *Gamble* [٤٠] investigated behavior of grade ٦٠ reinforcing bars of diameter (١٢.٧ mm) after exposure to fire. The bars were heated to temperatures of (٥٠٠-٨٠٠ ^{o}C), the furnace was held at peak temperature for about one hour and then slowly cooled simulating one possible condition in a severe fire. The bars were tested in tension after they had been cooled. The yield stresses were reduced to a minimum of ٧٣٪ of the original strength and the ultimate strength was reduced to a minimum of ٨٣٪ of the as rolled strength. The heating and cooling of the steel did not change the nature of the stress-strain curves. The modulus of elasticity remains constant at room and elevated temperatures.

M. Holemes and *R.D, Anchor* [٤١] studied the effect of elevated temperatures on the strength and stiffness properties of four reinforcing steels of varying size. The test program was designed to provide data on three major parameters (yield stress, ultimate strength, and elastic modulus). They found that the normalized results for the yield stress, ultimate strength and elastic modulus for all sizes are as follows:

A- There was no significant change in the normalized values below ٣٠٠ ^{o}C.

B- A ٥٠٪ reduction in both the yield stress and ultimate strength was obtained between ٥٢٠ ^{o}C and ٥٨٠ ^{o}C and between ٥٤٠ ^{o}C and ٧٠٠ ^{o}C for the elastic modulus.

٢.٧.٣ The Effect of Fire on Reinforced Concrete Slabs

J. Hannant and *P.S. Pell* [٤٢] investigated the thermal stresses in reinforced concrete slabs. An experimental and theoretical investigation into the stresses induced in steel and concrete in reinforced concrete slabs subjected to high temperatures and thermal gradient. They found that the observed stresses in the steel are dependent on time and previous temperature cycling of the slab. Initially, the stresses in the steel were in close agreement with the values derived from the elastic analysis, but as shrinkage and creep increased, with time and temperatures, large losses of tensile stress were measured until, in several cases, the steel developed compression even while the thermal gradients were considerable. The main cause of the loss of tensile stress in the steel was attributed to the increased rate of concrete shrinkage at temperatures near or above ١٠٠ ^{o}C, with secondary effects due to creep and reduction in the expansion coefficient.

Salse and Lin [٤٣] carried out a theoretical study on the influence of high temperature on concrete structures. It included a theoretical part for the structural design for reinforced concrete members subjected to fire. To determine the properties of concrete and steel reinforcement during fire exposure, the thermal distribution through the member section should be known, therefore, they used a thermal analysis by finite difference method.

They reached the following conclusions:

١- The resistance of a structural member to fire increases as the restraining force increases.

٢- Simple mathematical relationship may be used to find the resistance of sections at the negative and positive moment areas.

٣- The effects of restraining force were used to calculate the strength of the section in the ultimate moment areas only.

Shirly et al. [٤٤], carried out a study dealing with high strength reinforced concrete slabs and their resistance to fire. The study includes five specimens having dimensions of ٩٠٠x٩٠٠x١٠٢ mm reinforced with ١٩ mm diameter steel bars. Four high strength mixes were used along with one mix with normal strength for comparison. The specimens were subjected to a standard fire, and failure was determined when the average unexposed surface temperature reached ١٢١^{o}C.

The results showed that the behavior of the five slab specimens was the same, the fire endurance of the specimens were close, and there was no spalling or falling of the concrete surface due to high temperature exposure. Some cracks formed over embedded reinforcing bars during the fire tests. However, these cracks appeared in both the high and normal strength concrete specimens.

Gustaferro and *Carlson* [٤٥], interpretated the effect of end restraint on the fire resistance of prestressed concrete members based on data obtained in some of the fire tests as shown in Figure (٢-٦).

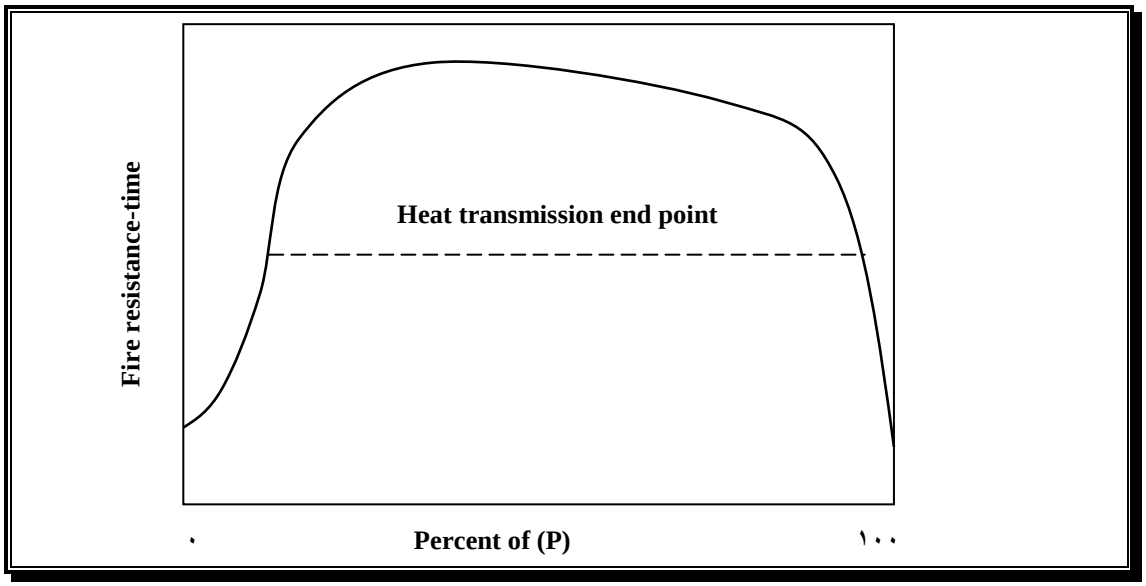

Figure (٢-٦): Effect of end restraint on fire resistance on prestressed concrete.

The value of (١٠٠٪ restraint) represents the fixed end condition while the (٠٪ restraint) represents a simply supported condition with no

resistance to thermal expansion. Other percentages represents intermediate degree of restraint. Each point on this curve represents the fire resistance for a certain degree of restraint. It is evident that some restraints improve the fire resistance, however, complete or nearly complete restraint can result in a reduction in the fire resistance. One of the end points of fire test listed under ASTM standard E١١٩ [٤٦] is the "heat transmission" end point which is reached when the average temperature of the unexposed surface of a slab rises more than ١٢١ ^{o}C. The relative position of the dashed line is principally a function of the slab thickness and the type of aggregate. The portion of the curve above the dashed line is principally of academic interest since the fire resistance would be determined by the elapsed time to the first end point. The portion of the curve to the left of the zone representing an end point by heat transmission indicates the structural end point, while the portion to the right indicates the end point by compression spalling or by compression failure.

Lie and Leir [٤٧], investigated the effect of different parameters on the temperature distributions on reinforced concrete slabs under fire exposure, using ٨٠٠x٩٠٠mm specimens with different thickness ٦٠, ١٠٠ and ١٥٠ mm. Moreover, a computer program was used depending on the finite difference method to calculate the temperature distribution in the fire exposed slabs taking into account the effect of time of exposure to the elevated temperatures and concrete thermal properties. The authors concluded that there is good agreement between the experimentally and theoretically calculated temperature distribution for all the specimens. They also found that an increase of moisture in concrete leads to disagreement between the experimental results and those calculated using the computer program. Furthermore, they observed that the slab thickness affects the temperature distribution significantly.

Hidayat [٤٨], carried out an experimental and theoretical investigation concerning the behavior of reinforced concrete slabs subjected to high temperatures. The experimental part included fabricating and testing ١٨ reinforced concrete slab specimens having dimensions of ٦٠٠x٦٠٠x٤٠٠ mm, with different steel ratios. The specimens were heated and cooled, then tested to failure under uniformly distributed load.

The analytical investigation included thermal analysis using the computer program fires – T٣ to predict the thermal distribution through the slab section, and a structural analysis of the slab specimens subjected to high temperatures.

He reached the following main conclusions:

١- All the heated slabs were found to be capable of resisting the service loads.

٢- The ultimate flexural strength of the slab specimens decreased with the increase of temperature.

٣- Good agreement between the thermal analysis and the experimental results were obtained, which confirms the validity of the method and the mathematical models used.

٢.٨ Temperatures Associated with Fires

The values of temperature associated with fires are according to the ASTM-E١١٩ standard curve which can be described approximately by the following expression [٤٦]:

If t < ٧٢٠٠ sec.

$$T_f = T_o + \frac{1}{1.8} [١٠٤٤ + \tanh (٠.٠٠٠٢٣٤١٣\ t) - ٤٩٨.٢ \tanh (٠.٠٠٠٢٧٠٤٤t) + ١٢٨٦ \tanh (٠.٠٠٢٤٧٥\ t)] \quad .....(٢-١٤)$$

If t ≥ ٧٢٠٠ sec.

$$T_f = ٩٢٧ + ٠.٠١١٥٧٤\ t \qquad .....(٢-١٥)$$

where;

f : for the fire,

t : time in seconds,

T : the fire temperature at time t (^{o}C), and

T_o : initial temperature (^{o}C).

The curve representing this function; known as the "standard time-temperature curve", Figure (٢-٧).

Lie and *Irwin* [٤٩] proposed a model to simulate the temperature – time curve for the standard ASTM-E١١٩ fire test

$$T = 20 + 750\left[1 - \exp\left(-3.79553\sqrt{t}\right)\right] + 170.41\sqrt{t} \qquad .....(٢-١٦)$$

where t is the time in hours.

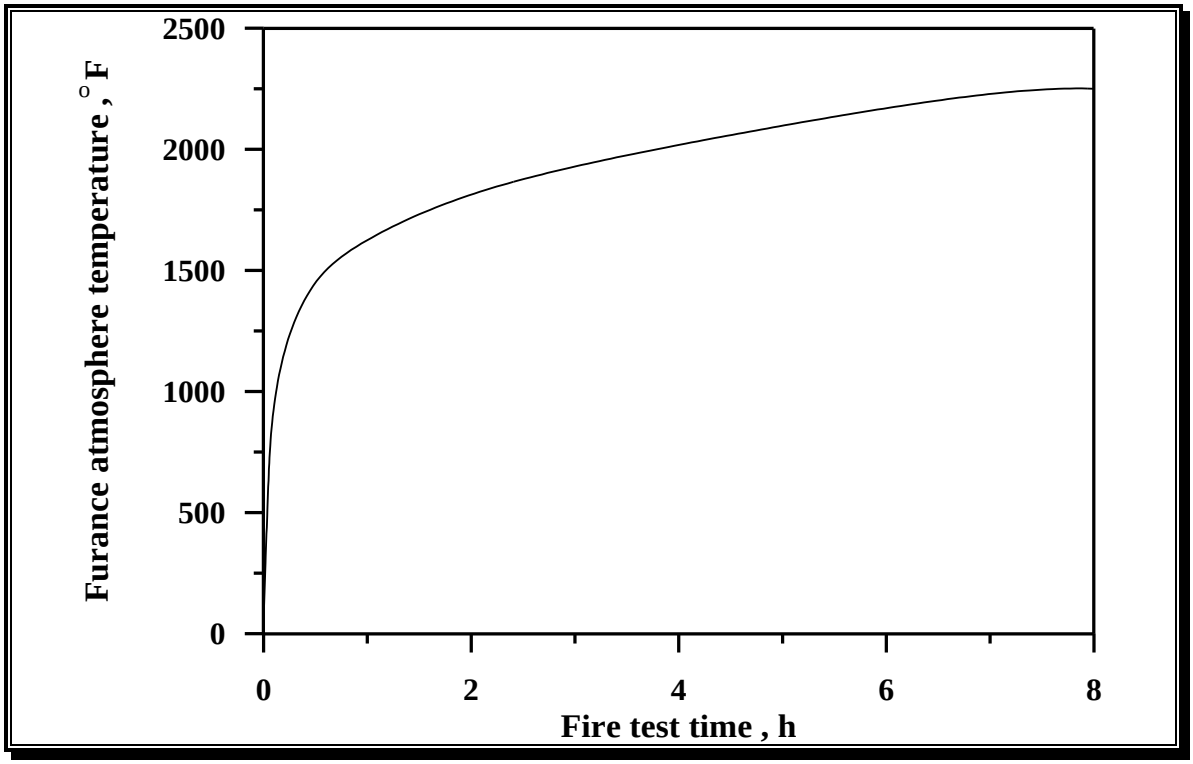

Figure (٢-٧): Standard time-temperature relationship of furnace atmosphere (ASTM E١١٩).

Concrete made with siliceous or limestone aggregate shows a change in colour with temperature, as this is dependant on the presence of certain compounds of iron, there is some difference in the response of different concrete. The change in colour is permanent, so that the maximum temperature during a fire can be estimated a posterior; the colour sequence is approximately as follows, pink or red between ٣٠٠ and ٦٠٠^{o}C, then grey up to about ٩٠٠ ^{o}C, and buff above ٩٠٠ ^{o}C. Thus the residual strength can be approximately judged [١٦, ٣٥].

٢.٩ Thermal Properties at Elevated Temperatures

A- Thermal Expansion of Concrete

Thermal expansion is a very important free strain associated with fire. It changes rapidly with temperature. An envelope model [٥٠] and a typical model for thermal expansion of concrete are shown in Figure (٢-٨).

A coefficient of thermal expansion of concrete is obtained from the slopes of Figure (٢-٨) as follows:

$$0 \le T \le 500^{o}C \quad \alpha_c(T) = 10.8\times10^{-6}/{}^{o}C \qquad \text{.....(٢-١٧)}$$

$$T \ge 500^{o}C \qquad \alpha_c(T) = 16.2\times10^{-6} \ /{}^{o}C \qquad \text{.....(٢-١٨)}$$

The free thermal strain in concrete for time step (i) is calculated as:

$$\Delta\varepsilon_{th},c(i) = \alpha_c(\overline{T_i})(T_i - T_{i-1}) \qquad \text{.....(٢-١٩)}$$

where;

$$\overline{T_i} - \text{average temperatu re during time step i} = \frac{\mathrm{T_i} + T_{i-1}}{2}$$

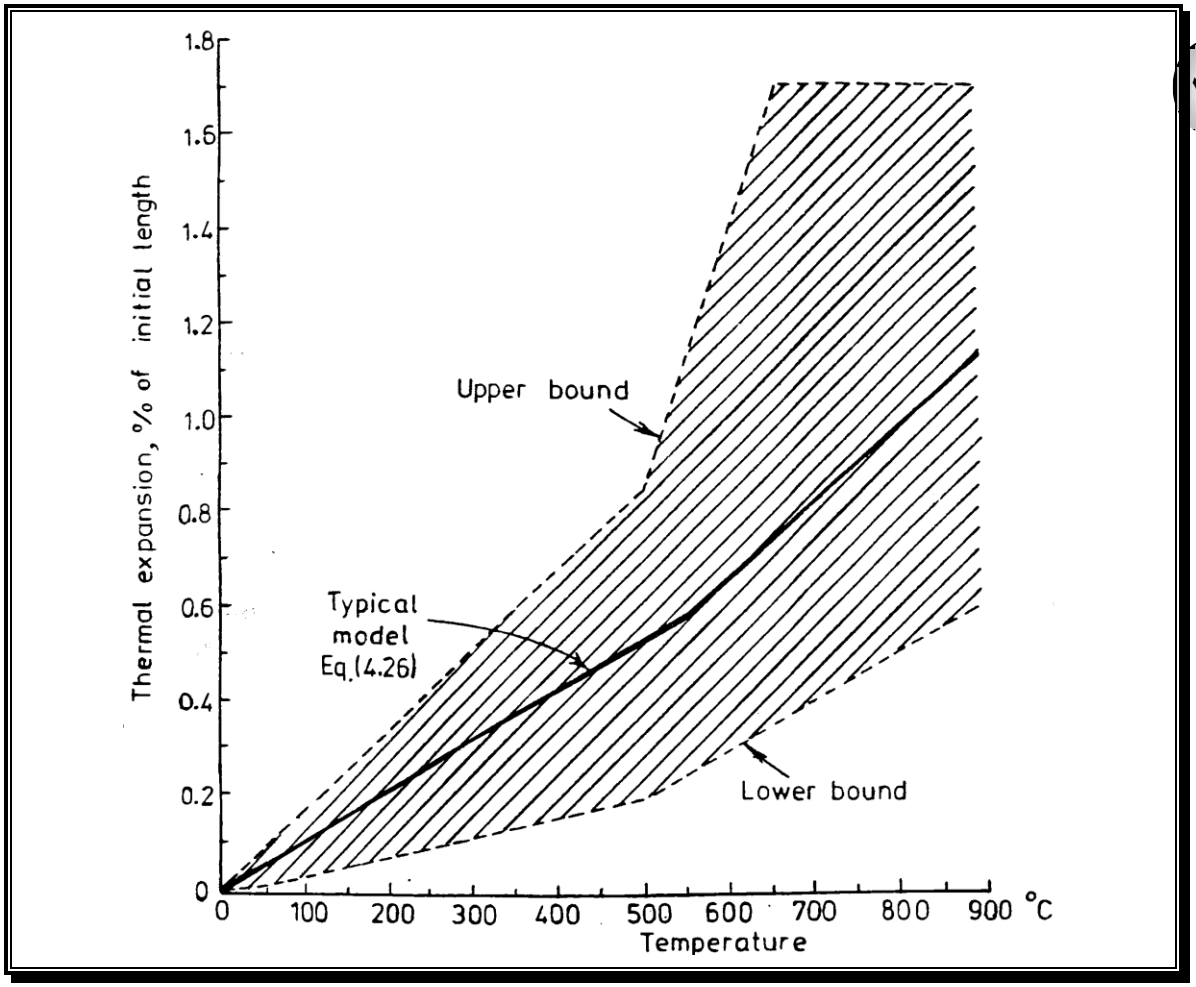

Figure (٢-٨): *Thermal expansion of concrete as a function of temperature.*

Figure (٢-٩) shows data on linear thermal expansion of concrete made with siliceous aggregate. The data were obtained by *Cruz* [٥١] using a dilatometric method but the results have not yet published. *Harmathy* and *Allen* [٥٢] studied the thermal expansion of ١٦ different concretes, used in masonry units. Among these, pumice concrete was found to exhibit considerable shrinkage at temperatures above ٣١٥^{o}C. *Dettling* [٥٣] pointed out that thermal expansion of concrete is influenced by aggregate type, cement content, water content, and age.

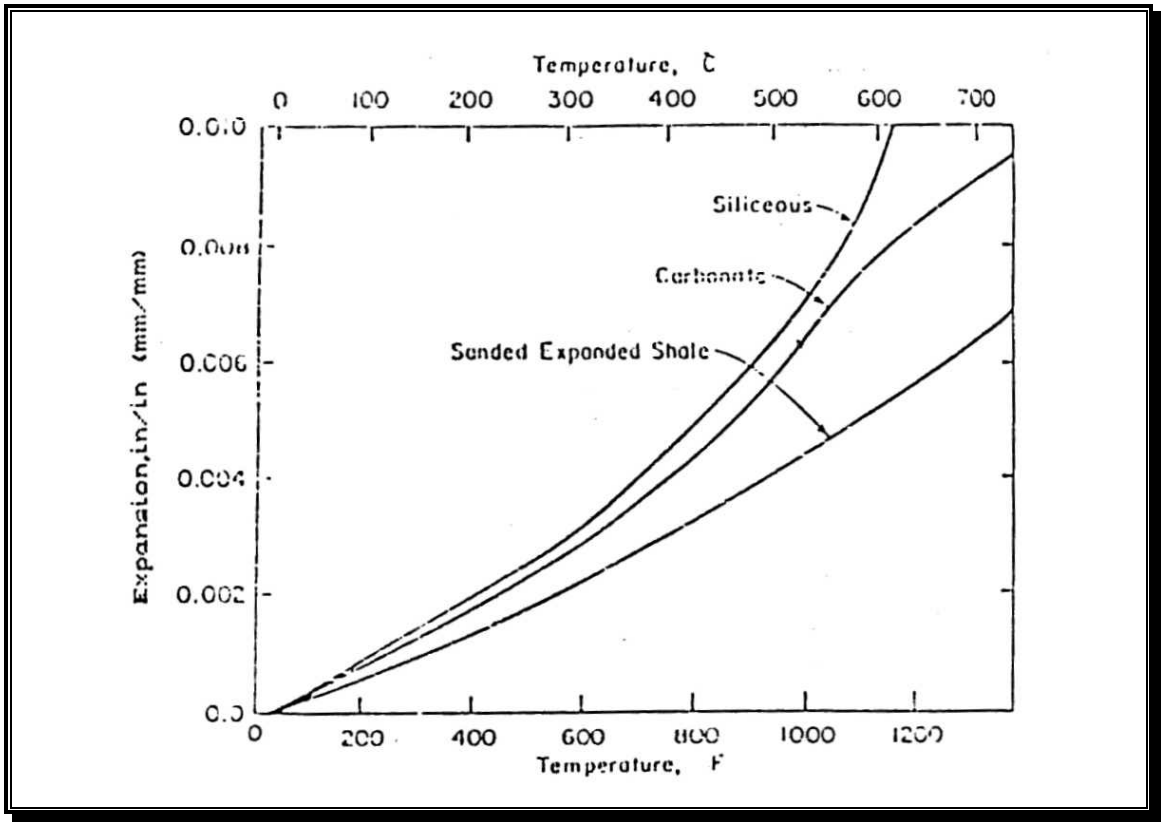

Figure (٢- ٩): *Thermal expansion of concrete at high temperature.*

The aggregates, depending on the type of their rock origins, have different expansion behaviors during heating. The coefficient of thermal expansion of various rocks usually ranges from less than $٣.٦x١٠^{-٦}$ /°C to more than $١٢x١٠^{-٦}$/°C at normal temperature [٥٤]. Testes by *Harda et al.* [٣٤] revealed that thermal expansion of concrete was very close to that of aggregate used in it. This is attributed to the high content of aggregates as compared with the cement paste. So, in spite of the high contraction of the cement paste, expansion of concrete is predominant. *Zoldner* [٥٤] stated that the quartz content in aggregate is the main factor influencing thermal expansion of aggregate. A higher quartz content to cause larger expansion due to heating.

During first heating, the cement paste is subjected to two opposite effects. An ordinary thermal expansion based on kinetic molecular movements, and a hygrothermal volume change associated with the

movement of internal moisture [٥٤, ٥٥]. Up to a temperature of ١٠٠ ^{o}C, the cement paste expands; then it will contract at higher temperatures [٥٥]. This contraction continues as temperature rises as shown in Figure (٢-١٠).

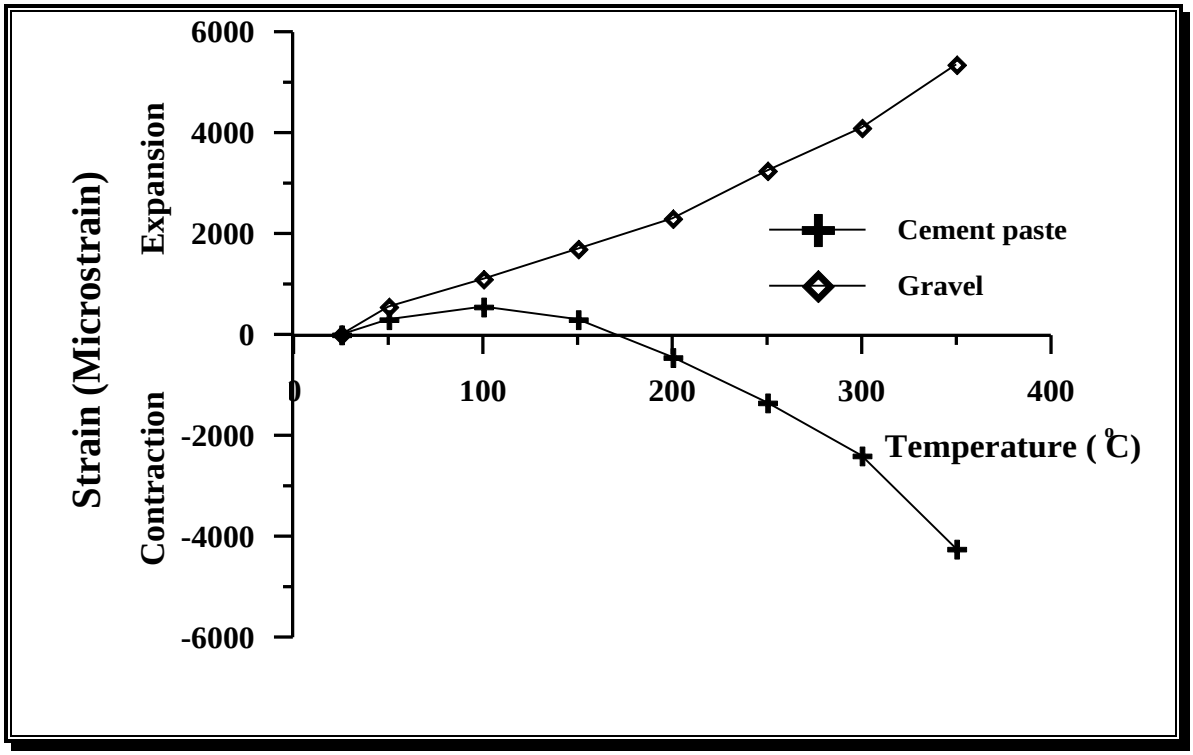

Figure (٢-١٠): *Free thermal strain of cement pate and gravel. (After Khoury et al., ١٩٨٥)* [٥٥].

B- <u>Thermal Expansion of Steel</u>

In order to study the behavior of reinforced concrete structures up to failure, the mechanical properties of steel should be specified. These properties such as modulus of elasticity, *Es*, yield strength, f_y and stress strain relation are temperature dependent.

It was stated earlier [٥٠] that up to ٧٠٠^{o}C thermal expansion coefficient of steel increases with rise in temperature. Thereafter, steel undergoes transformations in its composition (i.e. crystalline transformations) resulting in an appreciable discontinuity in the expansion curve (Malhotra) [٥٦]. However, the model suggested by *Nizamuddin* **[٥٠]** is shown in Figure (٢-١١) in addition to the test result published by

Takeuchi et al. [٥٧]. This model for calculation of the coefficient of thermal expansion, α_s, is shown by the formula:

$$\alpha_s = \left(\frac{T}{100} + 10.8\right) \times 10^{-6} \ , ^oC \ \ for \ 0\,^oC \le T < 650^oC \qquad .....(٢\text{-}٢٠a)$$

and

$$\alpha_s = 17.3 \times 10^{-6} \ , ^oC \qquad for \ 650^oC \le T \qquad .....(٢\text{-}٢٠b)$$

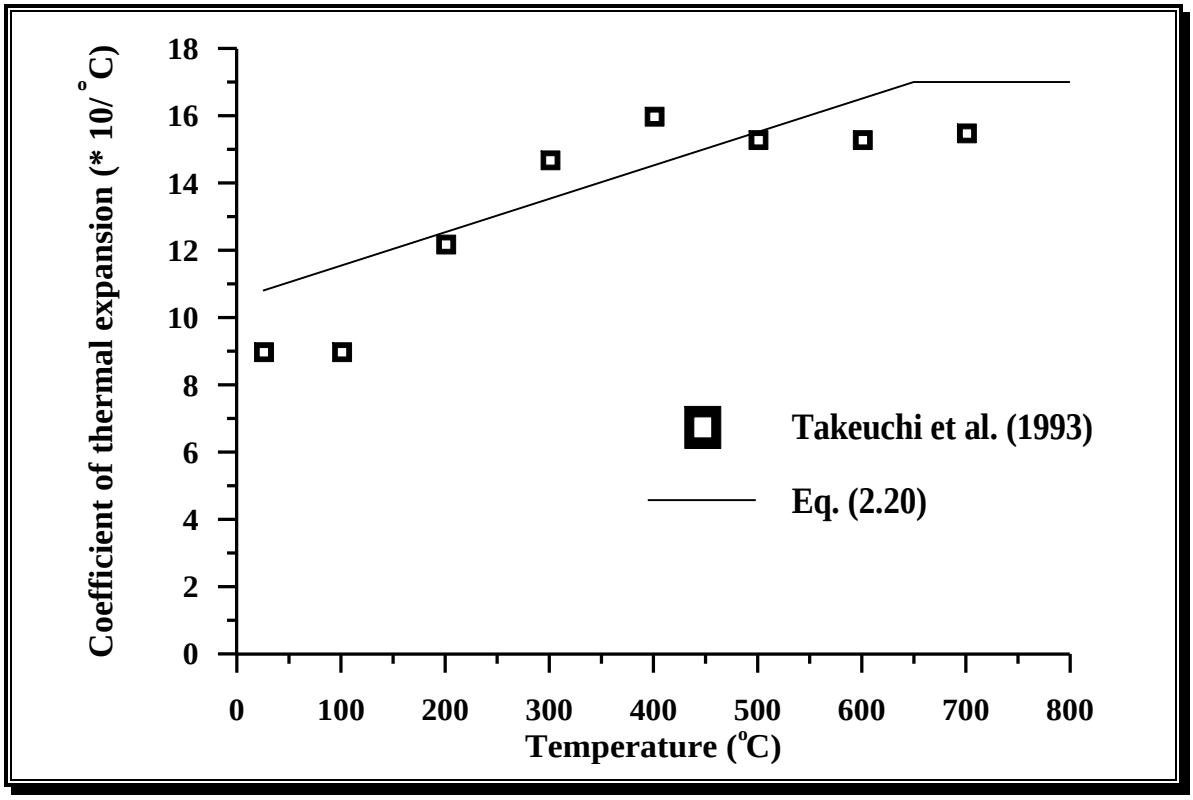

Figure (٢-١١): Coefficient of thermal expansion of steel at different temperatures.

٢.١٠ Deformation Properties at elevated Temperatures

A – Creep of Concrete at Elevated Temperatures

Creep is one of the time dependent free strains associated with fire that it increases rapidly with increasing temperature. Many investigators [٥٨, ٥٩] tried to study this strain by loading concrete after heating and different models were presented. However, this was discouraged when it became clear that transient thermal strain was significantly greater than the

basic creep and the elastic strain [٥٥,٥٦]. Moreover, heating of concrete before loading seems to occur rarely from structural point of view, and the structural element is heated mostly after loading.

The creep strain may be divided to the following components [٦٠]:

i- creep strain before heating which may be calculated using any creep law at ambient temperature,

ii- creep strain during heating which was considered as a part of load induced thermal strain (ε_{LITS}),

iii- creep strain at constant temperature exposure which was seen by *Khoury* ١٩٩٣) [٦١], and

iv- creep strain during and after cooling which was not considered in the published studies as far as known.

B- <u>Shrinkage of Concrete After Heating</u>

The time-dependent behavior of concrete increases in importance when concrete structures are exposed to elevated temperatures. This is especially so in the case of prestressed concrete structures, such as storage and containment vessels, which could lose their prestress due to excessive creep and shrinkage experienced at high temperatures [٣٧].

J. Hannant and P.S. Pell [٤٢] investigated the thermal stress in reinforced concrete slabs. An increase in temperature, particularly near ١٠٠^{o}C, was found to accelerate shrinkage, creep and change in expansion coefficient, all of which were related to loss of water.

Habeeb [٦٢] investigated the effect of high temperature on the mechanical properties of high strength concrete (HSC). The specimens were subjected to elevated temperature ranging between (١٠٠-٨٠٠ ^{o}C). Five temperature levels of (١٠٠, ٣٠٠, ٥٠٠, ٦٠٠ and ٨٠٠ ^{o}C) were chosen with three different exposure duration of ١,٢ and ٤ hours without any

imposed loads during heating. The specimens were heated and cooled under the same regime and tested either one day to one month after heating. For shrinkage of concrete before and after heating of [١٠٠x١٠٠x٥٠٠ mm] prisms were measured in this work. He observed that (HSC) was more sensitive to high temperature exposure than normal strength concrete (NSC). He found from the test results, that the additional shrinkage values due to the heating are between (٤٠٠-٨٠٠) microstrains, and there is no significant increase in shrinkage values due to the increase of exposure time from ١ hour to ٤ hours. Shrinkage values were not more than ١٠٪ of that at ١hour exposure.

٢.١١ Structural Behavior

The overall effect of non-linear temperature distribution through the depth of reinforced concrete slabs may be considered of three parts:

١- Owing to the main temperature induced in the cross-section, there will be an axial strain resulting in overall axial deformation if the slab is axially unrestrained and free to deform, such temperature strains are induced without stress.

٢- Owing to the main temperature gradient there will be a strain gradient causing an overall curvature of the section (remaining plane); if the slab is free to rotate, such temperature strains do not produce stresses.

٣- Owing to mechanical characteristics of the materials (steel and concrete) under the elevated temperatures, mainly the reduction in compressive strength concrete $f_{c'}$, and yield stress of reinforcing steel f_y.

٢.١١.١ Structural Behavior of Simply Supported (Unrestrained Slabs)

For a simply supported reinforced concrete slab, the rocker and roller supports indicate that the ends of the slab are free to rotate and expansion can occur without resistance. Therefore, no thermal stresses produce, and the reduction in nominal moment strength will affected only by the reduction produced in strength of structural materials due to exposure to high temperature. If the underside of the slab is exposed to fire, the bottom of the slab will expand more than the top, resulting in a deflection of the slab [٦٣].

٢.١١.٢ Structural Behavior of Continuous Slabs

Structures that are continuous or otherwise statically indeterminate, undergo changes in stresses when subjected to fire [٦٤, ٦٥]. Such changes in stress results for temperature gradients within structural members, or changes in strength of structural materials at high temperatures, or both. In this investigation there is no account of thermal stresses was considered due to temperature gradient by assuming that the heated portion of a slab can expand and push against the surrounding part of the slab, if a fire occurs beneath a small interior portion of large reinforced concrete slab. Concerned the effect of fire on the changes in strength of structural materials at high temperatures.

CHAPTER THREE

EXPERIMENTAL WORKS

٣.١ Introduction

This chapter describes the materials used in the production of the specimens, mix proportions and the methods of testing.

Considerable experimental work has been carried out to study the shrinkage cracking behavior of reinforced concrete members restrained from movement at their ends for different restrained cases. But, limited experimental work was carried out to study the effect of fire on some properties of reinforced concrete slabs. This research was designed to study the effect of fire on different cases of restrained reinforced concrete slabs after restrained shrinkage cracking had taken place. Hence, the first main aim of this research is to study the behavior of drying shrinkage cracks in reinforced concrete slabs for different restrained cases (crack width, crack length, crack spacing, cracking tendency and position of maximum crack width). The second main aim is to study the effect of fire on the behavior of these slabs after drying shrinkage had taken place for a period of ٢ months in the laboratory.

Because the experiments of this study were made using reduced-scale slab models, measurements for crack spacing, crack width and crack length were made also for actual (full scale) slabs, to link the results of this study with actual site observations.

٣.٢ Program of the Work

During this research, the study of cracking characteristics of slabs was based on four reduced scale reinforced concrete slabs cast in laboratory. The chosen dimensions were fixed for the four slabs as (٢٢٥٠*٢٢٥٠*١٠٠ mm) (length * width * thickness respectively). The slabs were all cast in the same period to prevent or minimize the variations in the exposure conditions. Ratio of steel reinforcement (ρ) was kept at (٠.٤٢٪) for the four slabs. Restraint cases were varied as (free slab, two end restrained, three end restrained and four end restrained) to investigate their effect on shrinkage and thermal cracking of the slabs when exposed to drying and fires.

The end restraint was provided by reinforced concrete rigid beams. Thus, the model used can be considered to represent a practical restrained slab situation.

The experimental work was carried out to decide upon the temperature range and duration of burning. It was decided to limit the maximum exposure to fire flame to about ٦٠٠^{o}C, with a duration of exposure to fire flame of ١.٥ hour which cover the range of situation in the majority of elevated temperature tests.

The specimens were cast, moist cured for ٧ days, air dried in the laboratory until age of ٦٠ days, then subjected to fire flame.

Finally, crack spacing, crack length and crack width measurements were carried out for each slab for a period of ٦٠ days before burning and other ٦٠ days after burning.

٣.٣ Experimental Work

٣.٣.١ Restraining Reinforced Concrete Rigid Beams

In order to provide different restrained cases from the ends to the slab models, square reinforced concrete rigid beams were cast with dimensions (٢٢٥٠*٣٧٥*٣٧٥ mm) (length * width * height respectively) for all beams as shown in Figure (٣-١). A period of ٣ months was allowed between the casting of the rigid beams and the casting of the slabs to permit a considerable amount of shrinkage to take place before casting the slabs.

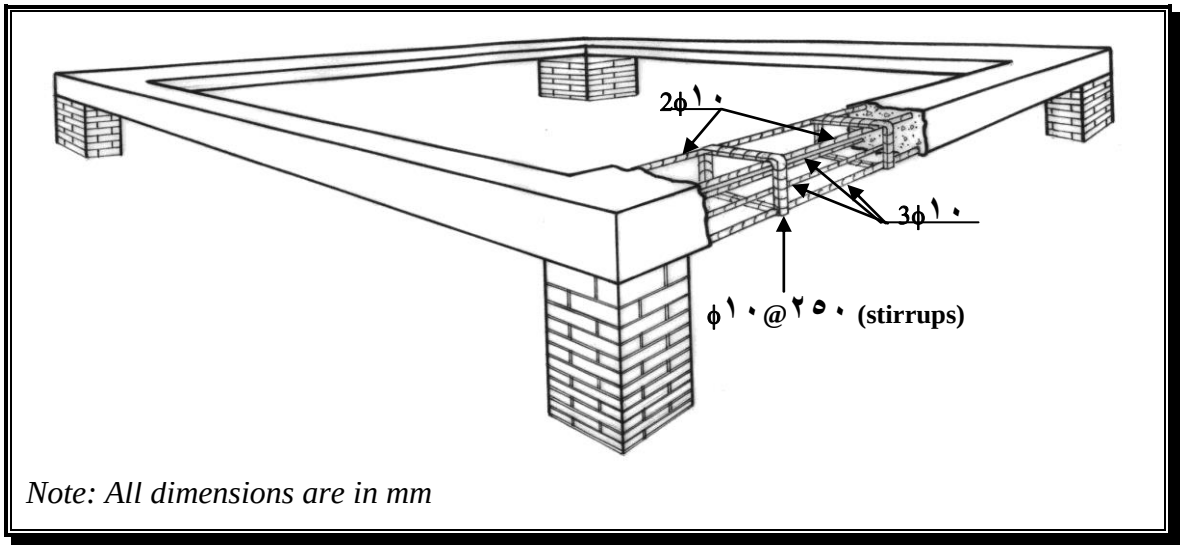

Note: All dimensions are in mm

Figure (٣- ١): Details of the restraining reinforced concrete rigid beams.

The mix proportions of the concrete used in casting of the rigid beams were (٤٣٥: ٥٢٥: ١٢١٥) kg/m^{٣} (cement: sand: gravel respectively), with a water to cement ratio of ٠.٤٥ and a slump of ٦٠ mm. The rigid beams were cured as for the slab models. This mix was designed according to British mix design method BS ٥٣٢٨: Part ٢: ١٩٩١ [٦٦] specifications to give a ٢٨-day cube compressive strength of ٣٨.٥ MPa.

The reinforced concrete rigid beams were used as end restraint. These beams were cleaned and greased from the upper surface to minimize the friction between the reinforced concrete slab and beams. In addition to the rigid beams, the edge surround beams and slab were cast at the same time. The edge surround beams provide the required end restraint. Figure

(٣-٢) shows the slab with the surround edge beams. The edges of the beams offer different end restraints to the slabs (two end, three end and four end restrained). These beams offer a better end restraint and at the same time allow shrinkage stress development very similar to that under field conditions.

Plates (٣-١) show the mixes of these beams were casted into the plywood formwork.

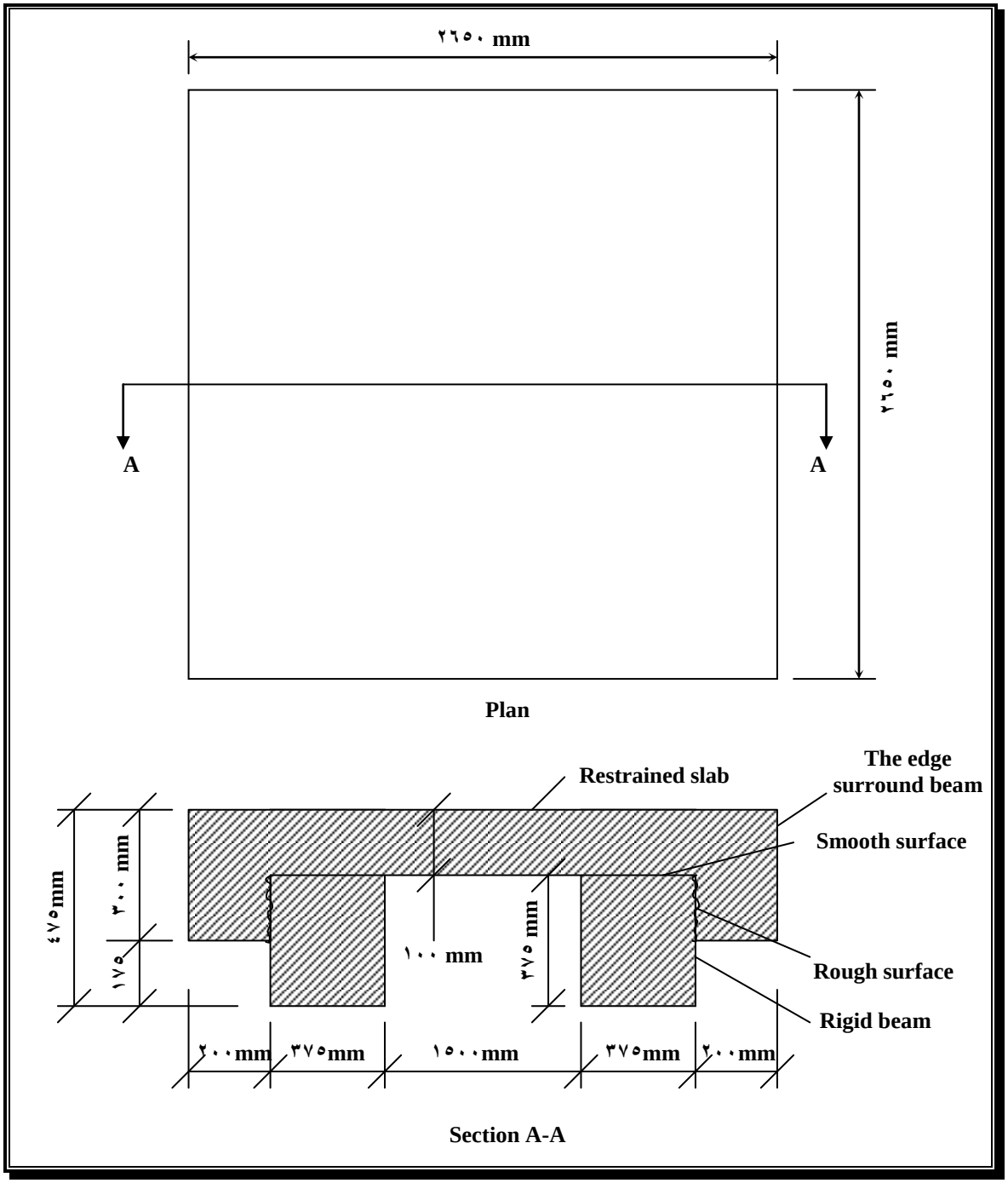

Figure (٣- ٢): Schematic diagram of the slab restraint.

٣.٣.٢ Slabs

Four slab models were cast on the above mentioned square rigid beams. These slabs were cast with different restrained cases (two end, three end and four end restrained), and another slab was cast without any restraint (free slab).

The chosen dimensions for the slabs were (٢٢٥٠*٢٢٥٠*١٠٠mm) (length * width * thickness) respectively. The edge beams which attain the action of restraint are of cross-section ٣٠٠*٢٠٠ mm and c/c span of ٢٤٥٠ mm. Plate (٣-٢) shows these slabs.

The mix proportions were (٥٤٥:٦٣٥:١١٩٥) kg/m^{٣} (cement: sand: gravel) respectively with an effective w/c ratio of ٠.٤٨ and a slump of ١٨٠ mm.

The ٧ and ٢٨ days compressive strength of this mix were ٢٣.٨ and ٣٢.٥ MPa respectively, whereas the ٧ and ٢٨ days flexural strength were ٤.٠٥ and ٦.٠ MPa respectively.

The reinforcement used is of deformed steel bars grade ٤٢٥ MPa with ١٠ mm-diameter for longitudinal bars (main reinforcement), and the steel ratio adopted in this work is (٠.٤٢٪) which is the minimum ratio allowed for shrinkage according to ACI Code ٣١٨ [٦٧].

In order to get a constant cover, small pieces of steel as chairs of ٢.٥ cm height were placed under the slab reinforcement and also under the beams reinforcement. Figure (٣-٣) shows the details of reinforcement for slabs and edge beams.

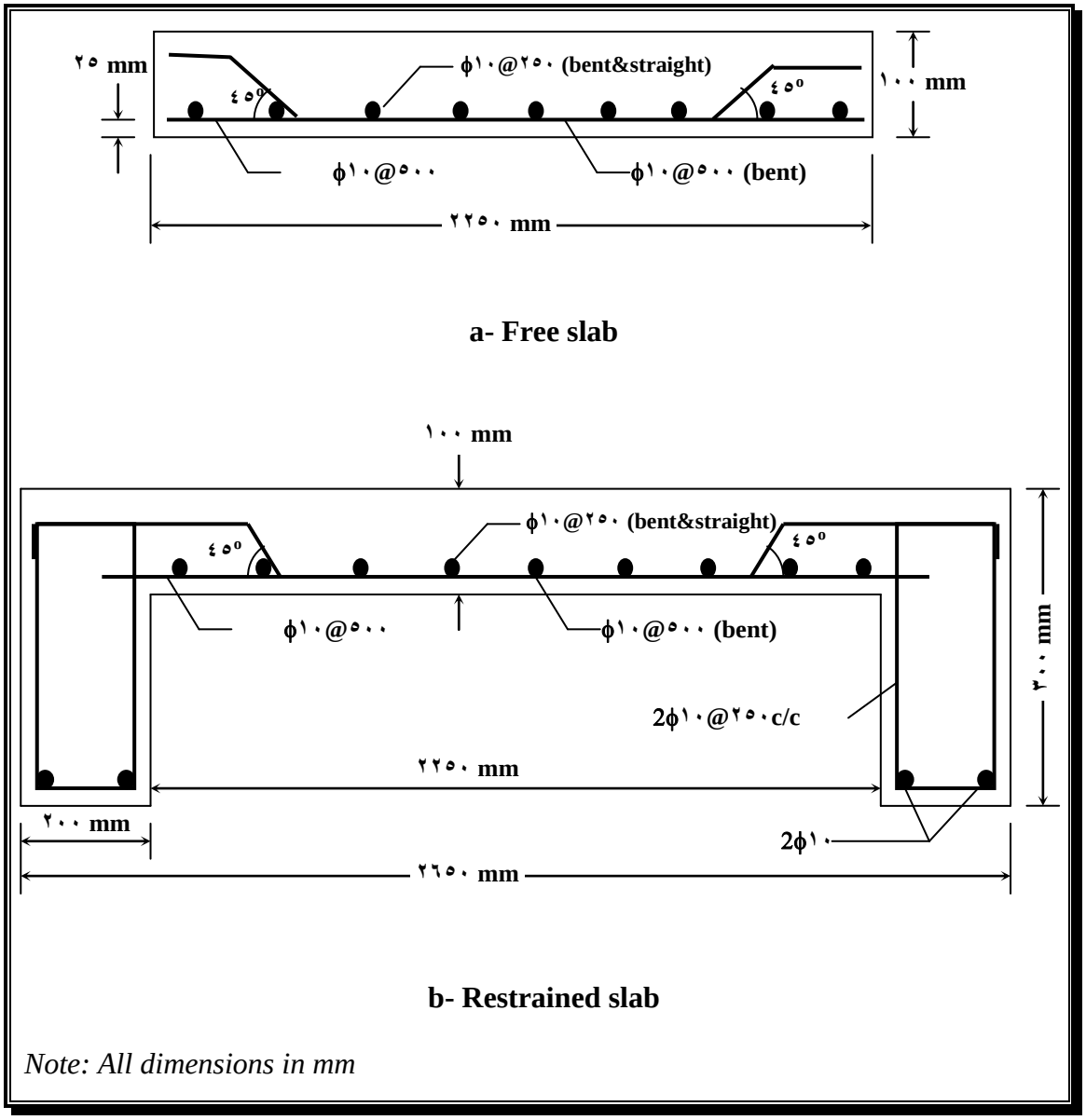

Fig.(٣-٣) *Details of the slabs* ***a-*** *without edge beams ,* ***b-****with edge beams*

٣.٣.٣ Materials and Mixes

٣-٣-٣-١ Cement

Ordinary Portland cement manufactured by the new cement plant of Kufa was used for concrete mixes throughout the present work. The cement was properly stored in the laboratory. This cement complied with the Iraqi specification No.٥/١٩٨٤ [٦٨]. The physical properties and chemical composition of the cement are given in Tables (A-١) and (A-٢).

٣-٣-٣-٢ Fine Aggregate

Al-Akhaidhur well-graded natural sand was used. The physical and chemical properties of the sand are listed in Table (A-٣). Its grading conformed to the Iraqi specification No.٤٥/١٩٨٤ [٦٩], Zone(٣).

٣-٣-٣-٣ Coarse Aggregate

The gravel used was brought from Al-Nibaii area with a maximum size of ١٩ mm. The gravel was washed, then stored in air to dry. The gravel used conforms to the Iraqi specification No.٤٥/١٩٨٤. The grading and other properties of this type of aggregate were tested and shown in Table (A-٤).

٣-٣-٣-٤ Water

Tap water was used throughout this work for both mixing and curing of concrete.

٣-٣-٣-٥ Reinforcement

Deformed steel bars of ١٠ mm diameter were used. The average yield strength of three samples is ٤٢٥ MPa. The stress-strain curve for the reinforcing steel used is shown in Figure (٣-٤).

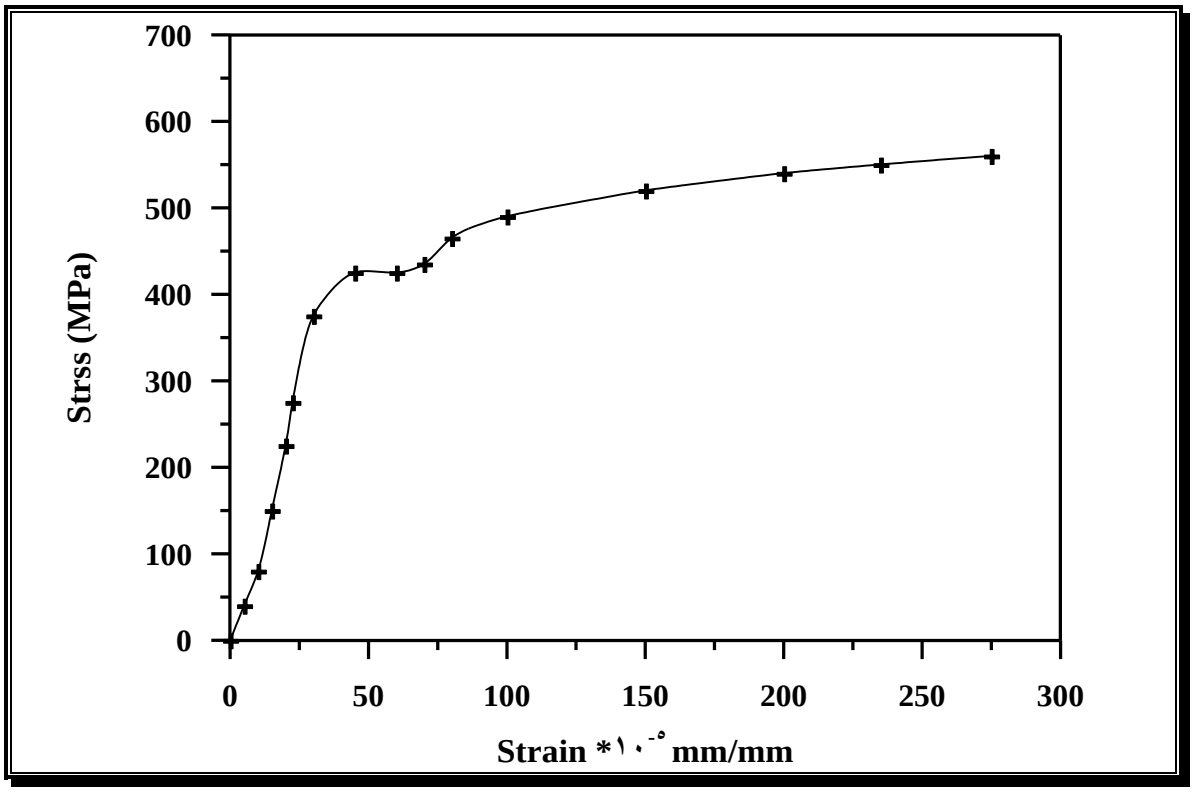

Figure (٣.٤): Stress strain curve for ١٠mm diameter mild bar used.

٣-٣-٣-٦ Mix Design and Proportions

The concrete mix was designed according to British mix design method BS ٥٣٢٨: Part ٢: ١٩٩١ [٦٦]. This mix was design to give the target design strength of ٤٠ MPa and a slump of (٦٠ mm).

The proportions of the concrete mix are summarized in Table (٣-١).

Table (٣- ١): *Mix Proportions*

		Weight proportion	Mix proportion kg/m^3			
Slump mm	**W/c ratio**	**Cement : Sand : Gravel**	**Water**	**Cement**	**Sand**	**Gravel**
٦٠	٠.٤٥	١.٠ : ١.٢ : ٢.٧	١٩٥	٤٣٥	٥٢٥	١٢١٥

٣-٣-٤ Testing Fresh and Hardened Concrete

٣-٣-٤-١ Slump Test

The workability of the fresh concrete mixes was measured by the slump test before casting these mixes in their molds. This test was conducted according to ASTM C١٤٣-٨٩a [٧٠].

٣-٣-٤-٢ Compressive Strength Test

For the hardened concrete, the compressive strength test was carried out according to BS. ١٨٨١: part ١١٦:١٩٨٣ [٧١], using a digital testing machine of ٢٠٠٠ kN maximum capacity. Three cubes (١٥٠ mm) were tested for each mix at each age for the determination of compressive strength. The cubes as tested were at right angles to the position as cast. The load was applied approximately at a constant rate and failure load is recorded to the nearest ١ kN.

٣-٣-٤-٣ Flexural Strength Test

Three points flexure tests were performed on three (١٠٠x١٠٠x٤٠٠ mm) prisms with a span of ٣٠٠ mm using the machine meeting the requirement of ASTM C٢٩٣-٧٩:١٩٨٩ [٧٢].

٣-٣-٥ Casting Procedure of the Slabs

٣-٣-٥-١ Mixing and Casting of Slabs

The concrete was mixed using an electrical drum type mixer with a maximum capacity of ٢٠٠ kg/batch. The interior surface of the mixer was cleaned and moisted before placing the materials.

Materials were put in the pan of the mixer, firstly coarse and fine aggregates were mixed together with small amount of mixing water. Cement and mixing water were added as mixing proceeded. By naked eye a homogeneous mix was observed. The total mixing time from the time of adding water was about ٥ min.

Then the concrete mixes were caste into the plywood formwork of the slab as can be seen in Plate (٣-٣). The concrete mixes were cast in two layers, compaction was achieved using a portable electrical vibrator, then traweled to maintain an even surface.

٣-٣-٥-٢ Curing and Exposure

To prevent plastic shrinkage cracking due to rapid evaporation from the upper surface of the slab. Wetted hessian sheets and polythene sheets were used to cover the upper surface of the slabs after ٣٠-٤٠ minutes from the casting as can be seen in Plate (٣-٤).

The formwork was strike after ٧ days from casting and the slabs were covered with wetted hessian and polythene sheets during the ٧ days as can be seen in Plate (٣-٤). The hessain sheets were wetted two times a day during this period.

The same curing procedure was adopted to the beams. The casting and exposure of the slabs were carried out during the period from first of October to the first of December (٢ months period) before exposure to fire flame and from first of December to the first of February (٢ months period) after exposure to fire flame.

٣-٣-٦ Strain and Crack Width Measurements

Surface strain measurements were carried out by using stainless steel demec points inserted in ٣ rows on the slabs. The rows were at ٢٥, ٢٥٠ and ١١٢٥ mm distance from all the edges. The spacing between demec points in the same row was ٢٠٠ mm apart. The demec points were positioned in the prisms and slabs (٥-١٥) minutes after casting.

An extensometer, Whittemore type, with an accuracy of (٠.٠٠٢ mm/division) was used to measure strain in the panels of the slab (the panel is the distance between two consecutive demec points in the same row, panel length = ٢٠٠ mm). The measurement devices are shown in Plate [٣-٥].

The measurements were registered early in the morning (about ٨ AM) every ٢ days until occurrence of the first crack. Then, measurements were taken at an average of ١٠ days for a total period of about ٦٠ days, until no appreciable change in demec readings were obtained, and a stable cracking pattern had been formed.

Crack widths were measured at ١٧ locations from the edges; these locations were at ٠, ٢٥, ٥٠, ١٠٠, ١٥٠, ٢٠٠, ٢٥٠, ٣٠٠, ٣٥٠, ٤٠٠, ٥٠٠, ٦٠٠, ٧٠٠, ٨٠٠, ٩٠٠, ١٠٠٠ and ١١٢٥ mm distance from the edge. The measurements were carried out before and after exposure to fire flame by using a portable microscope with ٤٠X magnification and a measuring field of ٢.٥ mm. A crack as can be seen under the portable microscope is shown in Plate (٣-٦). The crack pattern in the two and three end restrained of the

reinforced concrete slabs before and after exposure to fire flame are shown in Plates (٣-٧ and ٣-٨) respectively.

٣-٣-٧ Free Volume Change of the Slabs

In order to obtain an idea about the free volume change of the slabs, reduced-scale slabs with dimensions of (١٠٠٠x١٠٠٠x١٠٠ mm) were cast, and were exposed to the same conditions of restrained slabs. There was no connection between the slab and the rigid beams. The friction, in the plane of contact between the slab and the rigid beams was minimized by applying two layers of greased polythene sheets, then this slab was approximately free to shrinkage and move. The movements were measured by demec points and an extensometer as described in sec.(٣-٣-٦). Plate (٣-٩) shows the free movement slabs.

The first day movement of the slab was obtained by the use of ٢.٢ meter ⌐¬shape steel mold as shown in Figure (٣-٥) and plate (٣.١٠), in which an artificial crack (gap) was made in the mid-span of the web by using a ١.٥ mm steel diaphram. The beam was subjected to exposure conditions similar to that of the slabs. The increase in gap width after one day would represent the first day shrinkage [٢٢], see Plate (٣-١١).

The first day thermal strain of the slab, due to loss of its heat of hydration to the surrounding atmosphere from its peak temperature to the temperature when the first strain reading of the slab was taken, was measured by embedded thermometer in the concrete slab to determine the temperature drop, then the thermal strain by adopting a coefficient of thermal expansion of $١٠x١٠^{-٦}/\ ^{o}C$ [٢٣] for concrete.

In order to measure subsequent free shrinkage movements after the first day, two demecs which were inserted at the sides of the gap after ٥-١٥ minutes from casting, see Plate (٣-١١).

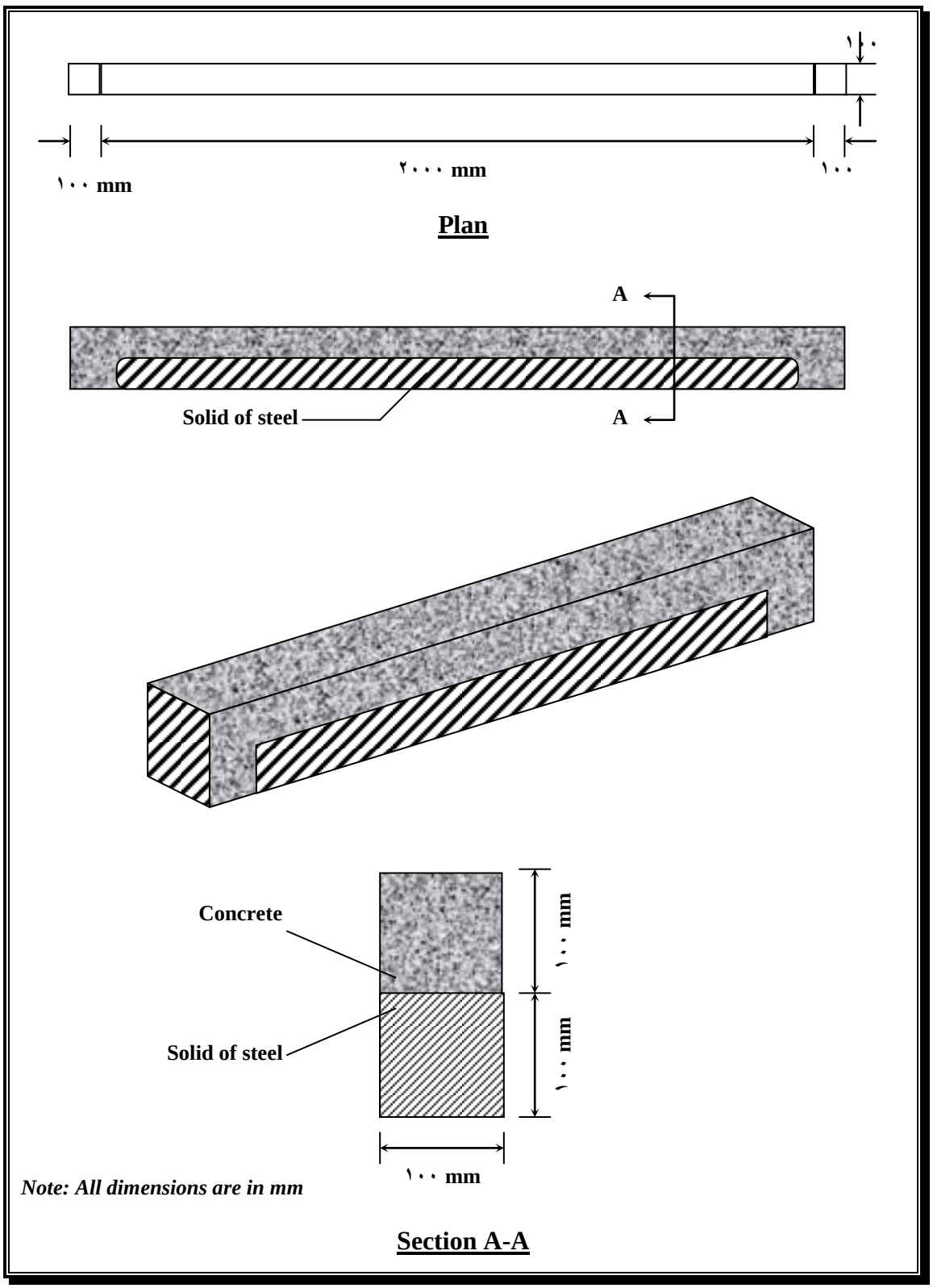

Fig.(٣-٥): *Schematic diagram of the ⌐¬ -shaped mold dimensions.*

٣-٣-٨ Tensile Strain Capacity Tests

The elastic strain capacity is the amount of strain that is instantly relieved due to the elastic recovery of restrained concrete upon cracking. It

is defined as the observed free contraction of concrete at the onset of cracking [٢٢].

Elastic tensile strain capacity of concrete was measured by using two methods:

i- The first is a direct method using the same ⌐¬-shaped steel mold described in article (٣-٢-٧). Plain beams were cast and allowed to shrink. Soon after the first crack occurred, the amount of strain which was relieved as a result of elastic recovery of restrained concrete, was measured between plug fixed points together with crack width measurement by a microscope. This crack opening was assumed to represent elastic tensile strain capacity of concrete.

ii- The second is an indirect method by dividing the flexural strength of concrete by the modulus of elasticity of concrete. According to ACI-Committee ٢٢٤ [١٠]. This method produces significantly inaccurate values of tensile strain capacity due to the non-linearity of stress distribution across the beam, which causes the modulus of rupture to be ٢٠-٤٠ percent higher than the true tensile strength of concrete.

٣-٣-٩ Burning and Cooling

The reinforced concrete slabs were burnt with direct fire flame from a net work of methane burners inside the frame. The fire flame hits the lower face of these slabs. The dimensions of this burner net are (١٥٠٠*١٥٠٠mm) (length * width respectively) as shown in Plate (٣-١٢). The bars of flame were intended to simulate the heating condition in an actual fire.

When the target was reached, the temperature was continuously measured by digital thermometers, one of them was positioned in the bottom surface of the slab in contact with the flame, while the other was

positioned at the unexposed upper surface of the slab, and by thermocouple that was inserted in the center of each slab to measure the temperature at the mid-depth (٥٠ mm from the exposed or unexposed surface). The measurement devices are shown in Plate (٣-١٣). After burning, the reinforced concrete slabs were allowed to cool in the laboratory to a room temperature of about ٢٣^{o}C.

٣-٣-١٠ Duration and Range of Temperatures

The duration of fire depends on the speed with which it can be put out. Total fire duration, including the time of the build-up of the fire, can vary from about one hour to about one day [٧٣,٧٤].

However, for this work, it was decided that exposure time of ١.٥ hour at the level of the maximum temperature would cover the range of situations occurring in the majority of elevated temperatures during fires [٣٦,٧٥,٧٦].

Although the maximum temperatures reached during fires of buildings are of the order of ١٠٠٠ to ١٢٠٠ ^{o}C [٣٦,٧٧] such high temperatures occur only at the surface of the exposed members. Considering the relatively small size modeling of the specimens to be tested, it was decided to limit the maximum fire flame exposure temperature to ٦٠٠ ^{o}C.

٣-٣-١١ Shrinkage of Reinforcement Concrete Slabs After Exposure to Fire Flame

Shrinkage of slabs was monitored during and after exposure to fire flame and cooling in the laboratory to room temperature was about ٢٣^{o}C. Shrinkage was measured after the slabs were cooled to room temperature, at ages of (١, ٣, ٧, ١٥, ٣٠, ٤٥ and ٦٠ days) after burning. Shrinkage strain of these slabs was measured during fire, the procedure of the measurement as shown in Plate (٣-١٤).

٣-٣-١٢ Deflection of Reinforced Concrete Slabs During and After Exposure to Fire Flame

When the slabs were subjected to fire flame, the cracks which were developed from previous drying shrinkage propagated and widened. The thermal cracks appeared in a honeycomb fashion all over the lower surface of these slabs. The deflection of the slabs was due to fire only and without applying any superimposed load. The deflections were recorded by a dial gauge with an accuracy of (٠.٠١mm/division) positioned at the center of these slabs. The deflection recording was at times (٥, ١٥, ٣٠, ٤٥, ٦٠, ٧٥ and ٩٠ minutes) during exposure to fire flame. Plate (٣-١٤) shows the procedure of deflection measurements mentioned above. Also, deflection after burning of these slabs was measured using the same procedure conducted during burning.

٣.٤ Site Observations

In addition to the four reduced-scale experimental slabs investigated, measurements were made on actual size slabs in a newly constructed building in Hilla city. The measurements covered; length, width and thickness of the slabs, amount and distribution of reinforcement, crack spacing, crack length and crack width for each crack at intervals of ٢٥٠ mm from the edge of the slab. Some of these parameters were measured directly on the slabs by a portable measuring tape and a microscope. Whereas, the amount and distribution of reinforcement and thickness of the slab were taken from their design engineering drawings. The procedure of cracking measurements as shown in Plate (٣-١٥).

CHAPTER FOUR

FINITE ELEMENT ANALYSIS

٤.١ Introduction

In this chapter, a brief review of some previous studies on the application of the finite element method to reinforced concrete structures will be presented. A review of the mathematical models for predicting long-term effects on concrete, such as creep and shrinkage, are described. In addition, a brief description of the convergence criteria used in the computer program is also described in this chapter.

A computer program was taken from reference [٧٨], and had been modified to represent the problem of shrinkage cracking in different restrained cases for reinforced concrete slabs. This program was written in Q-Basic Language.

In this chapter, the relationships and solution algorithm which were used in the steps of program are discussed.

٤.٢ Finite Element Modeling of Reinforced Concrete Structures

During recent years and because of the development of relatively powerful analysis techniques implemented in electronic digital computers, interest in nonlinear analysis of concrete as a structural material was greatly increased. The most important analysis procedure that is already in wide

use for both linear and nonlinear analysis of structures is the finite element method.

The first published paper in finite element analysis of reinforced concrete structures to include the effect of cracking was by *Ngo* and *Scordelis* [٧٩], ١٩٦٧, who carried out a linear elastic analysis of beams with predefined crack patterns. The purpose of the study was to determine bond stresses and stresses in the concrete and steel for a particular crack configuration. By the separation of nodal points, the cracks were modeled.

Non-linearity was first introduced by *Nilson* [٨٠], ١٩٦٨, by treating the concrete material as an orthotropic material. Discrete cracking was introduced by stopping the solution when the average value of the principal tensile stress in two adjacent elements exceeded the tensile strength, then changing the topology of the structure by disconnecting the elements at their common corners.

Scanlon[٨١] in ١٩٧٤ presented a finite element model which is capable of simulating the behavior of reinforced concrete slabs at working loads, including the effect of nonuniform reinforcing and tensile cracking. This study concentrates on technique for including the effect of creep and shrinkage.

Meyer and *Bathe* [٨٢], ١٩٨٢, studied the nonlinear analysis of reinforced concrete structures as one, two and three-dimensional elements, and the applicability of using nonlinear static and dynamic analysis in engineering practice.

In ١٩٩٠, [٨٣], *Hu* and *Schnobrich* developed a nonlinear model for cracked reinforced concrete subjected to inplane shear and normal stresses. In this model, a set of constitutive equations suitable for incremental F.E. analysis was derived.

٤.٣ Finite Element Method and Time Dependent Effects

The work of *Selona* (١٩٦٩) [٨٤] was to develop a mathematical model which predicted the time-dependent behavior of planar reinforced concrete frame structures subjected to service loads. The material behavior laws were developed for uniaxial creep, shrinkage and tensile cracking in the concrete and for instantaneous elastic-plastic strains in the reinforcing steel.

A finite element model which was capable of simulating the behavior of reinforced concrete slabs at working loads, including the effects of non-uniform reinforcing, tensile cracking, shrinkage and creep, was studied by *Scanlon* (١٩٧٤) [٨١]. The inelastic strains resulting from creep and shrinkage behavior were treated by the initial strain method [٨٥]. The CEB expressions based on available experimental data were used for the evaluation of creep and shrinkage strains.

Aldsted and *Bergan* (١٩٧٨) [٨٦] presented finite element models that were capable of predicting the long-term behavior of plane, slender reinforced concrete frames and which were subjected to loads up to their ultimate carrying capacities. Two models were adopted (distributed and discrete cracking).

Kang and Scordelis (١٩٨٠) [٨٧] developed a numerical procedure based on the finite element method for the material and geometric nonlinear analysis of planar reinforced and prestressed concrete frames including the time-dependent effects due to load history, temperature history, creep, shrinkage and aging of concrete and relaxation of prestress.

Chow (١٩٨٤) [٨٨] also developed a finite element analysis for the effects of creep and shrinkage in reinforced concrete beams. The ACI method was used to model the time dependent effects in the concrete.

It can be stated the present study is one of the first attempts which tries to analyze the problem of time dependent shrinkage cracks for different restrained cases of reinforced concrete slabs by using the finite element method.

٤.٤ Shrinkage Expressions

Three expressions to compute shrinkage strain can be estimated:

١- *Schorer* Expression

For the reason of the importance of ambient humidity on shrinkage, *Schorer's* equation has been used since (١٩٤٣) [٨٩]; which is:

$$(\varepsilon_{sh})_u = 12.5\times10^{-6}(90 - H_u) \qquad \text{.....(٤-١)}$$

where H is the ambient humidity.

٢- *Hyperbolic* Expression

One of the most widely used methods for modeling shrinkage versus time is the hyperbolic equation in the same form of Ross creep equation, which is;

$$\varepsilon_{sh(t)} = \frac{t}{35+t}(\varepsilon_{sh})_u \quad \text{for moist cured concrete} \qquad \text{.....(٤-٢)}$$

$$\varepsilon_{sh(t)} = \frac{t}{55+t}(\varepsilon_{sh})_u \quad \text{for steam cured concrete} \qquad \text{.....(٤-٣)}$$

٣- *Exponential* Expression

An exponential form of equation is proposed by *Lyse*, *Wallo* and *Kesler* (١٩٦٨):

$$(\varepsilon_{sh})_t = (\varepsilon_{sh})_u\left(1 - e^{-0.1t\frac{0.65}{V/S}}\right) \qquad \text{.....(٤-٤)}$$

where *V/S* is the volume-surface ratio in inches.

٤.٥ General Mathematical Modeling of Shrinkage

For the prediction of constitutive properties of shrinkage, a mathematical modeling needs to be used as the input for the finite element computer program [٩٠]. The selection of functions should satisfy the following points:

١- The function represents the available experimental data of concrete, such as age, environmental humidity and its variation, temperature and its variation, size and shape of cross section, curing conditions and their duration.

٢- The undetermined coefficients of the functions should be relatively easy to evaluate from the available experimental data.

٣- The function should be sufficiently simple to conduct the numerical evaluation in the finite element program.

Several practical models for predicting shrinkage at any time were proposed:

١- The model of ACI Committee ٢٠٩ [٧]

The ACI procedure for the evaluation of drying shrinkage strain at any time is based on the studies of *Branson et al.* [١٩٧٥]:

$$\varepsilon_h(t) = \frac{(t - t_o)}{35 + (t - t_o)} \times \varepsilon_{sh}\, u \qquad \text{.....(٤-٥)}$$

where t is the time in days since the concrete casting, t_o is the curing time and $(\varepsilon_{sh}\, u)$ is the ultimate shrinkage strain. Its average value is given by the following relation:

$$\varepsilon_{sh}\, u = 800 \times 10^{-6} \times CF^{s} \qquad \text{.....(٤-٦)}$$

Where CF^s is the shrinkage correction factor given as:

$$CF^{s} = F_H^s \times F_T^s \times F_S^s \times F_B^s \times F_F^s \times F_A^s \qquad \text{.....(٤-٧)}$$

where F_H^s, F_T^s, F_S^s, F_B^s, F_F^s *and* F_A^s are the shrinkage correction factors for humidity, minimum member thickness, slump, cement content, percent fines and air content respectively. All these factors assume the value of unity for the following standard conditions [٧]. For conditions other than the standard ones, the correction factors are calculate in Appendix (B-١).

٢- Euo-international committee of concrete model

The procedure recommended by CEB for drying shrinkage prediction is based on the following:

$$(\varepsilon_{sh})t = \alpha(\varepsilon_{sh} -) \times B_s(t_1) \quad \text{.....(٤-٨)}$$

in which $\alpha = \alpha_{ss} \times \alpha_{rh} \times \alpha_{sf}$ .....(٤-٩)

$\alpha_{ss}, \alpha_{rh}, \alpha_{sf}$ = factors to account for the size, relative humidity, and slump respectively.

$\varepsilon_{sh} -$ = Shrinkage strain at (t) = ∞.

Bs($t_١$) = factor to account for the rate at which shrinkage develops.

$t_١ = t - t_o$ [٩١]

The ACI model is adopted in the present study.

٤.٦ Mathematical Formulation of Creep

In the absence of experimental data, the following empirical expression for the prediction of creep deformation is recommended by ACI Committee [٧], which is:

$$C_t = \frac{(t-T)^{0..6}}{10+(t-T)^{0.6}} \times C_u \quad \text{.....(٤-١٠)}$$

where C_t is the creep coefficient defined as the ratio of creep strain at t days after loading to the initial instantaneous strain at loading. T is the age in days of concrete at load application. C_u is the ultimate creep coefficient to be determined from experimental data defined as creep strain at in finite time after loading to the initial strain at time of loading. The ultimate creep coefficient is calculated as follows;

$$C_u = 2.35 \times F_\tau^c \times F_H^c \times F_T^c \times F_S^c \times F_F^c \times F_A^c \qquad .....(٤-١١)$$

where F_τ^c, F_H^c, F_T^c, F_S^c, F_F^c *and* F_A^c are correction factors for age at loading, humidity, minimum member thickness, slump, percent fines and air content. All the above correction factors assume the value of unity for the standard conditions. The correction factors are calculated in Appendix (B-٢).

Creep deformation may be obtained by the superposition method which was stated by *D. Macttenry* as follows: [٩٢]

"The strains produced in concrete at any time (t_n) by a stress increment applied at any time, t_i, are independent of the effects of any stress applied either earlier or later than t_i". The principle of superposition is reasonably valid for stresses below approximately $0.4\, f_{c}'$, and for constant environment conditions.

Based on the above principle, for initial loading σ_o, applied at time t_o, the total deformation ε_t at time t_n is

$$\varepsilon_{tc} = \varepsilon_o + \varepsilon_o . C_{ut} \qquad .....(٤-١٢)$$

where $\varepsilon_o = \dfrac{\sigma_o}{E_o}$, E_o is the elastic modulus of concrete at time t_o and, C_{ut}, is the creep coefficient for a time interval (t_n-t_o), for any stress increment ($\Delta\sigma_i$) applied at time (t_i) the strain increment in the time interval (t_n-t_i) is $\Delta\varepsilon_i = \dfrac{\Delta\sigma_i}{E_i}$ and the total deformation is

$$\Delta\varepsilon_t = \Delta\varepsilon_i + \Delta\varepsilon_i \times C_{ut} \qquad \text{.....(٤-١٣)}$$

where, E_i is the elastic modulus at time (t_i), C_{ut} is the creep coefficient of concrete loaded at time (t_i) for an interval (t_n-t_i). The total deformation (ε_{nc}) at time (t_n) after number of stress changes is:

$$\varepsilon_{nt} = \frac{\sigma_o}{E_o} + \frac{\sigma_o}{E_o}.C_{uo}^n + \sum_{i=1}^{n}\left[\frac{\Delta\sigma_i}{E_i} + \left(\frac{\Delta\sigma_i}{E_i}\right).C_{ut}^n\right] \qquad \text{.....(٤-١٤)}$$

In simple cases such as shown in Fig.(٤-١), the stress history may be represented as a series of step. Knowing variation of (E) and (C_u) with time of initiation and duration of loading, the components of strain can be determined and the resultant strain can be obtained by superposition.

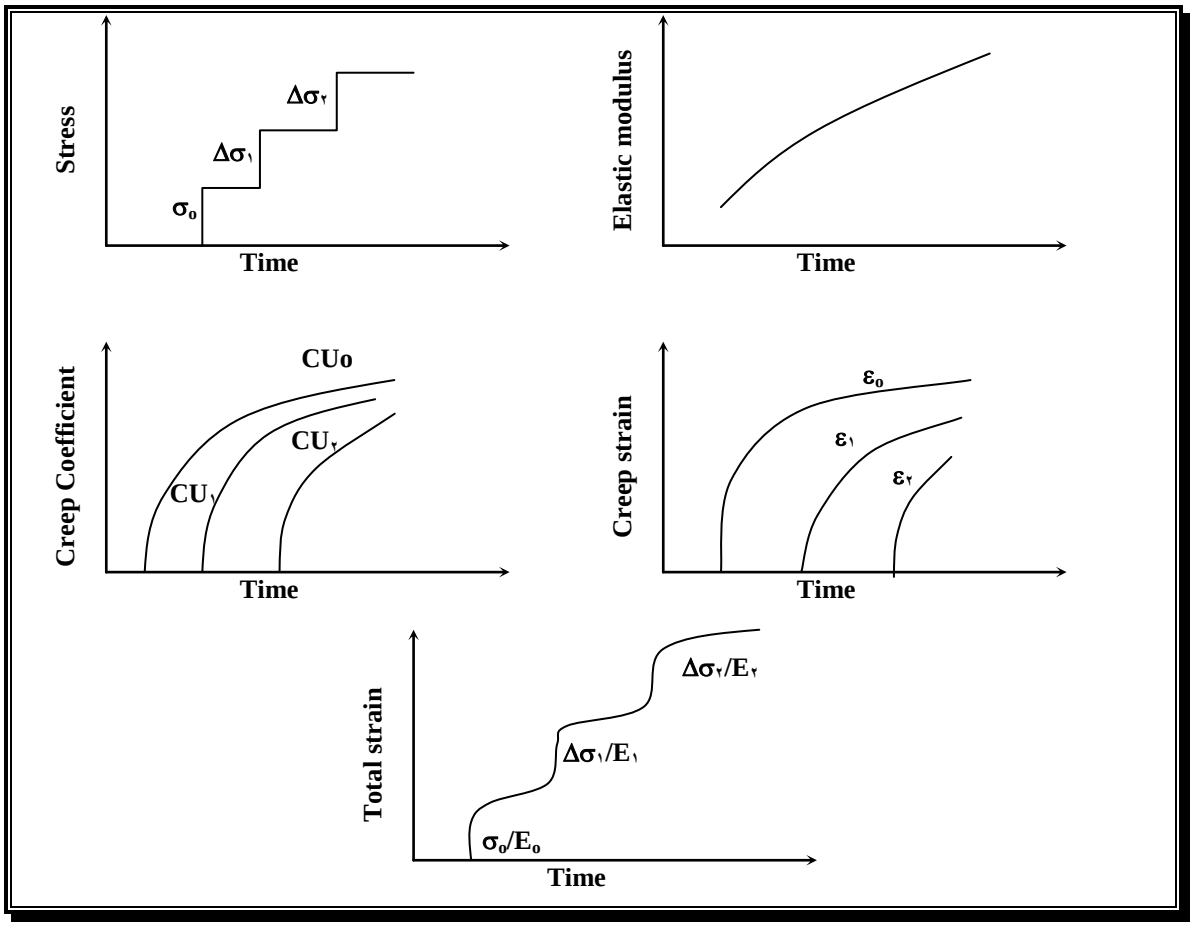

Figure [٤. ١] Determination of creep strain by superposition method. **[٩٢].**

However, using Eq.(٤-١٠) with the superposition formulation requires the storage of the complete creep history in order to calculate a new creep value which requires a lot of computational effort and memory storage.

٤.٧ Modeling of Concrete

Concrete is a heterogeneous nonlinear material and has completely different properties in tension as compared to compression. It is well known that the nonlinear response of concrete is caused by two major material properties, cracking in tension and plasticity in compression due to bond failure between aggregate and mortar and cracking of mortar itself. Time dependent effects such as creep, shrinkage and temperature volume change also contribute to the nonlinear response. These time dependent effects are considered in this research. There are several approaches for defining stress-strain relationship of concrete under various states. In general, they can be divided into four main groups:

a- Elasticity theory.
b- Plasticity theory.
c- Viscoplasticity theory.
d- Endochronic theory.

Excellent reviews and extensive references on modeling the concrete material are given in Reference [٧٨], [٧٩] and [٩٣].

٤.٨ Modeling of Steel Reinforcement

Steel is a homogenous material and usually has the same yield strength in both tension an compression. A typical stress-strain curve for steel is illustrated in Figure (٤-٢). Four regions can be distinct from this curve; initial linear elastic, yielding, strain hardening, and descending stage.

In the present investigation, the steel reinforcement is smeared into equivalent steel layers with uniaxial properties.

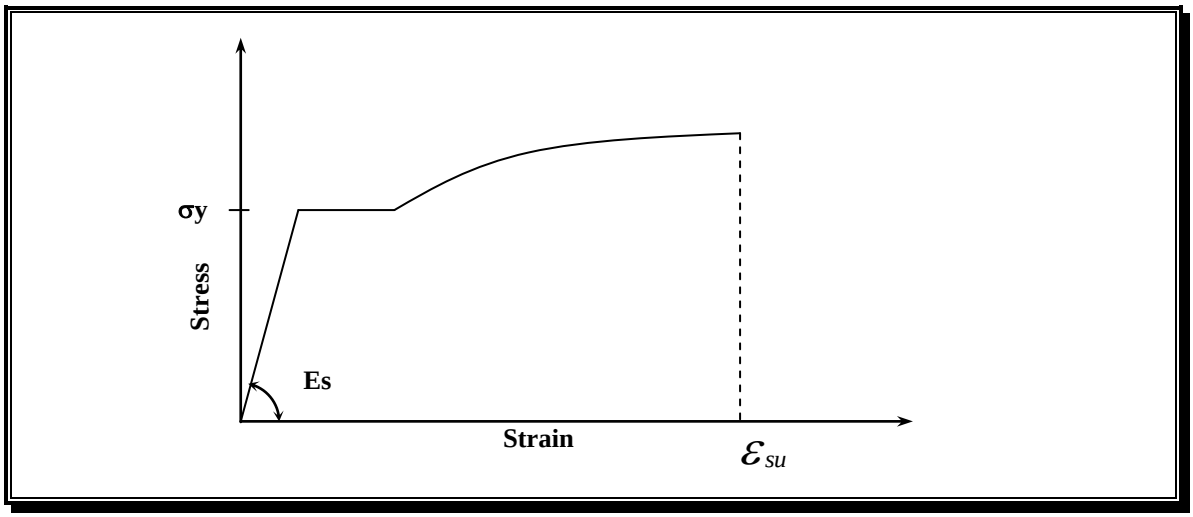

Figure (٤- ٢) Typical stress-strain curve for reinforcing steel.

٤.٩ Modeling of Cracked Concrete

Probably the main feature of plain concrete material behavior is its low tensile strength, which results in tensile cracking at a very low stress compared to the failure stress in compression.

In the finite element method, two main mathematical models are used for crack representations; discrete crack model and smeared crack model.

(a) <u>Discrete Crack Model</u>

This model represents the individual cracks as actual discontinuities in the finite element mesh. This model was firstly used by *Ngo* and *Scordelis* [٩٤] to analyze simply supported reinforced concrete beams. Cracking initiated when failure criterion at a certain node is achieved and crack discontinuity is represented by physically splitting that node. An obvious restriction of such a model is that the cracks must be formed along the element boundaries. This makes crack patterns mostly dependent on the local mesh refinement. Furthermore, when a crack forms the topology of

the mesh varies, and the updating procedures are time-consuming. These difficulties have resulted in a very limited acceptance of this model in general structural applications.

b- Smeared Crack Model

This model does not account for real discontinuities in the mesh. It was firstly introduced by *Reshid* (١٩٦٨) [٩٥]. Cracking concrete is assumed to remain a continuum and material properties are modified to account for the damage due to cracking. Concrete is initially isotropic, but cracking induces anisotropy. After cracking, concrete is assumed to become orthotropic, with the principal material axes oriented along the directions of cracking. Material properties are varied depending on the state of strain and stress. The Young's modulus is reduced in the direction perpendicular to the crack plane, and Poisson's effect is usually neglected due to the lack of continuity of the material. The shear modulus parallel to the crack plane is also reduced. *Lin* and *Scordelis* (١٩٧٥) [٩٦] introduced the retained shear modulus βG_o term, where G_o is the shear modulus of uncracked concrete and β is a reducing factor in the range of zero to one.

The smeared crack approach is used for most structural engineering applications, since it offers:

i- Unchanging of topology of the mesh throughout the analysis, and only the stress-strain relationship need to be updated when cracking occurs.

ii- Complete generality in possible crack direction.

iii- Computational efficiency.

In the present study the smeared crack model has been adopted.

٤.١٠ Concrete Representation

For different restrained cases, reinforced concrete slabs can be represented by ٤-node rectangular elements using polynomial function for the assumed displacement field:

$$U = \alpha_1 + \alpha_2 x + \alpha_3 y + \alpha_4 x y \quad \text{.....(٤-١٥)}$$

$$V = \alpha_5 + \alpha_6 x + \alpha_7 y + \alpha_8 x y \quad \text{.....(٤-١٦)}$$

The derivation of the strain displacement and stiffness matrices of the element can be found else where [٩٧].

Prior to cracking, the concrete is assumed to be isotropic, homogenous, and linearly elastic, thus, the stress-strain relationship for plane stress problem can be expressed as follows:

$$\begin{Bmatrix} \sigma_x \\ \sigma_y \\ \tau_{xy} \end{Bmatrix} = \frac{E_c(t)}{1-\nu^2} \begin{bmatrix} 1 & \nu & 0 \\ \nu & 1 & 0 \\ 0 & 0 & \frac{1-\nu}{2} \end{bmatrix} \times \begin{Bmatrix} \varepsilon_x \\ \varepsilon_y \\ \gamma_{xy} \end{Bmatrix} \quad \text{.....(٤-١٧)}$$

where;

$E_c(t)$ = modulus of elasticity of concrete at time (t).
ν = Poisson's ratio of concrete.

The aim of this study is to describe the time dependent shrinkage effect on concrete, as, the properties of concrete are time dependent, the ACI-Committee ٢٠٩ [٧] proposes the following form of strength-time relationship of concrete:

$$f_c'(t) = \frac{t}{a + bt} f_c'(28) \quad \text{.....(٤-١٨)}$$

where $f'_c(t)$ and f'_c(٢٨) are the concrete compressive strength at any time t and at ٢٨ days after casting, respectively, and the constants a and b depend

on cement type and curing method. For (٧) days moist cured concrete, type I-cement, a=٤, b=٠.٨٥.

The ACI Committee ٢٠٩, also proposes the following equations to calculate the direct tensile strength $f'_c(t)$ and the modulus of elasticity $E_c(t)$:

$$f_t'(t) = 0.007\sqrt{w.f_c'(t)}\ \text{, MPa} \qquad .....(٤\text{-}١٩)$$

$$E_c(t) = 0.043\, w^{1.5}\sqrt{f_c'(t)}\ \text{, MPa} \qquad .....(٤\text{-}٢٠)$$

where w, is the concrete unit weight in kg/m^3 and $f'_c(t)$ is in MPa.

A crack is assumed to initiate in the planes perpendicular to the maximum principal tensile stress if the stress criteria controls or perpendicular to the maximum principal tensile strain direction if the strain criteria controls [٩٣].

Smeared crack representation treats concrete as an orthotropic material with principal axes normal and parallel to the crack direction as in Figure (٤-٣).

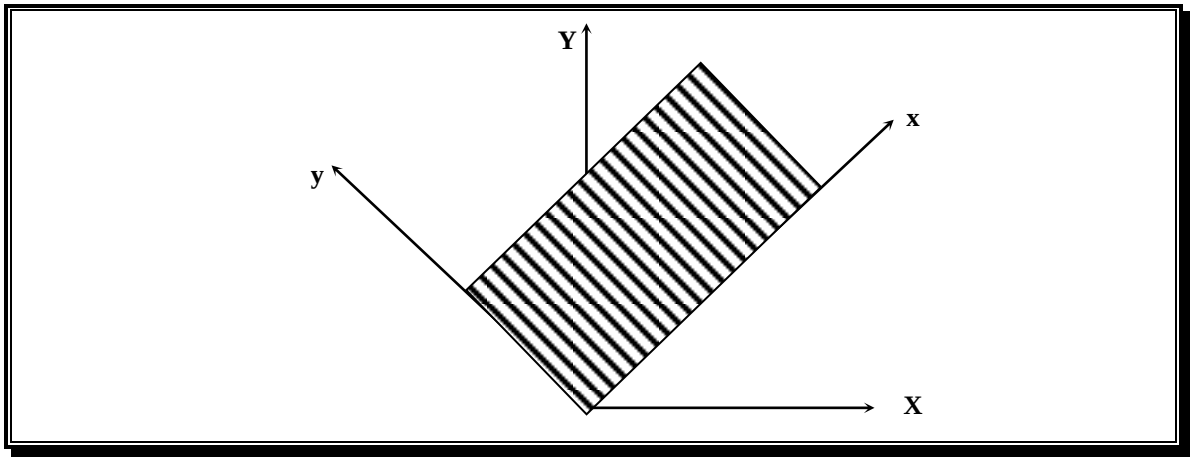

Figure (٤-٣) Crack coordinates. **[٨٣]**

The incremental stress-strain relationship associated with the crack coordinates [Eq.٤.١٧] becomes.

$$\begin{Bmatrix}\Delta\sigma_x\\ \Delta\sigma_y\\ \Delta\tau_{xy}\end{Bmatrix} = \begin{bmatrix}0 & 0 & 0\\ 0 & E_t & 0\\ 0 & 0 & \mu G\end{bmatrix} \times \begin{Bmatrix}\Delta\varepsilon_x\\ \Delta\varepsilon_y\\ \Delta\gamma_{xy}\end{Bmatrix} \qquad .....(٤\text{-}٢١)$$

In equation (٤-٢١) the modulus of elasticity of the concrete is reduced to zero in the direction normal to the crack. E_t is the tangent elastic modulus of concrete parallel to the crack direction. The Poisson's ratio is taken as zero due to the lack of interaction between the two orthogonal of directions. μ is the shear retention factor with $0 < \mu \leq 1$, $G = \frac{E_c}{2}$ is the shear modulus of cracked concrete.

At the instant of crack initiation only the stress perpendicular to the cracked plane and the shear stress parallel to the cracked direction are released; other stresses are assumed to remain unchanged. It follows that the stress state of the cracked material is reduced to the uniaxial stress state parallel to the cracked direction for plane stress problems [٩٣] as in Figure [٤-٤].

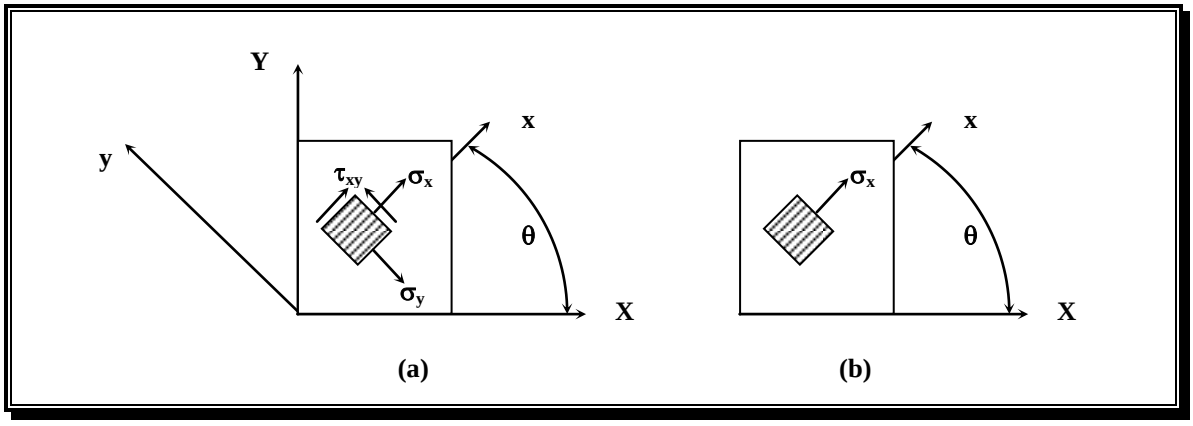

Figure (٤-٤) Stress distribution **(a)** just before crack and **(b)** just after a crack is formed. **[٩٣]**

The residual stress is computed as the difference between the stresses existing prior to cracking and the stresses which the material can sustain at the same strain level after cracking. A load vector equivalent to this residual stress is then computed for each cracked element according to:

$$\{P\} = \int_{vol.} [B]^T . \{\sigma\} . d\,vol. \qquad .....(٤-٢٢)$$

where $\{\sigma\}$ is the residual stress vector, [*B*] is the conventional nodal displacement strain matrix. Then, the application of the residual load vector to the structure causes stress redistribution due to cracking and results in additional deformation.

٤-١٠-١ Tension Stiffening

The use of the orthotropic constitutive Eq.(٤-٢١) to represent cracked concrete may not be realistic enough because the cracked concrete of the reinforced concrete element can still carry some tensile stress in the direction normal to the crack. This phenomenon is termed tension stiffening. In this study a general tension stiffening relationship suggested by *Bhide* [٨٣] is adopted. This relationship can be expressed as follows:

$$f_t = \frac{f_t'}{1 + 1000\,\varepsilon_t (\phi/90)^{1.5}} \qquad \text{.....(٤-٢٣)}$$

where;

f_t : the average tensile stress normal to the crack direction.

ε_t : the average tensile strain normal to the crack direction.

ϕ : measured in degrees counter clockwise from the steel direction to the crack direction.

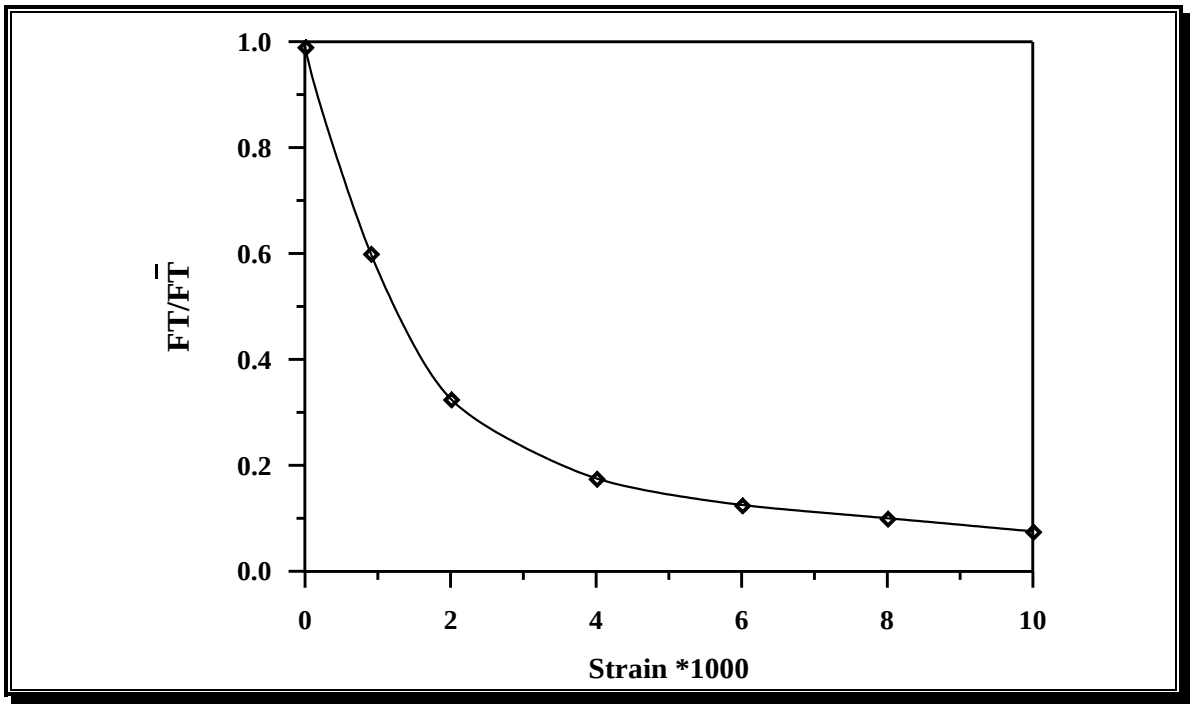

Figure (٤.٥): Tension stiffening curves by Bhide for Ø=٩٠٥. **[٨٣]**

٤-١٠-٢ Concrete Strength Parallel to the Crack Direction

After cracking has taken place, the concrete parallel to crack is still capable of resisting either tensile or compressive stresses. When it is subjected to tension, a pure linear elastic behavior is assumed as in Figure (٤-٦) and E_t is taken as $E_c(t)$ in Equation (٤-٢١). On the other side, when it is subjected to compression, experimental results show that the tensile cracks have caused a degrading effect not only on the compressive strength parallel to the crack but also on the compressive stiffness. This relationship is shown in Figure (٤-٧) and expressed by Eq.(٤-٢٤) below:

$$\frac{F_{cm}}{F_c'} = \frac{1}{0.8 + 0.34\frac{\varepsilon_t}{\varepsilon_o}} \le 1.0 \qquad \text{.....(٤-٢٤)}$$

It is used in this study to determine the degraded maximum compressive strength (f_{cm}), for concrete parallel to the crack direction, where, ε_o, is the strain corresponding to the maximum concrete compressive strength f'_c. After the peak strength (f_{cm}) is the determined the stress strain curve suggested by *Saenz* [٧٩] is used to calculate f_c.

$$f_c = \frac{E_c \times \varepsilon}{A + B\frac{\varepsilon}{\varepsilon_o} + C\left[\frac{\varepsilon}{\varepsilon_o}\right]^2 + D\left[\frac{\varepsilon}{\varepsilon_o}\right]^3} \qquad \text{.....(٤-٢٥)}$$

where A=١, B=(R+R_ε-٢): C=٢R-١: D=R .....(٤-٢٦)

$$R = \frac{R_E\left(R_\sigma - 1\right)}{\left(R_\varepsilon - 1\right)^2} - \frac{1}{R_\varepsilon} \quad : \quad R_E = \frac{E_c}{E_o} \qquad \text{.....(٤-٢٧)}$$

$$R\sigma = \frac{f_{cm}}{f_{cf}} \qquad \text{.....(٤-٢٨)}$$

$$R\varepsilon = \frac{\varepsilon_f}{\varepsilon_o} \qquad \text{.....(٤-٢٩)}$$

$$E_o = \frac{f_{cm}}{\varepsilon_o} \qquad \text{.....(٤-٣٠)}$$

In the present study it is assumed that $R\sigma = ٤$ and $R\varepsilon = ٤$, the tangent modulus (E_t) used in Eq.(٤-٢١) can then be calculated by differentiating Eq.(٤-٢٥) as follows:

$$E_t = \frac{d f_c}{d\varepsilon} = \frac{E_c\left[1+(2R-1)\left[\frac{\varepsilon}{\varepsilon_o}\right]^2 - 2R\left[\frac{\varepsilon}{\varepsilon_o}\right]^3\right]}{\left[1+(R+R_E-2)\left[\frac{\varepsilon}{\varepsilon_o}\right]-(2R-1)\left[\frac{\varepsilon}{\varepsilon_o}\right]^2+R\left[\frac{\varepsilon}{\varepsilon_o}\right]^3\right]^2} \quad .....(٤-٣١)$$

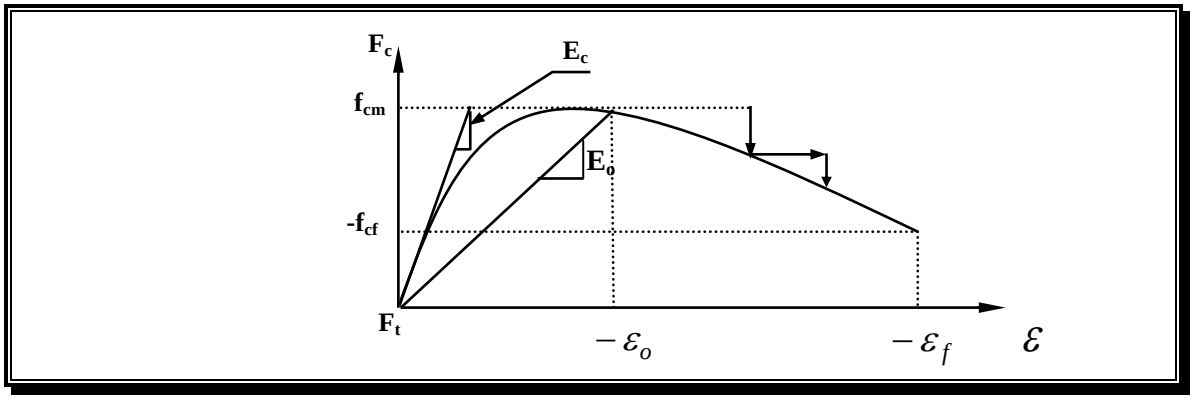

Figure (٤.٦): Stress – strain curve for concrete parallel to the crack direction. **[٨٣]**

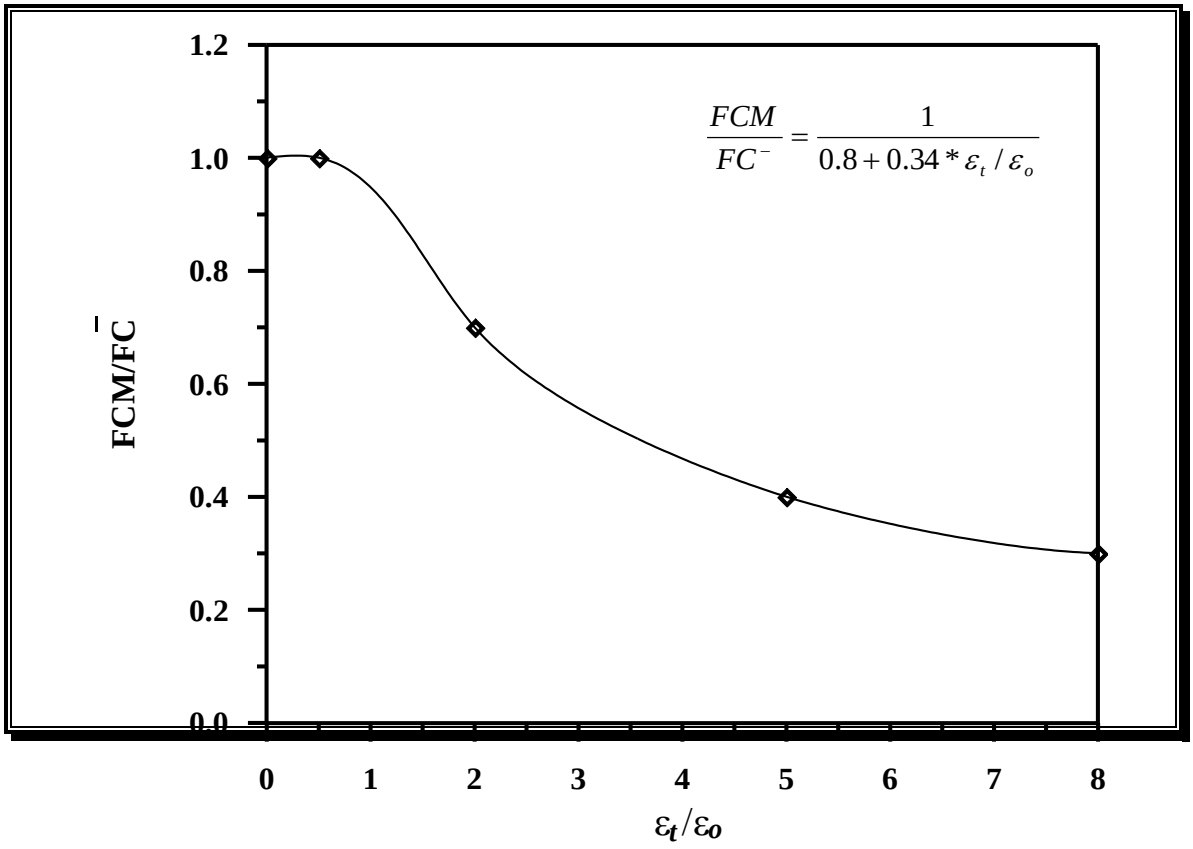

Figure (٤.٧): Degraded maximum compressive strength for concrete. **[٨٣]**

٤-١٠-٣ Shear Retention Factor

In plain concrete, the main shear transfer mechanism is the aggregate interlock and the main variables involved are the aggregate size and grading. In reinforced concrete dowel action will play a significant role, the main variables being the reinforcement ratio, the size of the bars and the angle between crack and bars, the shear transfer capacity being reduced as the width increases. A reduced shear modulus, μG, is retained with $(0 < \mu \leq 1)$ in the constitutive Eq.(٤-٢١) instead of dropping that capacity to zero. Using a reduced shear modulus not only improves the realism of the cracking representation during the finite element analysis but also removes most of numerical difficulties caused by the singularity of the composite material constitutive matrix.

Various forms of the shear retention factor have been proposed, however a constant value of μ = ٠.٢٥ is used in the present study.

٤.١١ Reinforcing Steel Representation

The material stiffness of the composite element is obtained by superposition of the material stiffness of the individual material components, concrete and reinforcement. An element of reinforced concrete subjected to plane stress is shown in Figure [٤-٨].

A stress-strain relation for the element can be written in the following form [٩٣].

$$\{\sigma_t\} = [D].\{\varepsilon_t\} \qquad .....(٤-٣٢)$$

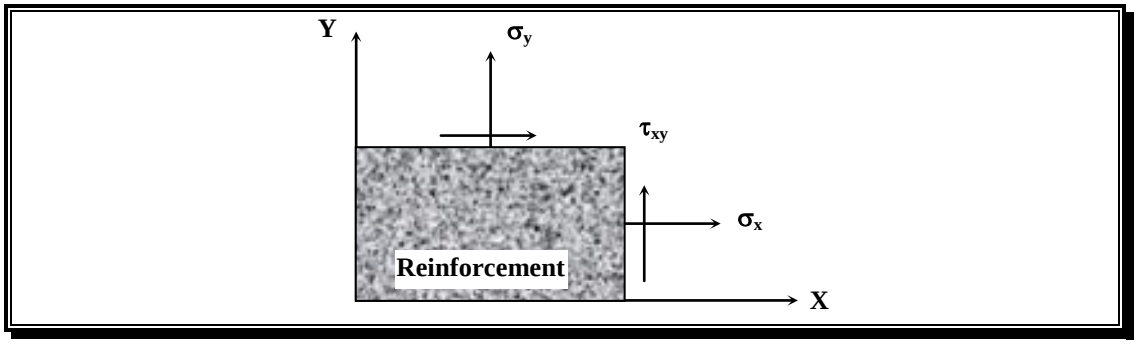

Figure (٤-٨) Total stress reinforced concrete element. **[٩٣]**

where the total stress vector $\{\sigma_t\}$ and the total strain vector $\{\varepsilon_t\}$ can be defined as follows:

$$\{\sigma_t\}=\begin{Bmatrix}\sigma_x\\ \sigma_y\\ \tau_{xy}\end{Bmatrix} \quad ; \quad \{\varepsilon_t\}=\begin{Bmatrix}\varepsilon_x\\ \varepsilon_y\\ \gamma_{xy}\end{Bmatrix}$$

[*D*] is the composite material stiffness matrix. The strains are similar for the two components steel and concrete, while the total stress vector is the sum of the component stress vectors,

$$\{\sigma_t\}=\{\sigma\}_c+\sum_{i=1}^{N}\{\sigma\}_i \qquad .....(٤\text{-}٣٣)$$

where $\{\sigma\}_c$ is the concrete stress vector and $\{\sigma\}_i$ is the reinforcement stress vector for the reinforcement in the $(i)_{th}$ direction.

Stress $\{\sigma_t\}$, $\{\sigma_c\}$, *and* $\{\sigma_i\}$ act on unit area of he composite cross section. It can be noted that the total stresses $\{\sigma_t\}$ don't represent real stresses but internal forces acting on a composite element. These stresses can be found from the strain as follows:

$$\{\sigma_c\}=[D]_c.\{\varepsilon_t\} \qquad .....(٤\text{-}٣٤)$$

$$\{\sigma_i\}=[D_i].\{\varepsilon_t\} \qquad .....(٤\text{-}٣٥)$$

in which $[D]_c$ and $[D_i]$ are the concrete and reinforcement material stiffness matrices respectively, by substituting Eqs.(٤-٣٤), (٤-٣٥) into Eq.(٤-٣٣), then comparing Eq.(٤-٣٢) with Eq.(٤-٣٣). The composite material stiffness matrices can be calculated as follows:

$$[D]=[D]_c+\sum_{i=1}^{N}D_i \qquad .....(٤\text{-}٣٦)$$

where, *N* is the number of reinforcing directions. The horizontal and vertical reinforcing steel is treated as an equivalent uniaxial layer material.

The stress-strain curve of reinforcing steel is modeled by an idealized bilinear curve identical in tension and compression. The incremental constitutive matrix for the (i)th steel layer [D_i] can be written as [٨٣]:

$$[D_i]=\begin{bmatrix} \rho E_s & 0 & 0 \\ 0 & 0 & 0 \\ 0 & 0 & 0 \end{bmatrix} \qquad .....(٤-٣٧)$$

where ρ and E_s are the steel ratio and the modulus of elasticity of reinforcement in the (i)th layer.

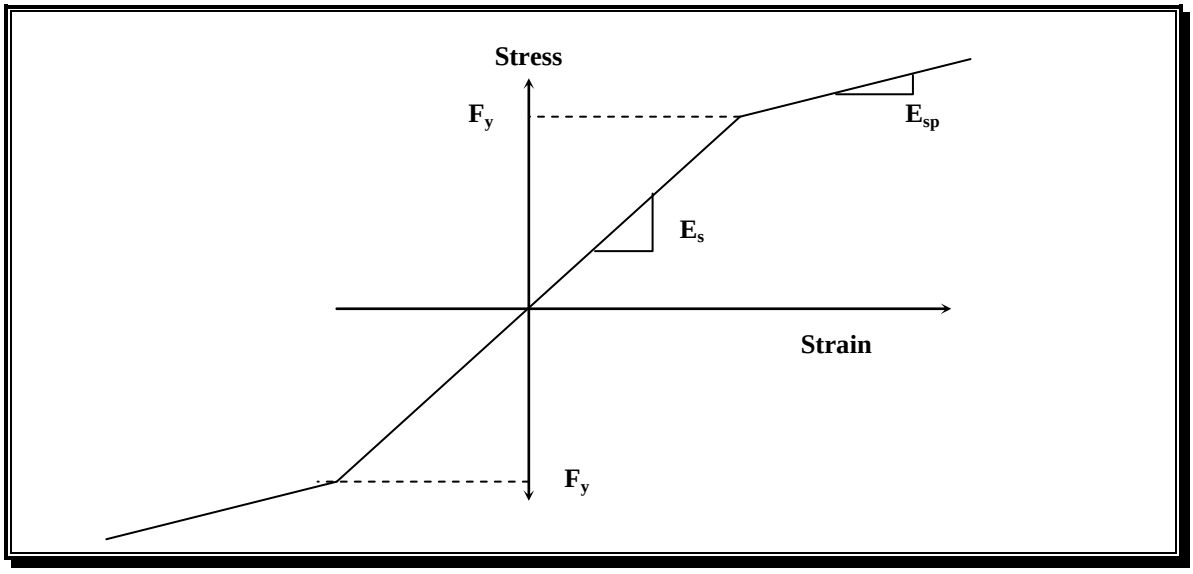

Figure (٤- ٩) Idealized stress-strain curve for steel.**[٨٣]**

٤.١٢ Non-linear Solution Procedures

The solution of linear elastic analysis for structural problems can be obtained directly from solving a set of algebraic equations in the following forms [٩٨]:

$$[K_G]\{d\}=\{F\} \qquad .....(٤-٣٨)$$

where;

$\{F\}$ is the nodal force vector,

$[K_G]$ is a function of material properties and structural displacements, and

$\{d\}$ is the unknown nodal displacement vector.

The solution of non-linear problems is usually attempted by either step by step method, constant stiffness method, or a combination of the two. In the latter procedure, the load is applied incrementally and with each increment successive iterations are performed to get more accurate results. Depending on the sequence of stiffness matrix computation combined method can be classified into two forms. Full Newton form is the first in which stiffness matrix is continually updated during each iteration. The second form is the modified Newton Raphson in which stiffness matrix is computed at beginning of each load step and remains constant during iterations until reaching convergence.

The most commonly used method in non-linear analysis of reinforced concrete structure is the modified Newton Raphson method, hence, it is adopted in this study.

٤.١٣ Convergence Criteria

A termination criterion for the iterative process should be used to stop iteration when a sufficient accuracy is achieved.

The convergence criterion for non-linear structural problems can usually be classified as:

A- Displacement convergence.

B- Forces convergence.

The convergence criterion used in the present study is based on the forces, and is called the forces convergence criterion. The violation of equilibrium is estimated by the magnitude of the residual unbalanced nodal forces, which are calculated during each iteration as follows:

$$\{\Delta f\} = \{F\} - \{I\} \qquad \text{.....(٤-٣٩)}$$

where $\{F\}$ is the applied load vector and $\{I\}$, is the internal force vector which depends on the nodal deformations $\{d\}$ [٨٦].

The convergence can be considered when

$$\frac{FNORM}{FNORMA} \leq force\ tolerance \quad [99] \qquad .....(٤-٤٠)$$

where

$$FNORM = \frac{\left[\sum_{i=1}^{NEQ}\left(\Delta f^{2}\right)\right]^{1/2}}{NEQ} \qquad .....(٤-٤١)$$

$$FNORMA = \frac{\left[\sum_{i=1}^{NEQ}\left(F\right)^{2}\right]^{1/2}}{NEQ} \qquad .....(٤-٤٢)$$

A tolerance force of (٢.٥٪) is taken throughout this study for the checking of solution convergence.

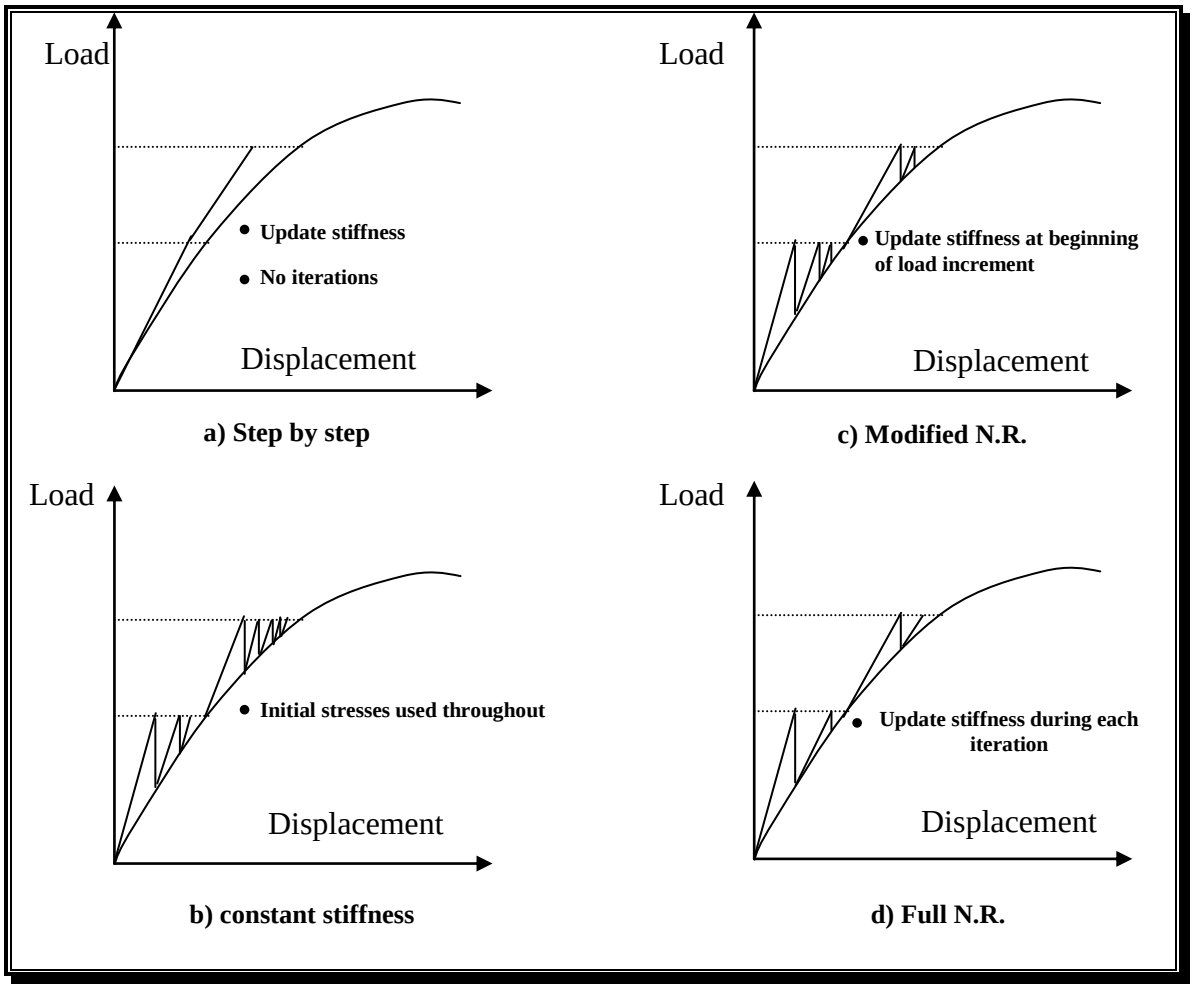

Figure (٤-١٠): Non linear solution.**[٩٨]**

٤.١٤ Computer Program

The steps of the computer program are

١- Input data

a- Control data such as number of element (*NEL*), number of node (*NON*), number of element in one row (*RE*), number of node in one row (*RN*) and in one column (*CON*), Length (*L*), and width (*w*) of the slab.

b- Reinforcement data such as giving number of layers, ratio, local coordinates, and modulus elasticity of steel.

c- Concrete properties such as compressive strength at (٢٨) days age, thickness of slab and Poisson's ratio.

d- Nodal number which gives the details of boundary condition.

٢- Automatic mesh generation

This step includes the estimation of node number and nodal connecting I_1, I_2, I_3, I_4 for each element.

٣- X and Y coordinates for each node are calculated automatically.

٤- Depending on the state of stress in each element and whether this element is close to be cracked, choose step of time (ΔTT) in days.

٥- Calculating concrete properties at a time equal to (TIC) which include duration of curing (٧days) by using equations (٤.١٨, ٤.١٩, ٤.٢٠). To represent shrinkage strain and creep strain, the ACI model Eq.(٤.٢) is used to calculate equivalent nodal force {EIF} in duration (ΔTT).

٦- Calculating total material stiffness from Eq.(٤.٣٦).

٧- Finding element stiffness matrix [Kele]. These stiffness matrices are assembled to form to global stiffness matrix. As a result of the symmetry of the global stiffness matrix, the coefficient is stored in rectangular matrix with dimension. (No. of equation, half band width), [K], at the same time, form external nodal force {ΔGf}, by assembling equivalent nodal forces for each element {EIf} during {ΔTT}.

٨- Solving [K].{ Δd}={ΔGf} for displacement increments {Δd} and adding it to pervious accumulative displacement vector {d} to get the total displacement.

٩- The incremental strains are evaluated using the following relationship:

$$\{\Delta\varepsilon_t\}=[B]\{\Delta d\} \qquad .....(٤.٤٣)$$

Incremental strains are calculated at each mid point of element and added to the previous accumulative strain $\{\varepsilon_{i-1}\}$ to get the total strain $\{\varepsilon_i\}$ as the follows:

$$\{\varepsilon_t^i\}=\{\varepsilon_t^{i-1}\}+\{\Delta\varepsilon_t\} \qquad .....(٤-٤٤)$$

١٠- From $\{\Delta\varepsilon\}$, $\{\Delta\sigma\}$ is found using the following relation:

$$\{\Delta\sigma_t\}=[D]_c.\{\Delta\varepsilon\} \qquad .....(٤-٤٥)$$

where [*D*] is either (elastic) material stiffness or cracked material stiffness. Then, add $\{\Delta\sigma_t\}$ to the previous stress to obtain total stresses. Stresses in steel are also calculated. Using concrete and steel stress to find element internal force, which represents the lack of equilibrium between external forces and equivalent internal forces which depend on nodal deformation. The steps (٦-١٠) are repeated until convergence is reached.

١١- The change in elastic restrained strain is found for each uncracked element which is used to calculate free creep strain by superposition

method. Change in elastic strain is calculated during (ΔTT) from the following relationship:

$$\{\Delta\varepsilon_e\} = \{\varepsilon_t\} - \{\varepsilon_f^s\} - \{\varepsilon_f^c\} - \{\varepsilon_e\} \quad \text{.....(٤-٤٦)}$$

where, ε_t is the total strain at time ($t=n_1$), ε_f^s free shrinkage strain at ($t=n_1$), ε_f^c free creep strain at ($t=n_1-\Delta TT$), ε_e the total elastic strain until ($t=n_1-\Delta TT$). This value of change in elastic strain in stored a matrix for obtaining the change in free creep strain at time ($t=n_1$) by subtracting free creep strain at ($t=n_1-\Delta TT$) from free creep strain at ($t=n_1$). This strain is converted to equivalent nodal force which is reapplied on the member, and steps (٦-١٠) are repeated until convergence occurs, then computation will follow step (١٢).

١٢- The change in restrained strain which occurs during (ΔTT) is found from the following equation:

$$\{\Delta\varepsilon_r\} = \{\varepsilon_t\} - \{\varepsilon_f^s\} - \{\varepsilon_f^c\} - \sum_{i=1}^{n-\Delta TT}\{\Delta\varepsilon_r\} \quad \text{.....(٤-٤٧)}$$

with the notice that free creep strain is calculated at time ($t=n_1$). This strain is added to previous value to find the total restrained strain. The same procedure is followed for stress to find total restraining stress.

١٣- Principal strains and stresses are then calculated.

١٤- Check cracking, if cracking happens in any element, the restrained stress normal to crack is released and return to step (٥).

CHAPTER FIVE

EXPERIMENTAL RESULTS AND ANALYSIS

٥.١ Free Volume Change of Slabs

Using the model described in Chapter Three, Article (٣.٣.٧), the free shrinkage strain of concrete slabs was measured under the same indoor exposure conditions of the restrained slabs. Figure (٥-١) shows the free shrinkage strain development in the slabs with drying period.

In the first day after casting, there was a contraction in the slabs due to the drop of the concrete slab temperature from its peak temperature (due to heat of hydration) to its temperature when the first demec reading was taken, which was carried out early in the morning. The temperature drop observed was about to ١٤^{o}C in the slab temperature. Thus the amount of free thermal contraction will be

$$e_{th} = C_T \times T \qquad \text{.....(٥-١)}$$

C_T : linear coefficient of thermal expansion of concrete which is taken as ١٠x١٠$^{-٦}$/^{o}C [٣٠, ١٠٠].

Therefore a total contraction strain of ١٤٠x١٠$^{-٦}$, due to the effect of temperature drop was recorded.

Free shrinkage strains of the slabs as illustrated in Figure (٥-١) were not uniform with distance from the edge to the center of the slabs. In general, the shrinkage strain at ٢.٥ cm from the edge was greater than the shrinkage strain at the center of these slabs because the surface area at ٢.٥

cm from the edge includes (edge and surface area) which was subjected to drying shrinkage more than that at the center which includes the surface area of slab only.

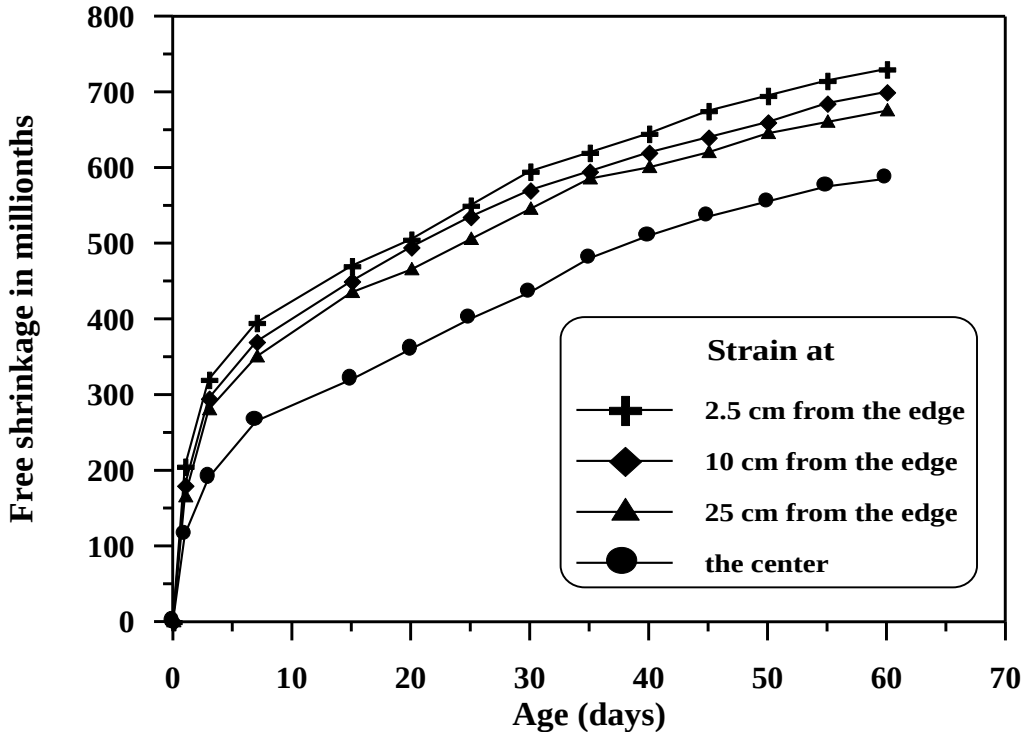

Figure (٥-١): Free shrinkage development with age for plain concrete free slab.

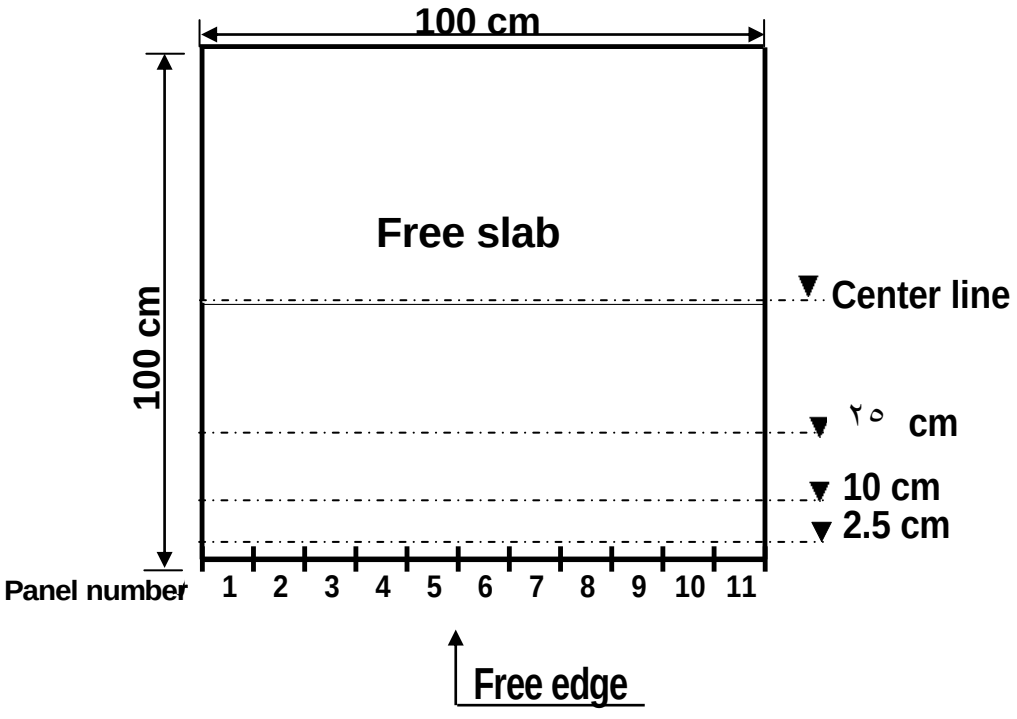

٥.٢ Restrained Movement of the Slabs

The measurement of movements of the slabs was carried out to investigate the effect of different restraint cases of the slabs on the cracking behavior (cracking age, cracking sequence, crack spacing, crack width, crack length and location of maximum crack width). These measurements were conducted for a drying shrinkage period of ٢ months and then behavior of cracking during (١.٥ hr) under fire, then after exposure to fire flame for a period of ٢ months.

Figures (٥-٢) and (٥-٣) show the internal restrained shrinkage strain development with age before and after exposure to fire flame of the reinforced concrete free slab respectively, at three rows (٢.٥, ٢٥ cm a part from the edge and at the center) of the slab.

Since the restraining effect of the ends decreases towards the center of the slab, therefore the movement of the slab will vary with the distance from the restraining ends. As described in Article [٣.٣.٦] the movement of the slab was obtained at three different levels [٢.٥, ٢٥ and ١١٢.٥ cm] distance from the edges by using a demec gauge (extensometer).

Figures (٥-٤ to ٥-٨) show the measured movement of most of the slabs studied. From this figure it can be observed that movements of the slab increase towards the centerline of the slab from the restrained edges. A gradual reduction in the readings of measured shrinkage strain at any panel would indicate a crack occurrence at that panel. An abrupt positive change would indicate that cracking had taken place at that panel which was denoted by zero strain in these figures.

In addition to the measurement of slab movement, the movement of the rigid beams was also recorded during the same period. The contraction of the rigid beams during the exposure period of the slabs was called “Loss of restraint – L.O.R.”. The average value of loss of restraint for each slab is illustrated in Table (٥-١).

Figure (٥-٢): Shrinkage development with age for reinforced concrete free slab before exposure to fire flame.

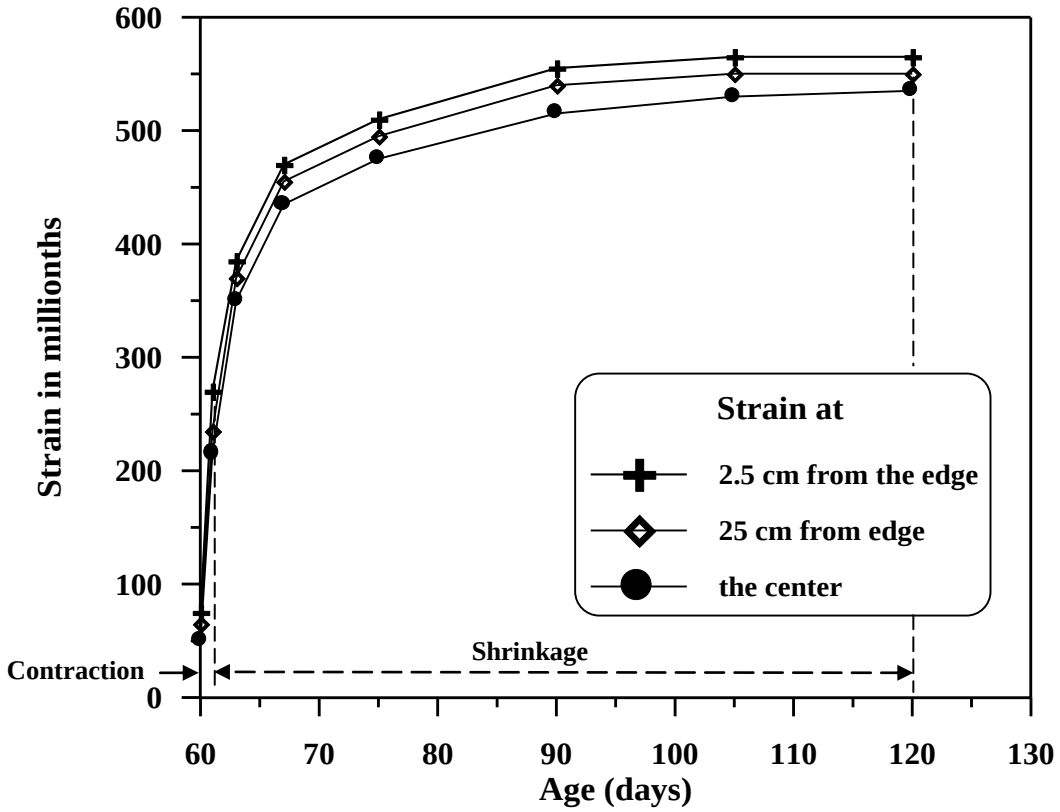

Figure (٥-٣): Relation between contraction, shrinkage and age for reinforced concrete free slab after exposure to fire flame.

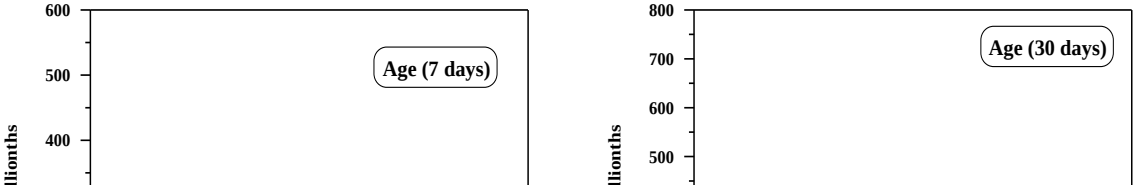

Figure (٥-٤): Strain development history for reinforced concrete free slab at ٢.٥ cm from the edge.

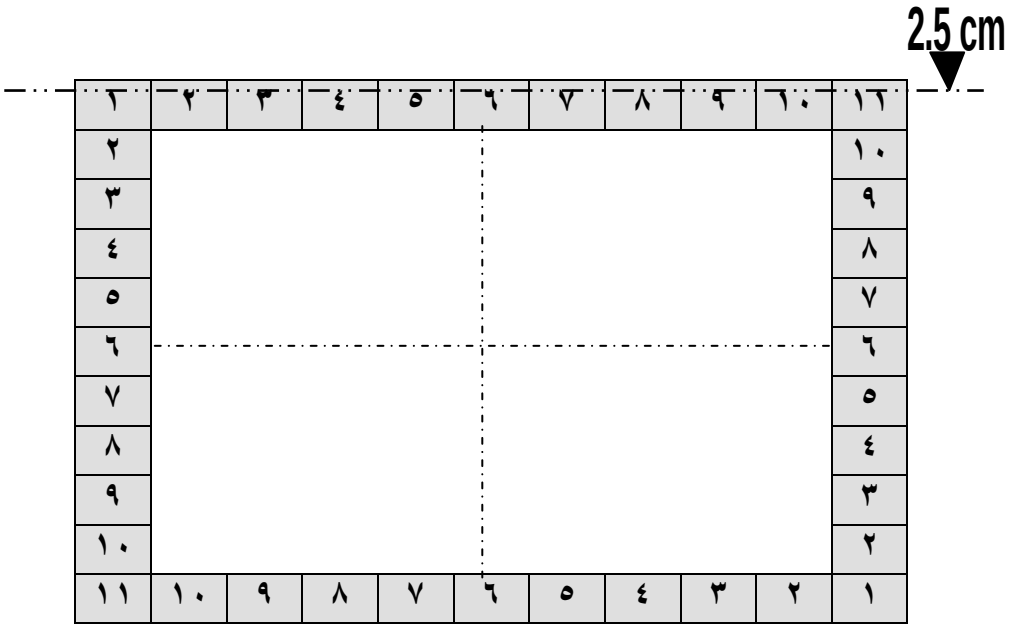

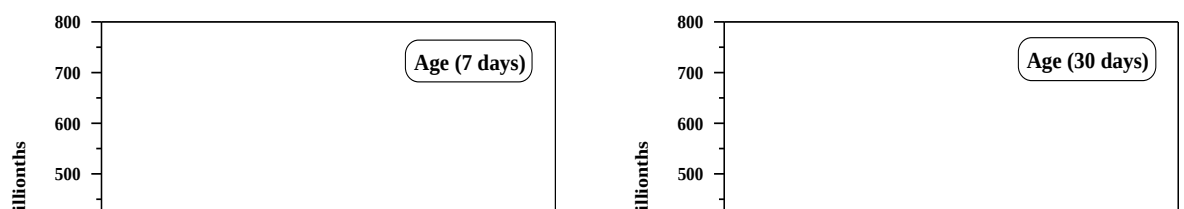

Figure (٥-٥): Strain development history for two end restrained of reinforced concrete slab at ٢.٥ cm from the free edge.

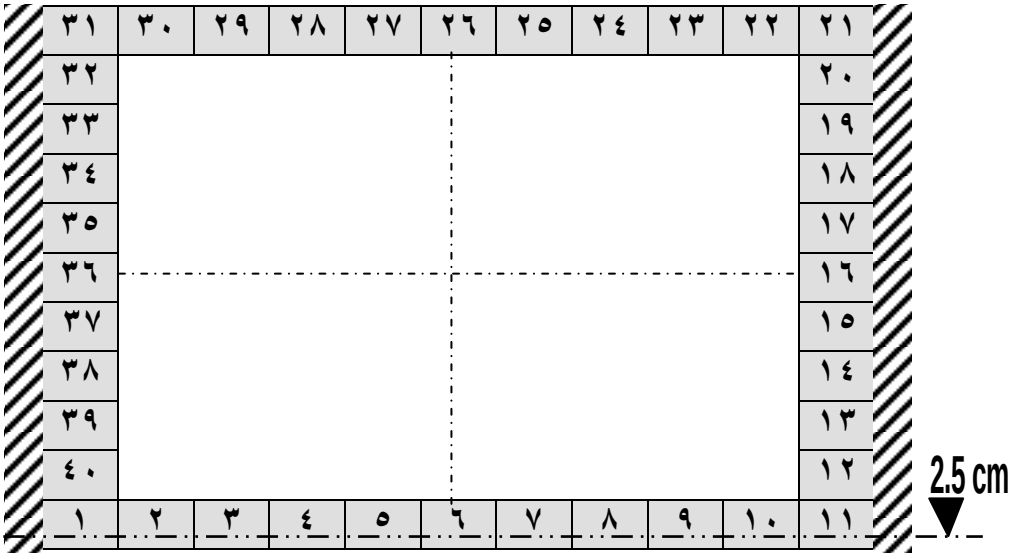

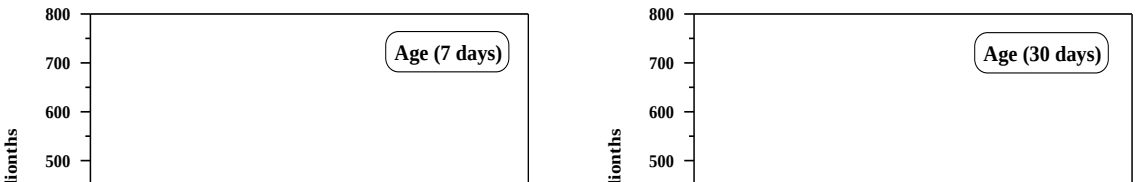

Figure (٥-٦): Strain development history for three end restrained of reinforced concrete slab at ٢.٥ cm from the restrained edge.

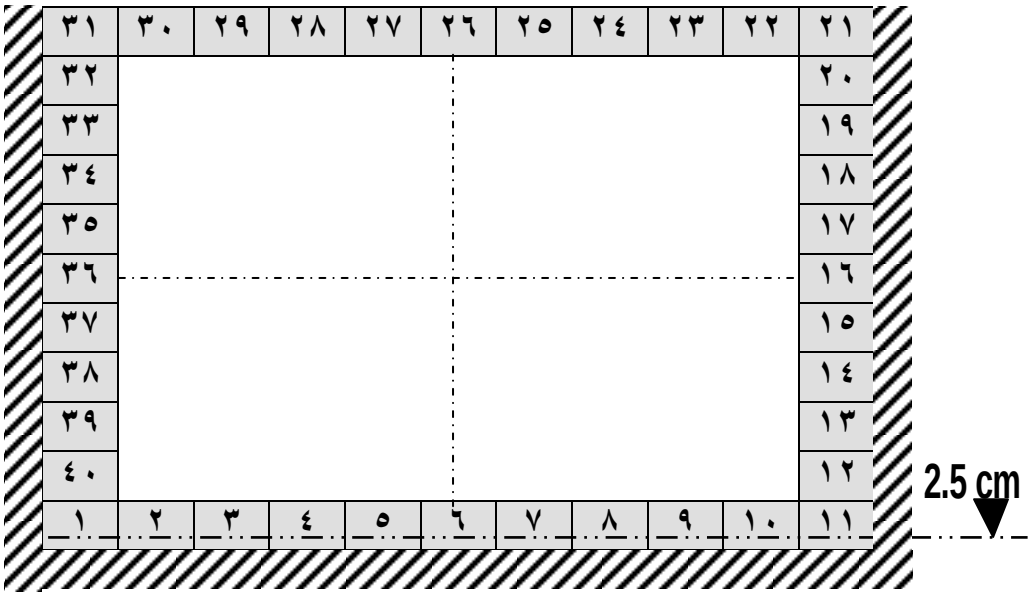

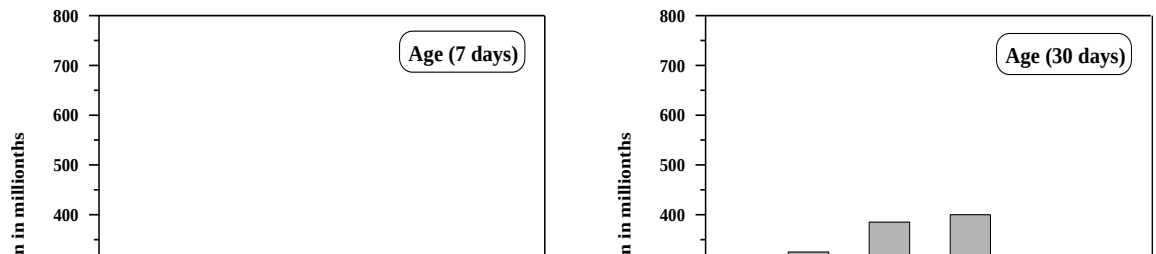

Figure (٥-٧): Strain development history for three end restrained of reinforced concrete slab at ٢.٥ cm from the free edge.

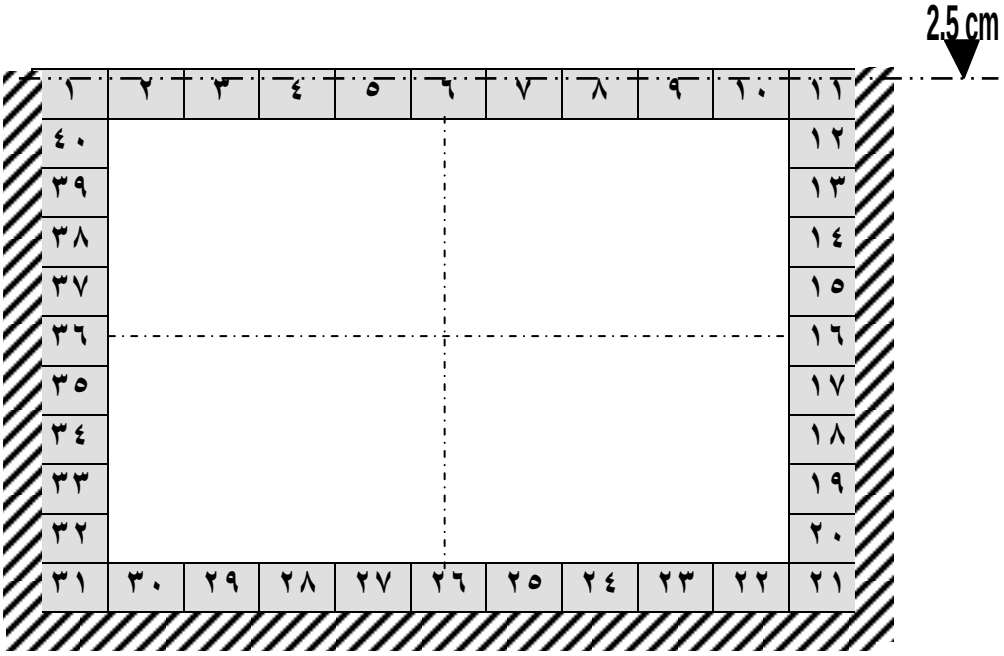

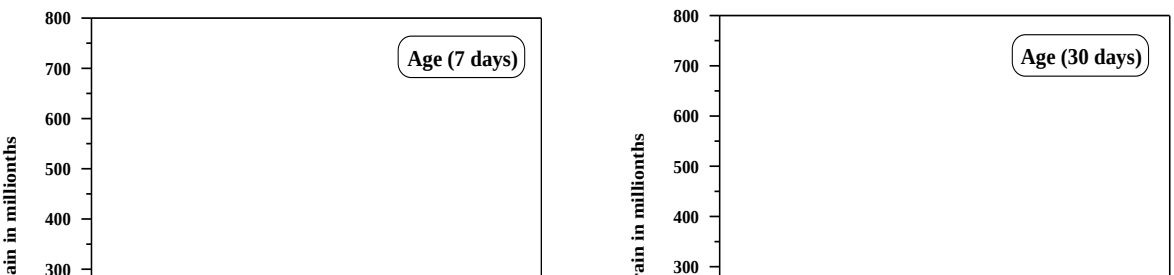

Figure (٥-٨): Strain development history for four end restrained of reinforced concrete slab at ٢.٥ cm from the restrained edge.

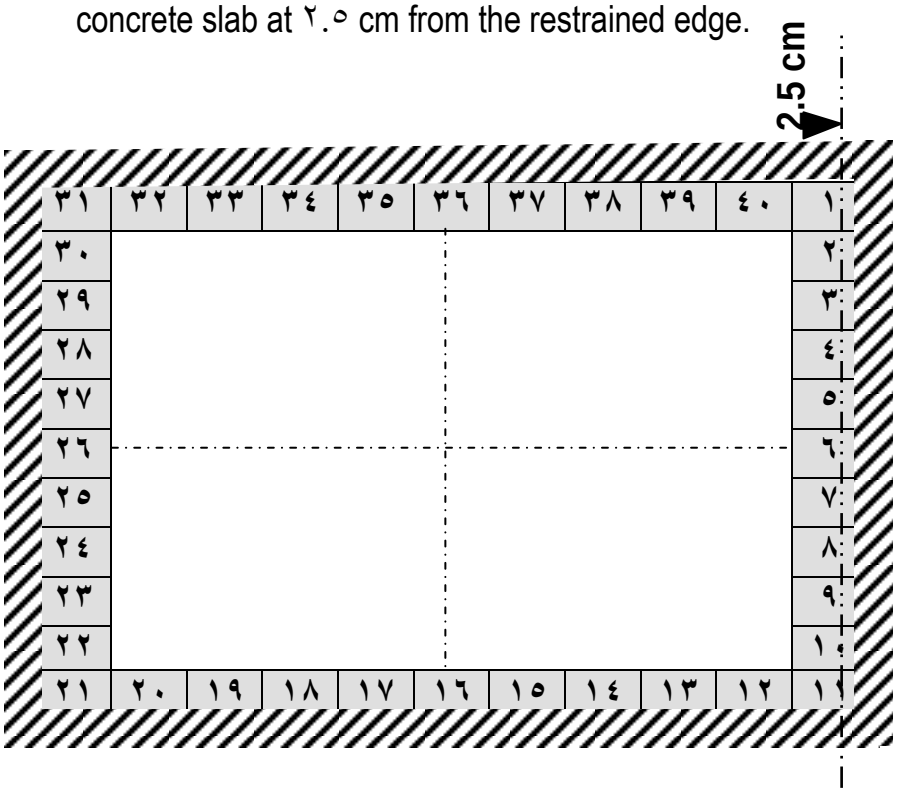

٥.٣ Elastic Tensile Strain Capacity Tests

Elastic tensile strain capacity of concrete was obtained directly by measuring the immediate movement after cracking of plain concrete of channel ⌐¬ - shaped beams. It was also measured indirectly by determination of tensile strength and dynamic modulus of elasticity. The elastic tensile strain capacity is taken as the tensile strength divided by the dynamic modulus of elasticity. The results of these tests are illustrated in Table (٥-١).

It was worth noting from the experimental results that the elastic tensile strain capacity of concrete measured by the direct method was greater than that of the indirect method and *Al-Rawi* also found [٢٢] such result.

As can be seen from the results of the present work that the tensile strain capacity of concrete is much higher than that reported in some of the literatures [٧, ٣١, ١٠١]. *Al-Rawi* [٢٢] also reported that tensile strain capacity values of concrete are much higher than those reported in previous literature. The results of the present work are in line with *Al-Rawi's* results.

Table (٥-١): Direct and indirect results of elastic tensile strain capacity.

	Loss of restraint L.O.R*١٠$^{-٦}$		Indirect method						Direct method
			٧ days			٢٨ days			
Mix Prop. Cement: sand: gravel w/c	Beam	Slabs	Ed GPa	Ru MPa	eult *١٠$^{-٦}$	Ed GPa	Ru MPa	eult *١٠$^{-٦}$	eult *١٠$^{-٦}$
١ : ١: ٢ ٠.٤٨	٤٥	٦٠	٤١	٤.٠٥	٩٩	٤٦	٦	١٣٠	١٤٥

Ed = Dynamic modulus of elasticity.
Ru = Tensile strength of concrete.
eult = Elastic tensile strain capacity.

٥.٤ Cracking of the Slabs

In Table (٥-٢) the cracking characteristics are summarized for slabs investigated at age of (٦٠ days) before exposure to fire flames. Table (٥-٣) presents the site observations and cracking data for drying shrinkage only of actual size slabs are summarized for a newly constructed building in Hilla city.

The experimental and site observation results clearly indicated that there is no difference in the characteristics of shrinkage cracking.

Table (٥-٢): Cracking data of the slabs before exposure to fire flame.

Slabs		ρ%	Number of cracks	Maximum Lc (cm)	D-wmax from edge (cm)	Observed spacing of cracks at edge (mm)		Maximum crack width (mm)
						Min.	Max.	
Two end restrained		٠.٤٢	٨	٢٨	٠	٣٢٠	٦٩٠	٠.٢٤
Three end restrained	From free edge	٠.٤٢	٤	٢٢.٥	٠	٢٨٠	٥٨٠	٠.٢
	From restrained edge		٣	٣٢	١٢	٤٦٠	١٢٦٠	٠.٢٥٥
Four end restrained		٠.٤٢	١١	٣٣	١٢.٥	٣٨٥	١٠٩٠	٠.٢٧٥

Lc = Length of crack.
D-wmax = Position of maximum crack width.

Table (٥-٣): Cracking data of the observation slabs.

Slabs		ρ%	Number of cracks	Maximum Lc (cm)	D-wmax from edge (cm)	Observed spacing of cracks at edge (mm)		Maximum crack width (mm)
						Min.	Max.	
Three end restrained	From free edge	٠.٣٢٣	٤	١٠٥	٠	٦٠٠	١٢٥٠	٠.٣
	From restrained edge		٩	١١٠	٥٠	١٠٠٠	٢٢٥٠	٠.٣٥
Four end restrained		٠.٣٢٣	١٣	١٤٧.٥	٣٥	٧٥٠	١٨٧٥	٠.٤٠

Lc = Length of crack.
D-wmax = Position of maximum crack width.

٥.٤.١ Cracking Age and Sequence

The cracking age can be used as an index for the vulnerability to cracking [٢٨].

Table (٥-٤) shows the effect of restraint on the cracking age. From this table, it is obvious that the slabs which cracked first are the four, three and two end restrained respectively, which means that the cracking age decreases if restraint increases (as shown in the table below).

Table (٥-٤): Effect of different restraint cases on the cracking age of reinforced concrete slabs before exposure to fire flame.

Types of restraint	Cracking age (days)
Two end restrained	٢١-٤٥
Three end restrained	١٨-٤١
Four end restrained	١٦-٤٣

The schematic pattern of crack development when stress is relieved by creep is shown in Figure [٢-١]. Cracking could occur only when the stress induced by restrained shrinkage strain, reduced by creep, reaches the tensile strength of the concrete. Since the restraint is highest at the center line of the slab for four end restrained and three end restrained from the restrained edge [٢٣, ٣٠], the first crack must occur at this position assuming that concrete is homogeneous and other characteristics are uniform. This is confirmed by the experimental results for three and four end restrained reinforced concrete slabs. While, the first crack in the two end restrained slab generally occurs at the weakest section of the slab, as the force induced due to restrained shrinkage exceeds that provided by the concrete section. This section is either weaker in tension than the rest of the slab (due to non-homogeneity of concrete), or it is under higher restraint which tends to increase the cracking force imposed at section.

Figures (A-١ to A-٣) show the development of crack pattern of slabs during two months period of observation before exposure to fire flame. Only one side of four end restrained slab, as indicated in Figure(A-٣), deviated from this trend. This may be attributed to the existence of non-homogeneity in the rigid beams or in the slab.

Generally, cracking sequence became slower with age as shrinkage became more exhausted with time.

After the formation of first crack, the formation of further cracks became rather more difficult. This is because the tensile strength of concrete slabs increases with increasing age and the remaining amount of restrained volume change decreases with age. The positions of further cracks depend on the new arrangement of degree of restraint along the slab.

From Figures (A-١ to A-٣) it can be concluded that the first crack always occurs within the middle third of the restrained edge slab length. The cracks at and near the center line of slab propagated towards the point of intersection of centerlines of these slabs, whereas, the cracks near edge of slabs extended in a direction inclined to the other restrained edge (at the corner). The same trend was also observed in full size slabs, as can be seen from Figure (A-٤). The propagation of cracks depends on the direction of tensile stresses.

Table (٥-٥) gives the cracking sequence of crack formation in slabs during exposure to fire flame for the slabs studied in this work. Similar trend have been observed by *Nizomuddin* et al. [١٠٢].

The crack propagation continued although the rate of free volume change was decreasing. This may be due to the facts that cracks propagate at a decreasing stress field once they have initiated [٢٣], and the crack propagation is much easier than crack initiation.

Table (٥-٥): Observed sequence of crack formation in slabs during exposure to fire flame.

Time of observation (min)	Observations
١٠	Cracks were formed on top surface of these slabs due to drying shrinkage propagation and extended in width and length. Radial cracks were observed on bottom surface of slabs at and near centerlines.
٢٠	Radials cracking on bottom of slab were continuing to initiate and propagate with some cracks now extending toward the edge of slab.
٣٠	More cracks were visible on edge of slab at top surface. Some of these cracks extended perpendicular toward the slab center.
٤٥	One crack near the centerline of four end restrained reinforced concrete slab was visible on top surface of slab and extended to approx. ٢.٥ cm toward center of slab.
٦٠	Cracking at top surface continued. The crack noticed at ٤٥ min now extended to approx. ٢٠ cm. Some of cracks, especially the cracks formed at the middle of the edge of slab noted increasing in depth from top to bottom of slab.
٧٠-٩٠	Some top surface cracks particularly near middle of slab extended to ٥٠-٧٥ cm, and propagated to full depth of these slabs.
٩٥	Some cracks were noticed on top and bottom surfaces and extended from the free edge to the restrained edge for two and three end restrained slabs.
١٠٥	Radial cracks were formed at the lower surface of these slabs and were visible at the middle of slab and extended perpendicular towards the edges of slab. These cracks stopped at a distance of (١٠-٢٠) cm from the edges of the slab. Also, it was noticed that cracks appeared in a honeycomb fashion in the lower surface for all the slabs investigated.

٥.٤.٢ Crack Spacing

As stated in the literature review, it was reported by *Hughes* [١٠٣] that the minimum crack spacing, S_{min}, is equal to the bond slip distance, in end restrained members. *Al-Rawi* [١٠٤] proved experimentally the soundness of this statement.

By adopting the same procedure, described in Sec.(٣.٣.٦), from strain measurement, *Al-Rawi* determined the distance over which the bond slip occurs.

In the present work, the data obtained from the demec gauge readings were misleading in determining the bond slip distance. Thus, the consideration of minimum and maximum crack spacing was based on the observation of crack locations.

Table (٥-٢) shows the information obtained with respect to the minimum and maximum observed crack spacing.

Figures (A-٥ to A-٧) and (A-٤) show the final crack pattern in the experimentally investigated slabs before and after exposure to fire flame and in some of actual size observed slabs without burning, respectively. From these figures, it appears that the cracks are generally more numerous in the proximity of the edge than at some distance from it. It can be stated that the maximum crack spacing in the slabs increases with increasing distance from the edge. Also, the observed crack spacing was largely affected by the different restrained cases investigated, which play an active part in distribution of cracks before and after exposure to fire flame.

Al-Rawi [٢٦] presented the following equation, for the prediction of minimum crack spacing, S_{min}, in members subjected to end restraint:

$$S_{\min} = 0.85K\frac{d}{\rho} \qquad \text{.....(٥-٢)}$$

In the present work the following equation is suggested for two and three end restrained slabs and for cracks in free edge.

$$S_{\min} = 0.85K\frac{d}{(\rho + \rho_R)} \quad .....(٥-٣)$$

ρ_R : this factor was estimated by STATISTICA program version ٥.٠ from experimental data with coefficient of correlation r=٠.٩٨, as follows

$$\rho_R = 0.9 - 1.1\left(\frac{l}{L}\right)^{0.6} \quad .....(٥-٤)$$

where;

k : a constant depending on the type of reinforcement which can be taken as ٠.٨ for indented deformed bars and ٠.٦٧ for ribbed deformed bars.

d : bar diameter.

ρ : reinforcement steel ratio.

ρ_R : effect of end restraint as a ratio.

L : slab length or width.

l : distance from the to the position of calculated crack width.

From the above equation it can be noticed that the effect of end restraint can be expressed in terms of additional steel ratio (ρ_R). Thus, in reinforced end restrained slabs, the total steel ratio is equal to the summation of the actual steel ratio and the calculated ratio (ρ_R). Also, this equation is applicable from the edge to the center of slab.

The equations which can be used for calculating minimum crack spacing for cracks which appear from restrained edge for three and four end restrained reinforced concrete slabs can be written as follows:

$$S_{\min} = 0.85K\frac{d}{(\rho + K_{R1})} \quad .....(٥-٥)$$

For three end restrained from restrained edge.

$K_{R١}$: this factor was estimated by STATISTICA program version ٥.٠ from experimental data with coefficient of correlation r=٠.٩٨ .

$$K_R = 1 - 1.1\left(\frac{l}{L}\right)^{0.4}$$

For four end restrained slab.

$$S_{\min} = 0.85K\left(\frac{d}{\rho + 0.8K_{R_2}}\right) \quad \text{.....(٥-٦)}$$

K_{R_2} Is taken from Figure (٥-٩).

Based on the information in Figure (٢-٢) of ACI committee ٢٠٧[٢٣] which was used to find the degree of restraint at center section of base restrained walls, a new relationship demonstrated in Figure (٥-٩) is suggested. This suggested relationship could be used to estimate the degree of restraint at center sections of restrained slabs.

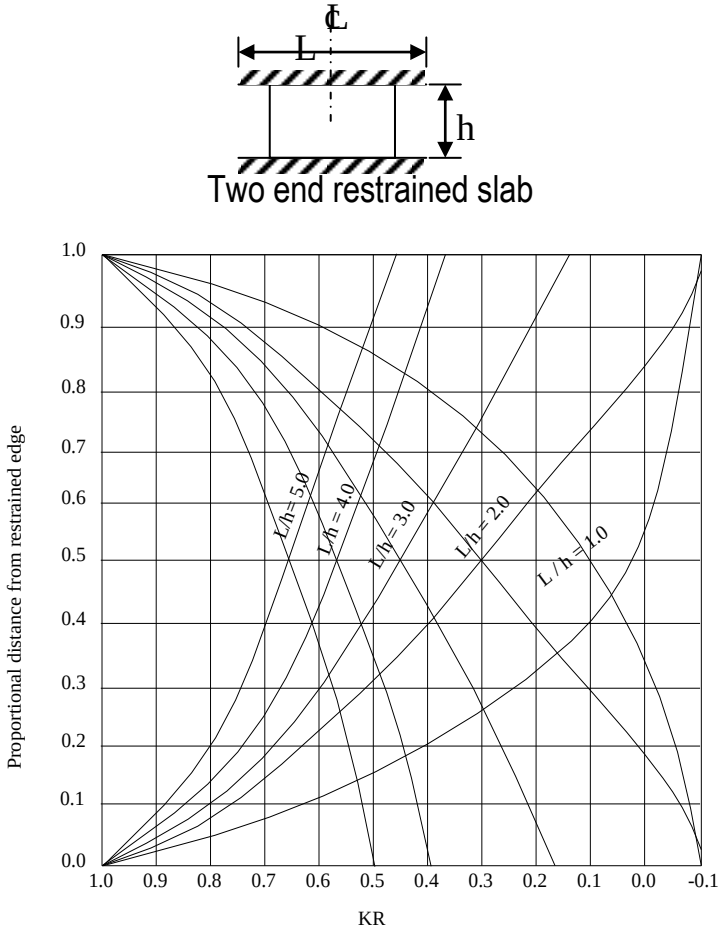

Figure (٥-٩): Degree of tensile restraint at center section.

The experimental results clearly indicate that the maximum crack width occurred at a level of about (٠.٣ and ٠.٢٥) times the crack length for cracks which appear from the restrained edge before and after exposure to fire flame respectively. To minimize the crack spacing at that level, the upper surface of the rigid beams was finished with high roughness. The

maximum crack width is associated with maximum crack spacing [٣٠, ١٠٣, ١٠٤,١٠٥].

٥.٤.٣ Crack Length and Crack Location

The experimental and site observation results clearly indicate that the maximum crack width increases with increasing maximum crack length as can be seen in Figures (٥-١٠ and ٥-١٢) as follows:

$W_{max} = ٠.٠٠٨\ L_c + ٠.٠٠٠٦$ for experimental slabs before burning.

$W_{max} = ٠.٠٠٢\ L_c + ٠.٢٧٤$ for experimental slabs after burning.

$W_{max} = ٠.٠٠٢٦٥\ L_c + ٠.٠٠٠٧١٣$ for actual size slabs without burning.

From these figures, it is obvious that if the prediction of maximum crack length is satisfactory, an assumption of maximum crack width can be made. Hence, the reduction of the width of cracks which is developed in reinforced concrete slabs is associated with the reduction in maximum crack length before and after exposure to fire flame.

Regarding the model used during the present study, it can be seen (from cracking history figures) that early cracks initiated mainly within the middle third of the slab rather than at its ends. Also that end portions showed that the strain values are higher than the internal portions. This means that the restrained shrinkage strain is higher at the middle of the slab than at its ends. This leads to suggest that stress concentration in these regions is higher.

Al-Rawi [٢٦] attributed this behavior to the generation of a strain gradient at the end parts which increases the loss of restraint and reduces the possibility of cracking. While at interior zones, higher restraint would be developed due to the build up of friction forces and the absence of strain gradient, hence, cracks would be expected to appear at the interior zones and away from the ends.

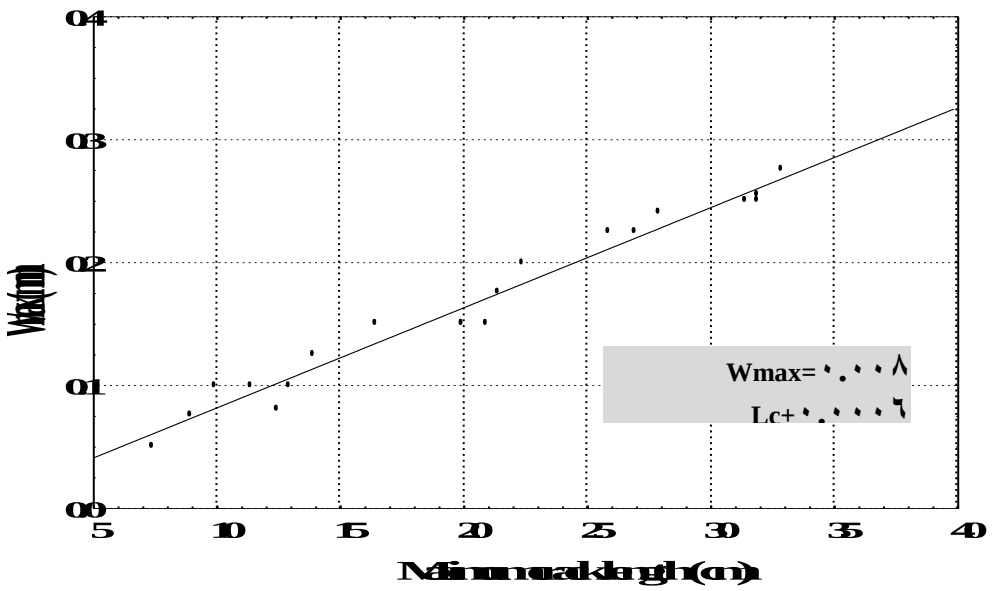

Figure (٥-١٠): Relation between maximum crack width and maximum crack length for experimental slabs investigated before exposure to fire

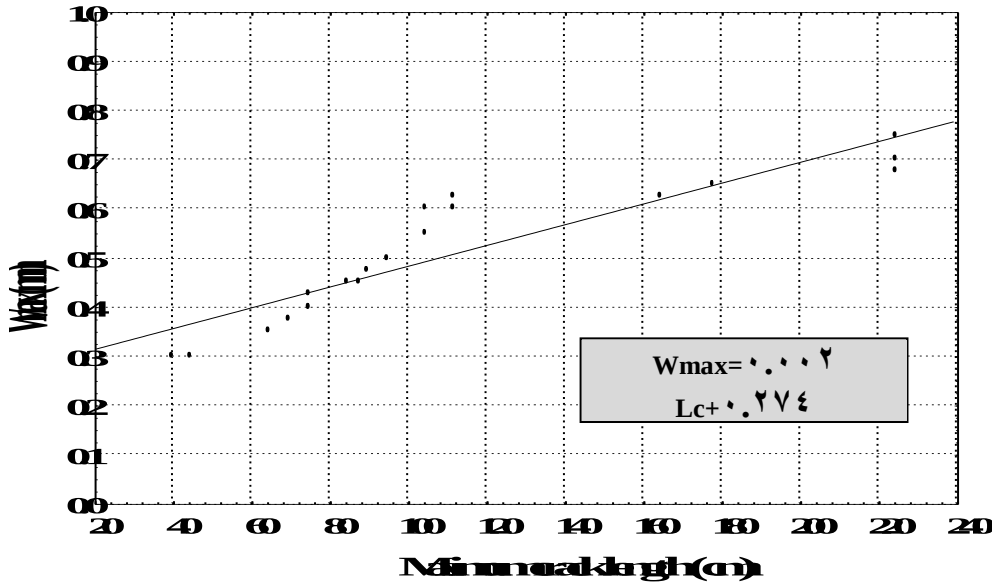

Figure (٥-١١): Relation between maximum crack width and maximum crack length for experimental slabs investigated after exposure to fire

The level of maximum crack width in a slab was designated as (D-w_{max}). It was observed that D-w_{max} for cracks which appeared from the restrained edge for the experimental and site observed slabs (three and four end restrained) was related to its maximum crack length (L_c). For experimental slabs, D-w_{max} was found to be equal to (٠.٣٥ L_c+١.١١ and ٠.١٤ L_c+١٣.٨) before and after exposure to fire flame respectively, and (٠.٢٩٧ L_c+٣.١١٣) for site observed slabs without exposure to fire flame as shown in Figures (٥-١٩ to ٥-٢١).

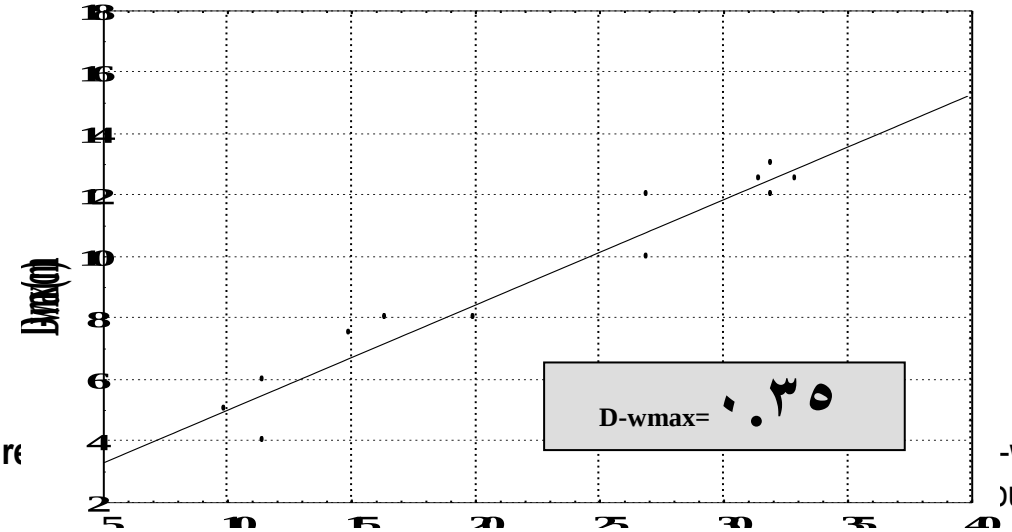

Figure (-wmax)
our end

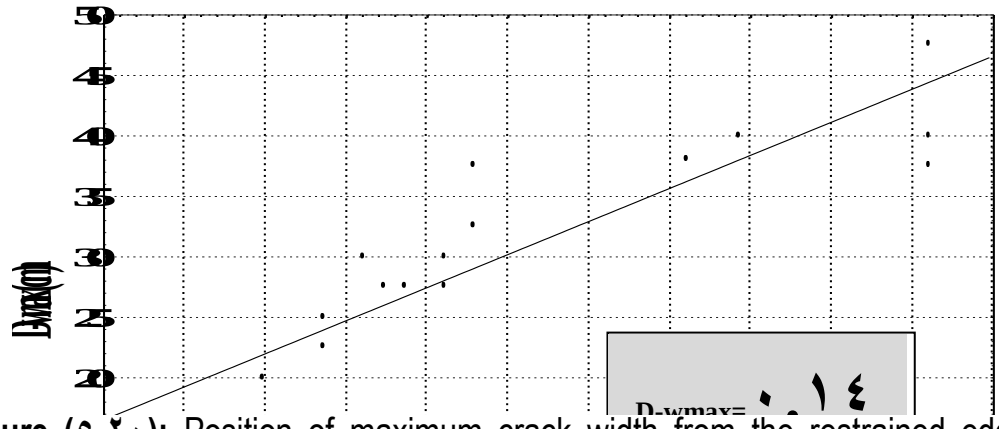

Figure (٥-٢٠): Position of maximum crack width from the restrained edge (D-wmax) as a function of crack length for the experimental three and four end restrained slabs investigated after burning.

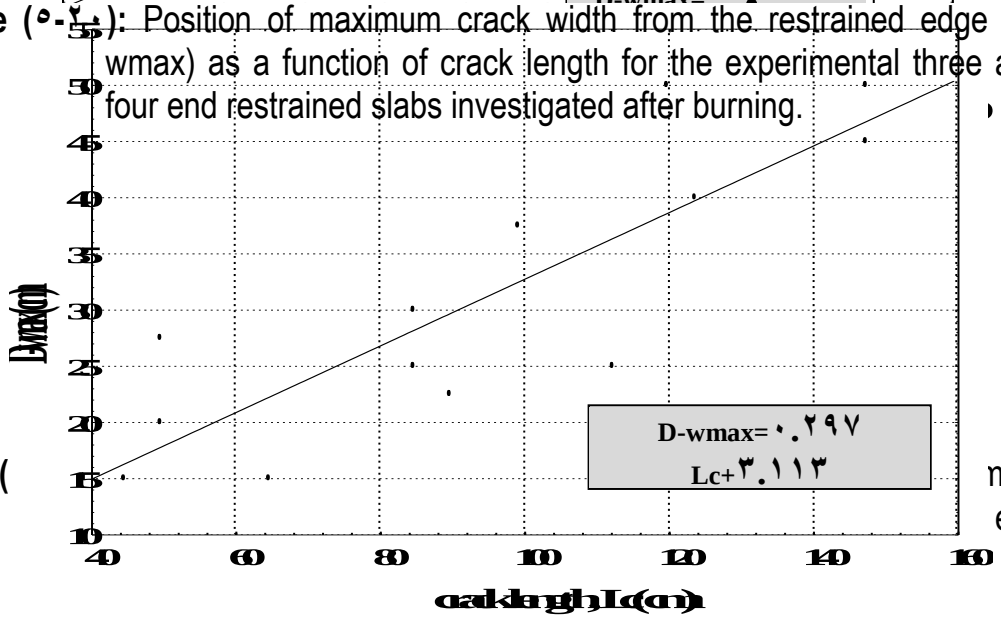

Figure (nax)
end

There is a further aspect to be considered in the investigated slabs (three and four end restrained), which is occurring the maximum crack width at a certain level from the restrained edge (٠.٢-٠.٥ and ٠.١٥ – ٠.٣٨)L_c before and after exposure to fire flame respectively. Moreover, the maximum crack width also occurs at a certain level from the restrained edge in site observed slabs (٠.٢٣-٠.٥٥)L_c. In the investigated slabs, the crack width decreases, from the level of maximum crack width (D-w_{max}), to zero at the end of the crack, and to a certain value at the beginning of the crack.

By using the strain distribution in the concrete and steel adjacent to a crack, as suggested by *Al-Rawi* [٢٦], the maximum crack width that may occur in the slab at the three different levels has been calculated. The equation used to calculate crack width developed by *Al-Rawi* [٢٦] was adopted by considering the strain distribution in Figure (٥-٢٢) and using non-linear estimation analysis (STATISTICA program version ٥.٠). Hence, the equation used to calculate crack width for two and three end restrained for cracks which appear from the free edge at any level of the slab, is as follows:

$$Wc_{\max} = S_{\max}\left[a \times e_{shn} - b \times C_f - C \times \frac{e_{ult}}{2}\right] \qquad .....(٥\text{-}٧)$$

Where:

a,b,c : constants (estimated statistically using STATISTICA program)

a = -١٠.٠٦
b = -٢٦.٩٢
c = ٥٠.٢٢

Coefficient of correlation (r=٠.٩٩٨).

The notations of the model referred to are as follows:

- S_{max} : Maximum crack spacing, (mm), Eq.(٥-٣).

- e_{sh} : Shrinkage strain plus strain due to decrease in temperature.
- L.O.R. : Loss of restraint due to ends contraction before cracking.
- e_{ult} : Elastic tensile strain capacity.
- e_{shn} : Net shrinkage stain, ($e_{shn}=e_{sh}$-L.O.R).
- C_f : Final creep strain, ($C_f = K^* e_{shn}$).

It was assumed that the value of final creep strain to be constant (K) of the net shrinkage strain, where K equals to ٠.٦ and ٠.٦٥ for reinforced and plain concrete walls respectively [١٩].

The equation which is used to calculated crack width for three and four end restrained slabs for cracks which appear from the restrained edge at any level of the slab by considering the strain distribution in Figure (٥-٢٢) and using STATISTICA program can be written as follows:

$$Wc_{\max} = S_{\max}\left[a\left(R_b - 0.7R_a\right)e_{shn} - b\times C_f - C\times\frac{e_{ult}}{2}\right] \quad .....(٥-٨)$$

Where:

a,b,c = constants (estimated statistically using STATISTICA program version ٥.٠)

a = ٠.٨٣

b = -٣.٩

c = ٢٣.٤٦

Coefficient of correlation (r=٠.٩٨٥)

- S_{max} : Maximum calculated crack spacing, (mm), Eq.(٥-٥ and ٥-٦) for three and four end restrained from the restrained edge respectively).

-R_b : Degree of restraint before cracking (at slab center)

$R_b = 1 - 1.1\left(\frac{l}{L}\right)^{0.4}$ For three end restrained.

And R_b = from Figure (٥-٩) for four end restrained.

- Ra : Degree of restraint after cracking,

$$R_a = 1 - \frac{e_{sr}}{e_{sf}} \text{ (Assumed)}$$

e_{sr} : restrained strain in the slab.

e_{sf} : free strain in the slab, ($e_{sf} = e_{shn}$ (١-R_b)).

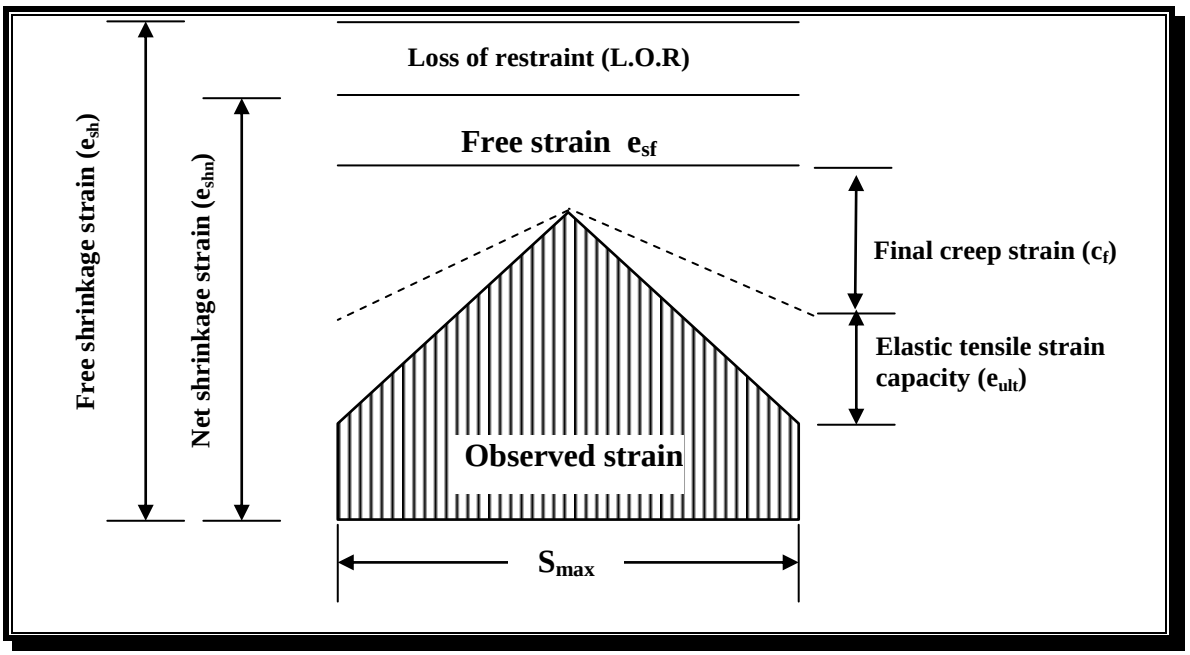

Figure (٥-٢٢): Sketch of strain distribution in the concrete adjacent to a crack.

It was assumed a reduction factor of ٣٠٪ of the restraint of the slab after cracking, due to the slippage between the slab and the restrained rigid beams.

From the Equations (٥-٧ and ٥-٨), it can be seen that there is an internal contradiction. This contradiction appears when using STATISTICA program. This program can not be performed and utilized without internal contradictions. Nevertheless, a function is acceptable if it is capable of reproducing the predicted data close enough to the comparable observed data provided by the prototype within reasonable limits [١٠٦].

Using the above Equations (٥-٧ and ٥-٨), with the experimentally measured values for e_{sh}, e_{shn}, e_{ult} and L.O.R, the crack width for experimental slabs at three different levels are calculated. Tables (٥-٧ to ٥-٩) summarize the required parameters to calculate maximum crack widths by using Eqs.(٥-٧ and ٥-٨) for two end , three end restrained from the free edge and three end, four end restrained from the restrained edge respectively.

The maximum crack widths calculated (w_c) at the three levels using Eq.(٥-٧ and ٥-٨) are summarized in the mentioned tables together with the maximum crack widths that are measured experimentally (w_o) before exposure to fire flame.

Based on the experimental results, an equation to estimate crack width in mid span of these slabs after burning was suggested as follows:

$$Wc_{\max} = (T_d - T_b)\,\alpha_c\ L\ K \qquad \text{.....(٥-٩)}$$

Where;

T_b, T_d : temperature of the unexposed surface before and during burning respectively, (^oC).

α_c : Coefficient of thermal expansion of concrete, (α_c = ١٢ * ١٠$^{-٦}$) [٣٠].

L : half-length of slab, (mm).

K : reduction factor depends on restraint.

(K = ٠.٠٤٥, ٠.٤, ٠.٤٢٥ and ٠.٤٥) for (free, two, three and four end restrained slabs respectively). These values for K obtained by STATISTICA program.

To ensure the validity of the present method for the experimental reduced scale slabs and actual size slabs, Equation (٥-٧ and ٥-٨) have been used to calculate the maximum crack width for actual size slabs (three end restrained from the free edge and four end restrained from the restrained edge respectively) (a newly constructed building in Hilla city). The

characteristics and measured cracking data for these slabs are illustrated in Table (٥-٣).

To be able to calculate maximum crack widths for these slabs, some assumptions must be made. These assumptions are:

- Elastic tensile strain capacity, (e_{ult} = ١٤٠*١٠$^{-٦}$).
- Strain due to temperature change, (e_{th} = ٢٠٠*١٠$^{-٦}$).
- Loss of restraint due to ends contraction, (L.O.R = ٦٠*١٠$^{-٦}$).

For calculating maximum crack width, value of free shrinkage strain namely e_{sh} = ٥٠٠*١٠$^{-٦}$ was adopted. The value is approximately equal to the measured value for concrete with thick section exposed to Iraq environmental conditions [١٠٧]. The maximum crack width at the levels of ٥٠, ١٠٠٠ mm from the restrained edge of four end restrained slab and at the level of maximum observed crack width of these slabs were calculated using the present method. Table (٥-١٠) summarizes the observed and calculated maximum crack widths (using Eq.(٥-٨)) with the measured and assumed parameters mentioned above. An example of the calculation of maximum crack width for different restrained cases of reinforced concrete slab is given in Appendix D.

The calculated crack width mentioned above, and the actual crack width (which is measured by the microscope and using demec point readings) are compared in Figures (A-١٠ to A-١٢).

Tables (٥-١١ to ٥-١٣) give a comparison between values of crack width at different levels of slabs, using different procedures reviewed in the literature with both calculated and observed crack width.

Also, Table (٥-١٤) summarizes the observed and calculated maximum crack widths (using Eq.(٥-٩)) at center of each slab with the measured parameters mentioned above.

Finally, the results of calculated maximum crack widths, using the methods proposed by various researchers and bodies [١٩, ٢٣, ٢٦, ٢٨, ٢٩, ٣٠], together with the observed maximum crack widths for both experimental and site observed slabs were compared with the present theoretically

predicted values. This comparison is shown in Figures (٥-٢٣ to ٥-٢٦). It is clear that there is a very close agreement between the observed maximum crack widths and the calculated maximum crack widths using the present methods for both experimental and actual size slabs before exposure to fire flame. Also, from Table (٥-١٤), it can be concluded that the calculated maximum crack width for investigated slabs by using Eq.(٥-٩) which gives a good agreement with the experimental results after exposure to fire flame.

Table (٥-٧): Maximum crack width calculations for two end restrained slab.

Level (cm)	S_{max} (mm)	e_{sh} (*١٠$^{-٦}$)	L.O.R. (*١٠$^{-٦}$)	e_{shn} (*١٠$^{-٦}$)	Cf (*١٠$^{-٦}$)	e_{ult} (*١٠$^{-٦}$)	W_c (mm)	W_o (mm)
٢.٥	٩١٠	٧٣٠	٦٠	٦٧٠	٤٠٠	١٥٠	٠.٢٣٨	٠.٢٤
١٠	٩٩٠	٧٠٠	٦٠	٦٤٠	٣٨٥	١٥٠	٠.١٥٩	٠.١٦
٢٥	١٠٨٥	٦٧٥	٦٠	٦١٥	٣٧٠	١٥٠	٠.٠٠٩	٠.٠١

Table (٥-٨): Maximum crack width calculations for three end restrained slab from the restrained edge.

Level (cm)	S_{max} (mm)	e_{sh} (*١٠$^{-٦}$)	L.O.R. (*١٠$^{-٦}$)	e_{shn} (*١٠$^{-٦}$)	Cf (*١٠$^{-٦}$)	e_{ult} (*١٠$^{-٦}$)	R_b	R_a	W_c (mm)	W_o (mm)
٢.٥	٩٢٠	٧٣٠	٦٠	٦٧٠	٤٠٠	١٤٥	٠.٨٢	٠.٦٥	٠.١٠٨	٠.١٠٠
١٠	١٠٠٥	٧٠٠	٦٠	٦٤٠	٣٨٥	١٤٥	٠.٦٨	-٠.٠٨	٠.٢٢٩	٠.٢٤٥
٢٥	١١٨٥	٦٧٥	٦٠	٦١٥	٣٧٠	١٤٥	٠.٥٤	٠.٠٥	٠.٠٦٦	٠.٠٧٥

Table (٥-٩): Maximum crack width calculations for the four end restrained slab from the restrained edge.

Level (cm)	S_{max} (mm)	e_{sh} (*١٠$^{-٦}$)	L.O.R. (*١٠$^{-٦}$)	e_{shn} (*١٠$^{-٦}$)	Cf (*١٠$^{-٦}$)	e_{ult} (*١٠$^{-٦}$)	R_b	R_a	W_c (mm)	W_o (mm)
٢.٥	١٠١٠	٧٣٠	٦٠	٦٧٠	٤٠٠	١٤٥	٠.٨٨	٠.٧٥	٠.١١٥	٠.١٢
١٠	١١٤٠	٧٠٠	٦٠	٦٤٠	٣٨٥	١٤٥	٠.٧٢	-٠.٠٥	٠.٢٧	٠.٢٦
٢٥	١٢٦٠	٦٧٥	٦٠	٦١٥	٣٧٠	١٤٥	٠.٦٠	٠.٠٧	٠.٠٩٩	٠.٠٩

Table (٥-١٠): Maximum crack width calculations in site observation four end restrained slab.

Level (cm)	S_{max} (mm)	e_{sh} (*١٠$^{-٦}$)	L.O.R. (*١٠$^{-٦}$)	e_{shn} (*١٠$^{-٦}$)	Cf (*١٠$^{-٦}$)	e_{ult} (*١٠$^{-٦}$)	R_b	R_a	W_c (mm)	W_o (mm)
٥	١٣٩٠	٧٠٠	٦٠	٦٤٠	٣٨٥	١٤٠	٠.٨٢	٠.٧	٠.٠٦٥	٠.١٠
٣٥	١٥٥٠	٧٠٠	٦٠	٦٤٠	٣٨٥	١٤٠	٥	-٠.٠٥	٠.٣٨٨	٠.٤٠
١٠٠	٢٠٧٠	٧٠٠	٦٠	٦٤٠	٣٨٥	١٤٠	٠.٧٠	٠.٠٢	٠.١٦	٠.١٨
							٠			

							٠.٤٢ ٢			

Notes: W_c for free shrinkage = ٥٠٠ * ١٠$^{-٦}$.

e_{th} = ٢٠٠ * ١٠$^{-٦}$.

e_{ullt} = ١٤٠ * ١٠$^{-٦}$.

Loss of restraint = ٦٠ * ١٠$^{-٦}$.

Table (٥-١١): Comparison between values of calculated maximum crack width using different methods for two end restrained of experimental reinforced concrete slab from the free edge.

Distance from the edge (cm)	Calculated crack width in mm.				
	BS: ٥٣٣٧	Al-Rawi	Evans and Hughes	W_c	W_o
٢.٥	٠.٦٠٠	٠.٤٠٠	٠.٥٢٨	٠.٢٣٥	٠.٢٤
١٠	٠.٥٧٣	٠.٣٧٥	٠.٥٠٠	٠.١٥٩	٠.١٦
٢٥	٠.٥٥٠	٠.٣٢٥	٠.٤٨٠	٠.٠٠٩	٠.٠١

Notes:
- BS: ٥٣٣٧, (Ref.٢٩)
- Al-Rawi, (Ref.٢٦)
- Evans and Hughes, (Ref.٢٨)
- W_c : calculated crack width as obtained from Eq.(٥-٧).
- W_o : Observed crack width.

Table (٥-١٢): Comparison between values of calculated maximum crack width using different methods for different restrained cases of reinforced concrete slabs.

Distance from the edge (cm)	Calculated crack width in mm.				
	Al-Rawi	ACI-Committee (٢٠٧)	Harrison	W_c	W_o
٢.٥	٠.٠٨٢	٠.٠٢٣٢	٠.١٧٧	٠.١٠٨	٠.١٠٠
١٠	٠.٣٦	٠.٠٧٥	٠.١٢٩	٠.٢٢٩	٠.٢٤٥
٢٥	٠.١٧٧	٠.١٣٤	٠.٠٨٥	٠.٠٦٦	٠.٠٧٥

A- Three end restrained of the reinforced concrete slab from the restrained edge.

Distance from the edge (cm)	Calculated crack width in mm.				
	Al-Rawi	ACI-Committee (٢٠٧)	Harrison	W_c	W_o
٢.٥	٠.٠٦٨	٠.٠٢٥	٠.١٩٤	٠.١١٥	٠.١٢٠

١٠	٠.٣٧١	٠.٠٨٠	٠.١٤٠	٠.٢٧٠	٠.٢٦٠
٢٥	٠.٢١٧	٠.١٦٠	٠.١٠٠	٠.٠٩٩	٠.٠٩٠

B- Four end restrained of the reinforced concrete slab from the restrained edge.

Notes

- Al-Rawi, (Ref.١٩).
- ACI Committee ٢٠٧, (Ref.٢٣).
- Harrison, (Ref.٣٠).
- W_c : Calculate crack width as obtained from Eq.(٥-٨).
- W_o : Observed crack width.

Table (٥-١٣): Comparison between values of calculated maximum crack width using different methods in site observed four end restrained slab.

	Calculated crack width in mm.				
Distance from the edge (cm)	Al-Rawi	ACI-Committee (٢٠٧)	Harrison	W_c	W_o
٥	٠.٠٩٥	٠.٠٣٦	٠.٢٨٣	٠.٠٦٥	٠.١
٣٥	٠.٦٣٧	٠.٢٠٦	٠.٢١٧	٠.٣٨٨	٠.٤
١٠٠	٠.٢٥٥	٠.٣	٠.١٣	٠.١٦	٠.١٨

Notes

- Al-Rawi, (Ref.١٩).
- ACI Committee ٢٠٧, (Ref.٢٣).
- Harrison, (Ref.٣٠).
- W_c : Calculate crack width as obtained from Eq.(٥-٨).
- W_o : Observed crack width.

Table (٥-١٤): Maximum crack width calculations at mid span for different restrained cases of reinforced concrete slabs after exposure to fire flame.

Slabs	T_b °C	T_d °C	K	α_c*١٠$^{-٦}$	L (mm)	W_c (mm)	W_o (mm)
Free end	٢٣	١٤٥	٠.٠٤٥	١٢	١١٢٥	٠.٠٧٤	٠.٠٧
Two end restrained	٢٣	١٤٥	٠.٤	١٢	١١٢٥	٠.٦٥٩	٠.٦٤٥
Three end restrained	٢٣	١٤٥	٠.٤٢٥	١٢	١١٢٥	.٦٩٩	٠.٦٧٥
Four end restrained	٢٣	١٤٥	٠.٤٥	١٢	١١٢٥	٠.٧٤	٠.٧

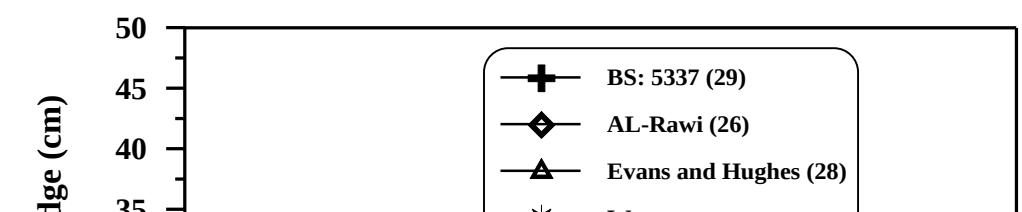

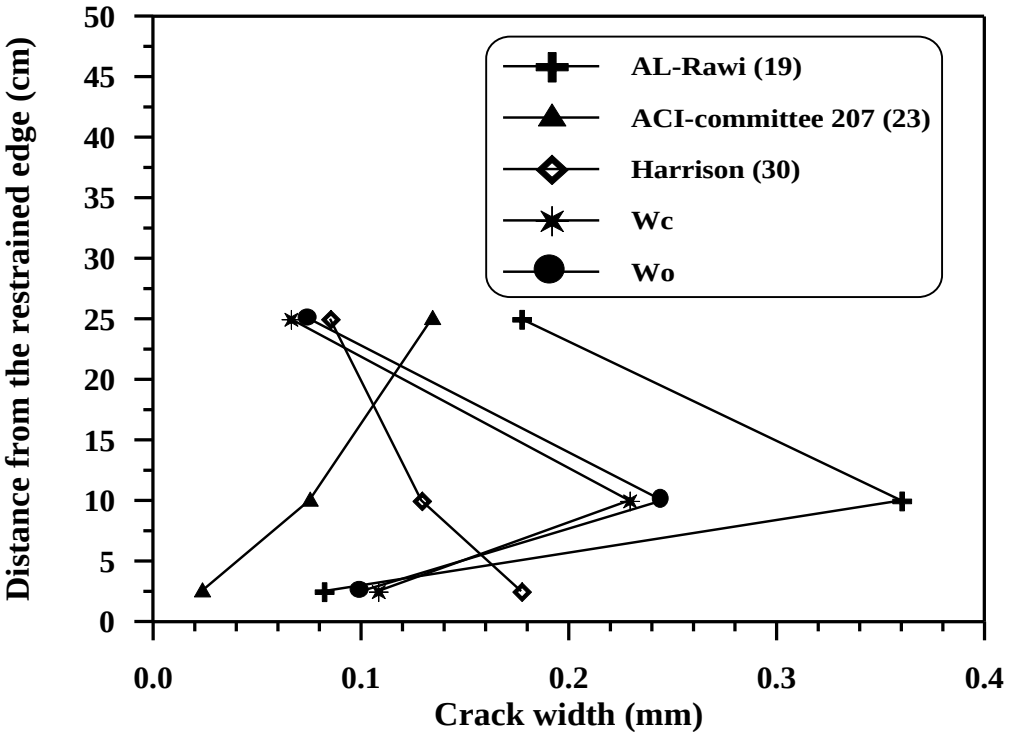

Figure (٥-٢٤): Comparison of the observed and calculated maximum crack width at different levels for three end restrained slab.

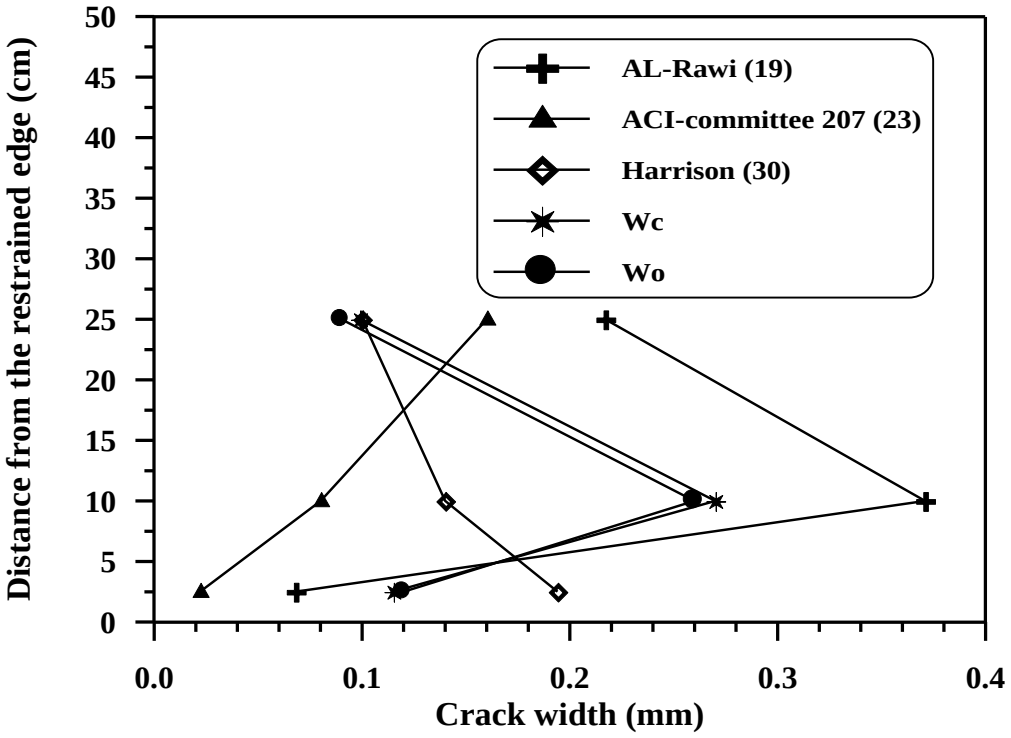

Figure (٥-٢٥): Comparison of the observed and calculated maximum crack width at different levels for the four end restrained slab.

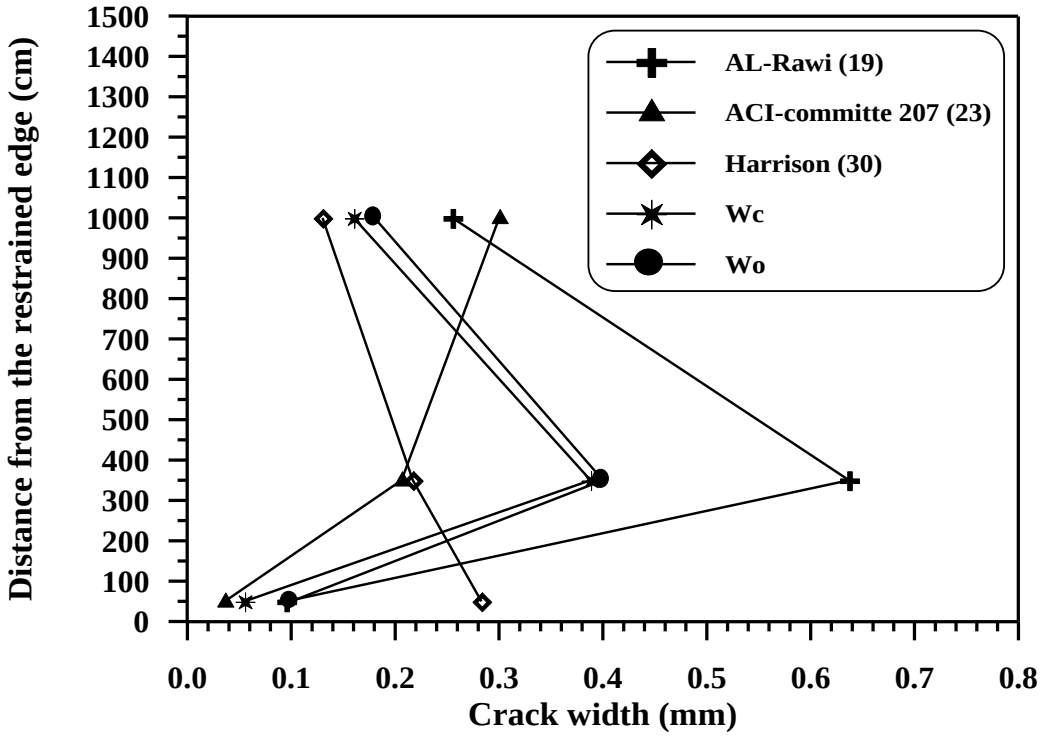

Figure (٥-٢٦): Comparison of the observed and calculated maximum crack width at different levels in site observed four end restrained slab.

٥.٥ Shrinkage Before, During and After Burning

The values of restrained shrinkage of the reinforced concrete free slab before, during and after exposure of fire flame are shown in Table [٥.١٥], and plotted in Figure (٥-٢٧) against age. Figure (٥-٢٨) shows the restrained shrinkage strain of this slab during burning at temperature ٦٠٠^{o}C for period of exposure of (١.٥ hour), at three rows (٢.٥, ٢٥ and ١١٢.٥) cm from the edge of the slab.

From Figure (٥-٢٧), it can be seen that the test results for shrinkage increasing before burning, decreasing during exposure to fire flame and then increasing after burning until constant at the later ages (after ٣٠ days).

The values of drying shrinkage at age of ٦٠ days before burning were added to each corresponding shrinkage value after burning to plot the Figure (٥-٢٩).

Figures (٥-٣٠ and ٥-٣١), it is obvious that the comparison between shrinkage development of the slab before and after exposure to fire flame

with age. From these figures it can be concluded that the shrinkage strain at ٦٠ days age before burning was higher than that the shrinkage strain at ٦٠ days age after burning. It can also be seen from the above figures that the rate of shrinkage strain after burning is greater compared to that before burning during the early ages. A similar trend has been observed by many researchers [٣٧, ٦٢].

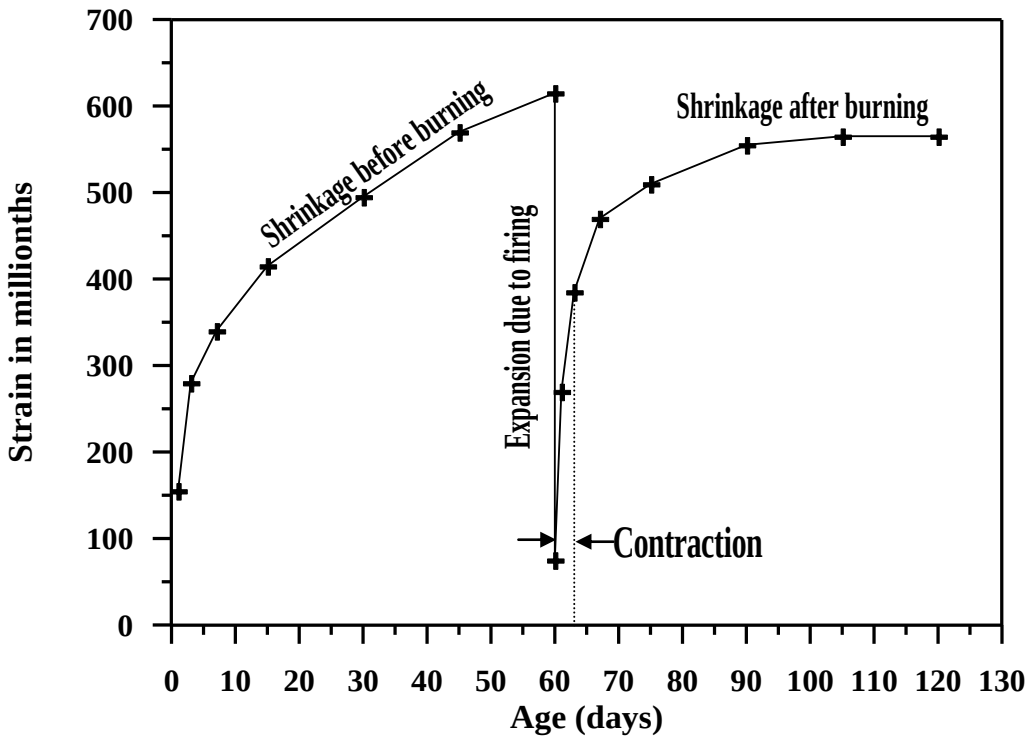

Figure (٥-٢٧): Relation between strain before, during and after burning of the reinforced concrete free slab.

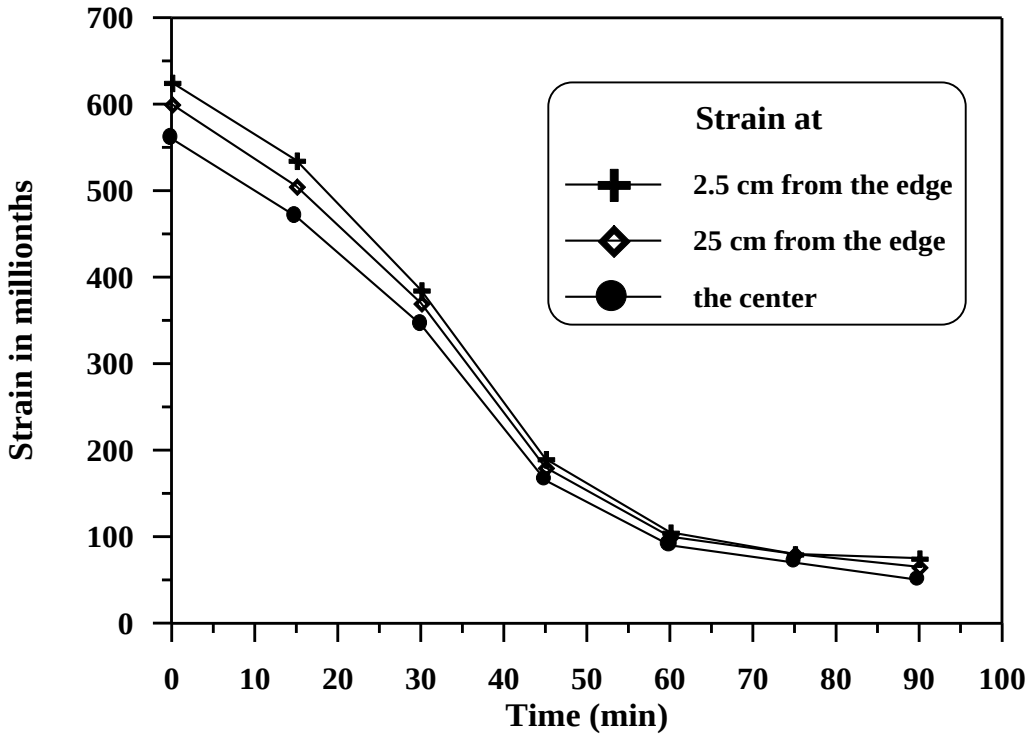

Figure (٥-٢٨): Measured strain of the reinforced concrete free slab width time during exposure to fire flame.

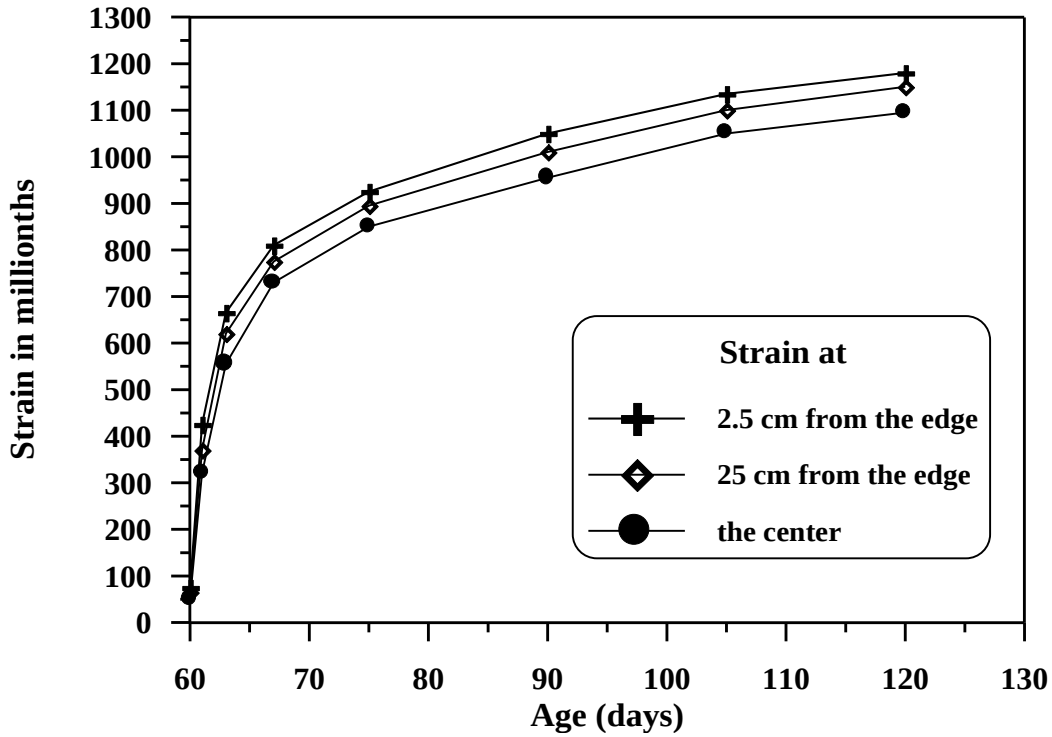

Figure (٥.٢٩): Relation between additional shrinkage before and after burning with age of reinforced concrete slab.

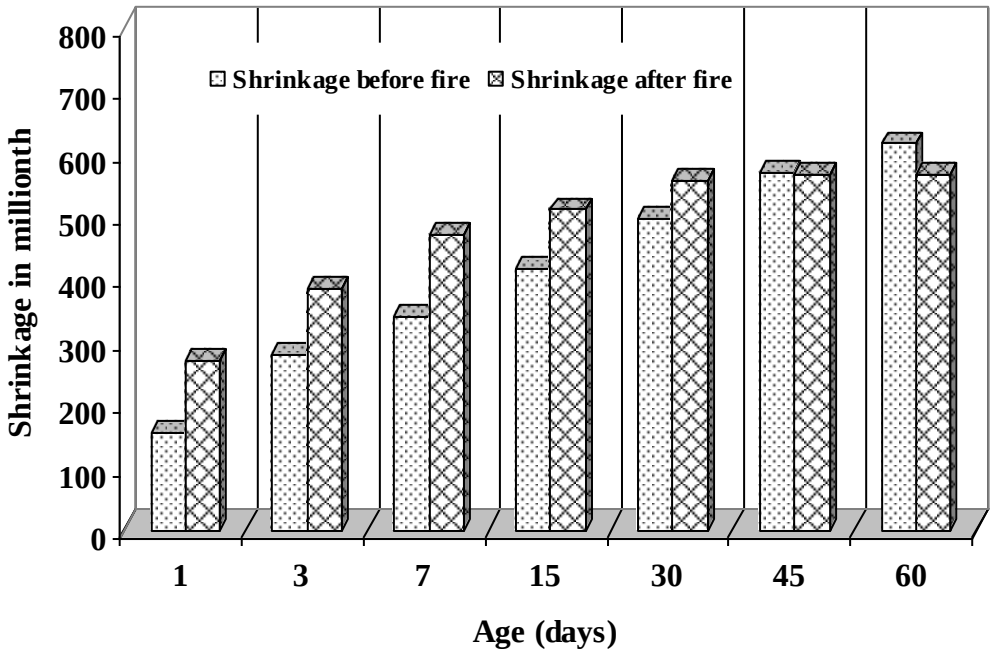

Figure (٥-٣٠): Relation between shrinkage and age at ٢.٥cm from the edge of the reinforced concrete free slab before and after exposure to fire

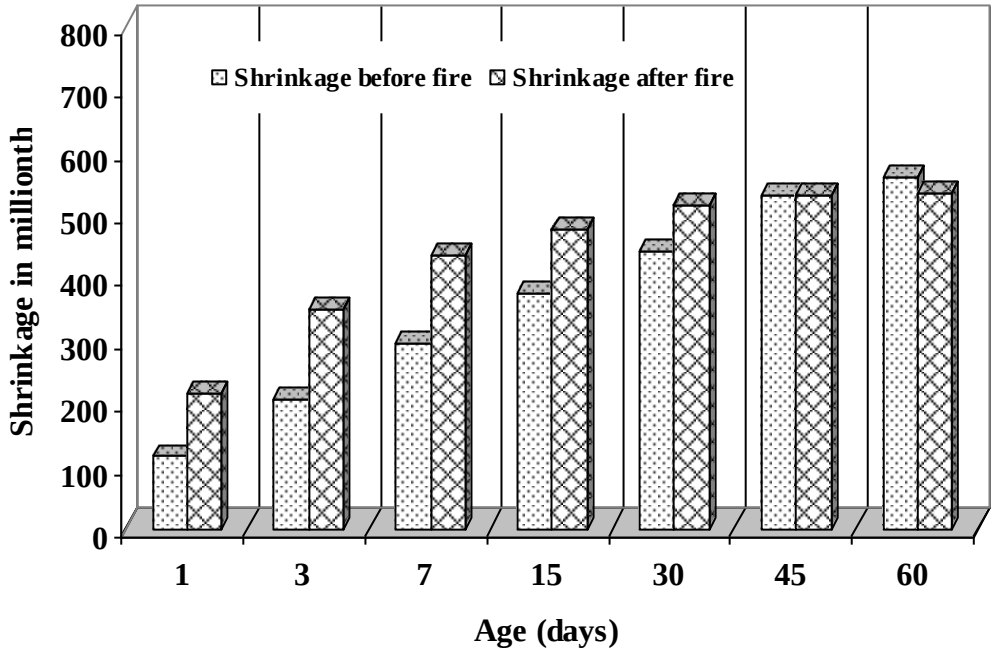

Figure (٥-٣١): Relation between shrinkage and age at the center of the reinforced concrete free slab before and after exposure to fire flame.

٥.٦ Surface Conditions and Fire Endurance of Tested Slab

The aim of design for fire safety should be to limit damage due to fire. The unexposed surface of each tested slab was observed throughout ١.٥ hr fire test. In the four tested slabs more cracks developed from the edge of these slabs towards the center during exposure to fire flame.

At the exposed surface, as exposure to fire flames continued more cracks appeared and propagated towards the edge of the slab and stopped at about ١٠-٢٠ cm distance from these edges. The main drying shrinkage cracks which appeared before burning proceeded and widened due to burning as well as initiating new cracks which appeared due to burning at upper and lower surface of the slab. These crack developments were noticed accompanied with deflection development. Cracking through the depth was observed at approx. (٧٠, ٧٨ and ٨٥ min) for (two, three and four end restrained) of reinforced concrete slabs respectively.

Figure (٥-٣٢) shows the temperature-time curves for the exposed, mid-depth and unexposed surface for slab. At the beginning the slabs are at room temperature, measured to be ٢٣^{o}C. The experimental results clearly indicate that the temperature near the surface to fire is higher and decreases towards the top of the slab thickness similar behavior was observed by other investigators [٤٧, ٤٨ , ١٠٨].

Fire endurance periods are determined normally by physical tests conducted according to the provisions of ASTM E١١٩-٨٨ [٤٦]. Under this standard, the fire endurance of a member or assembly is determined by the time required to reach any of the following three end points: [٤٦]

١- The passage or propagation of flame to the unexposed surface of the test assembly;

٢- A temperature rise of ١٦٣^{o}C at a single point or ١٢١^{o}C as an average on the unexposed surface of the test assembly; and

٣- Failure to carry the applied design load or structural collapse.

Based on the results of this work, it was noticed that the test results agreed with (ASTM E١١٩) [٤٦]. While, these slabs were subjected under fire exposure to fire flame temperature of (٦٠٠^{o}C) at ١.٥ hr, the fire endurance of all the slabs investigated was reached when the average temperature rise of the unexposed surface exceeded the allowable (١٢١^{o}C), then these slabs were considered failed according to ASTM E١١٩ [٤٦]. Similar results of the endurance for slab thickness (١٠cm) were obtained by others [٤٤,١٠٩].

Also, based on the results obtained, it was found that the fire endurance of reinforced concrete slabs increases as the restraining force increases (٠.٨,١.١٥,١.٣ and ١.٤) hr for (free, two, three and four end restrained) respectively. This conclusion is in a good agreement with that obtained by Salse and Lin [٤٣].

Finally, results indicate that the fire endurance is imposed by increasing the restraint on these slabs.

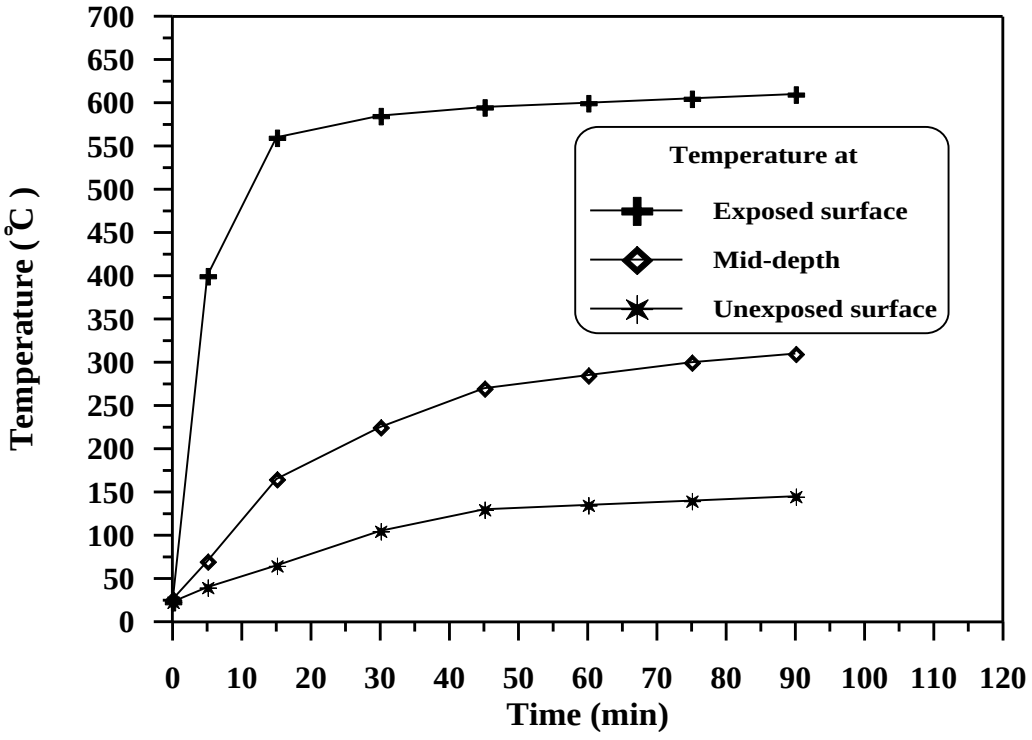

Figure (٥-٣٢): Slab temperature as a function of time at various depths (Slab thickness: ١٠cm) .

٥.٧ Deflection Behavior of Reinforced Concrete Slabs

The mid span deflection of these slabs was measured throughout each test. Because of the differences in restrained cases for these slabs, differences in mid span deflection of these slabs were expected. Deflection of these slabs which occurs immediately when were subjected to fire flame temperature of (٦٠٠^{o}C) for (٩٠ min) period of exposure was measured. This deflection is called immediate deflection or short-term deflection or instantaneous deflection. The principal factors that influence this type of deflection are the span length, conditions of end restraint, magnitude and distribution of the load, section properties including steel percentage and material properties [١١٠]. In the present work, deflection due to the influence of fire only without any applied load was measured.

The test results for mid span deflection during and after exposure to fire flame are summarized in Table (٥-١٦), and the relation between the deflection during burning and time is illustrated in Figure (٥-٣٣), the temperature at the lower surface is about ٦٠٠^{o}C. From this figure it can be noticed that the rate of deflection increases rapidly during the early minutes of fire test, then remains nearly constant for the latter period of exposure to fire flame, this phenomena was observed only for free and two end restrained slabs. While, the rate of deflection of three and four end restrained increases slowly during the early minutes period of exposure, then increases rapidly for the latter period of exposure to fire flame. This can be attributed to the early cracking and lower modulus of elasticity for each slab tested, on the other hand to the number restraint beams. This note agrees with the conclusions of other researchers [٣٩ , ٤٨].

Figure (٥-٣٤) shows the mid span deflection with age for all the slabs after exposure to fire flame. From this figure, it is obvious that the deflection of free end restrained slab during (٢٤ hr) after burning decreases more rapidly if compared with four end restrained, whereas, two and three

end restrained slabs behave in between. Based on the results obtained, it can be concluded that the deflection of slabs is highly sensitive to the restraint under and after exposure to fire flame.

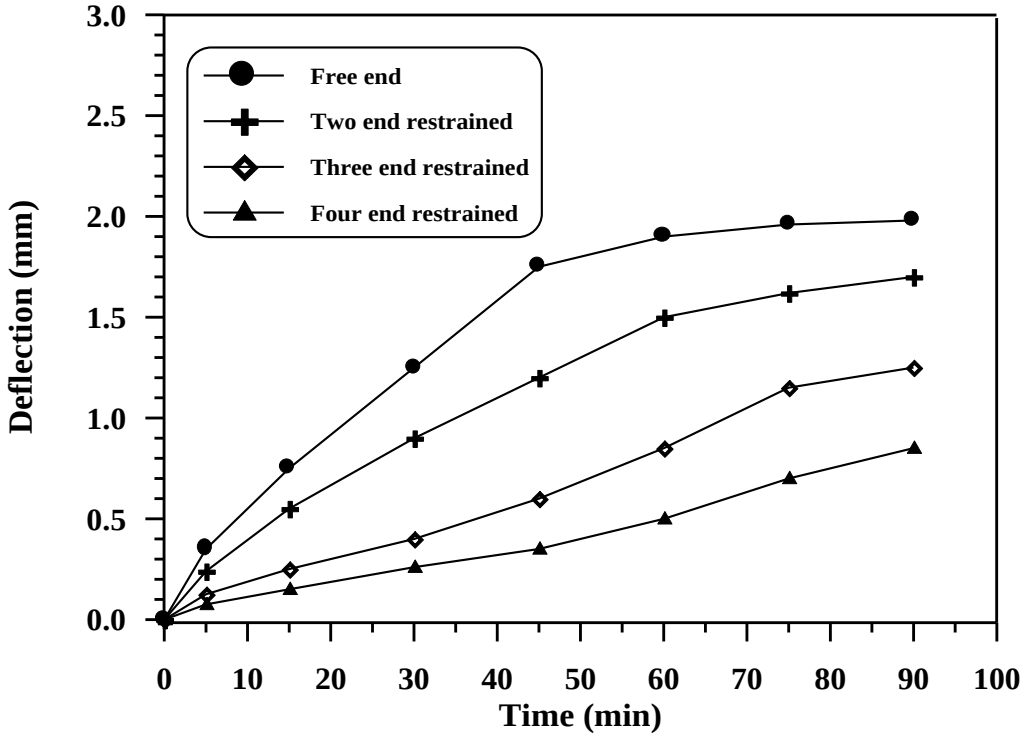

Figure (٥-٣٣): Relation between mid-span deflection of reinforced concrete slabs with time during exposure to fire flame.

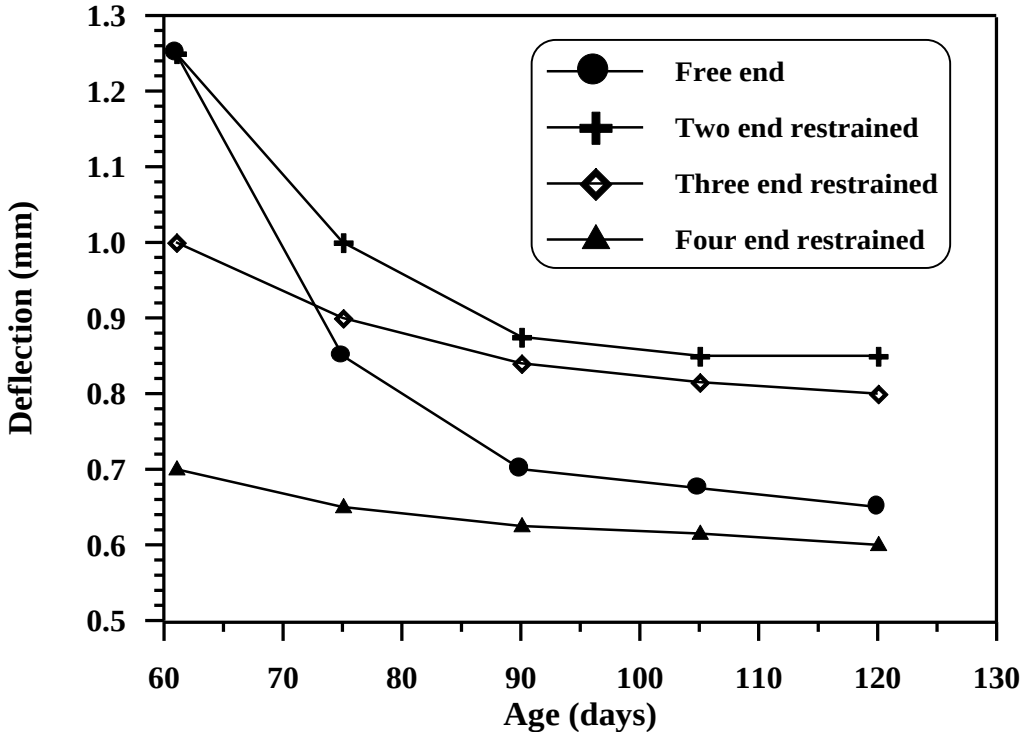

Figure (٥-٣٤): Relation between mid-span deflection of reinforced concrete slabs with age after exposure to fire flame.

Table (٥-١٦): Measured deflection at mid-span of the reinforced concrete slabs during and after burning.

A-During exposure to fire flame.

Time (min)	Deflection (mm)			
	Free slab	Two end restrained	Three end restrained	Four end restrained
٠	٠	٠	٠	٠
٥	٠.٣٥	٠.٢٤	٠.١٢٥	٠.٠٧٥
١٥	٠.٧٥	٠.٥٥	٠.٢٥	٠.١٥
٣٠	١.٢٥	٠.٩	٠.٤	٠.٢٦
٤٥	١.٧٥	١.٢	٠.٦	٠.٣٥
٦٠	١.٩	١.٥	٠.٨٥	٠.٥
٧٥	١.٩٦	١.٦٢	١.١٥	٠.٧
٩٠	١.٩٨	١.٧	١.٢٥	٠.٨٥

B-After exposure to fire flame

Age (days)	Deflection (mm)			
	Free slab	Two end restrained	Three end restrained	Four end restrained
٦١	١.٢٥	١.٢٥	١	٠.٧
٧٥	٠.٨٥	١	٠.٩	٠.٦٥
٩٠	٠.٧	٠.٨٧٥	٠.٨٤	٠.٦٢٥
١٠٥	٠.٦٧٥	٠.٨٥	٠.٨١٥	٠.٦١٥
١٢٠	٠.٦٥	٠.٨٥	٠.٨	٠.٦

٥.٨ The Effect of Fire Flame on the Reinforcing Steel Bars

The effect of fire flame on the properties of reinforcing steel bars is summarized in Table (٥-١٧). At ٦٠٠^{o}C, both burning and subsequent cooling was observed to have little effect on mechanical properties of the reinforcing steel bars. The residuals in the yield stress and in the ultimate stress were (٩٠.٥٪ and ٩١.٨٪) respectively for the bar ١٠ mm diameter. The modulus of elasticity was not affected by burning and cooling at this temperature. Similar behavior was observed by others [٣٤, ٣٩,٤٨, ١١١].

Table (٥-١٧): The effect of fire flame on properties of steel bars.

Bar diameter (mm)	Exposure temp. (^{o}C)		Yield stress N/mm^{٢}		Residual stress %		Ultimate stress N/mm^{٢}		Residual stress %		Modulus of elasticity Es(GPa)		Residual %	
	**	*	**	*	**	*	**	*	**	*	**	*	**	*

١٠	٢٣	٢٥	٤٢٥	٤٤٥	١٠٠	١٠٠	٦٤٩.٥	٦٧٢	١٠٠	١٠٠	٢١٠	٢١٠	١٠٠	١٠.٠
	٦٠٠	٦٠٠	٣٨٤.٦	٤٠٧	٩٠.٥	٨٩	٥٩٨.٤	٦٢٩.٥	٩١.٨	٩١.٧	٢١٠	٢١٠	١٠٠	١٠.٠

** **Present study.** * **Hidayat, (Ref.٤٨).**

CHAPTER SIX

ANALYTICAL RESULTS AND DISCUSSION

٦.١ Introduction

The present chapter deals with theoretical representation of the problem. The finite element method is applied to represent shrinkage cracking for some different restrained cases of reinforced concrete slabs. The results obtained experimentally were compared with the results obtained by finite element analysis. Table (٦-١) gives the details of the material properties that are used in the analysis.

The required data for applying the ACI-Committee ٢٠٩ equations [٧] [Appendix (B)] to predict shrinkage and creep values in the slabs investigated are used as follows:

t_o=٧day; S=١٨٠ mm; f=٠.٣٧٥; A=٤٪; B=٥٤٥ kg/m^3; Hu=٤٠٪. The thickness of the slabs and duration of drying are equal to (٠.١ m) and (٦٠) days respectively.

During analysis if the tensile strain in the element reaches (١٤٥*١٠$^{-٦}$) cracking is assumed to initiate.

Onset of crack, tensile stress in reinforced concrete element will drop to direct tensile strength estimated from Eq.(٤-١٩).

A tolerance of ٢.٥٪ has been used to monitor the convergence of the finite element solutions. Number of elements and nodes which are used to solve these cases are (١٧٦, ٢٠٤) respectively.

Table (٦-١): Material properties of the reinforced concrete slabs investigated.

Material Properties		Value
Concrete	Young's modulus, Ec, GPa	٢٥.٤
	Compressive strength, f_c', MPa	٣٢.٥
	Tensile strength, f_t', MPa	٣.٤٣
	Poisson's ratio, v	٠.١٧
Steel	Young's modulus, Es, GPa	٢١٠
	Yield strength, fy, MPa	٤٢٥
	Diameter of all bars (mm)	١٠
	Reinforcement ratio, ρx,%	٠.٤٢
	Reinforcement ratio, ρy,%	٠.٤٢

٦.٢ Sequence of Cracking

Theoretically the first crack usually occurs at the mid of the restrained edge slab length, since the restraint is highest at this position of three and four edge restrained slab. Also, the first crack usually occurs at the weakest section in the free edges in two end restrained slab. As each new crack forms at approximately the mid point of the uncrack portions of the slab, the previously formed cracks will propagate vertically [٧٨]. Hence, the first crack propagates and new cracks initiate at approximately mid length of the uncracked portions of the slab. This sequence of cracking is shown in Figures (٦-١) and (٦-٢).

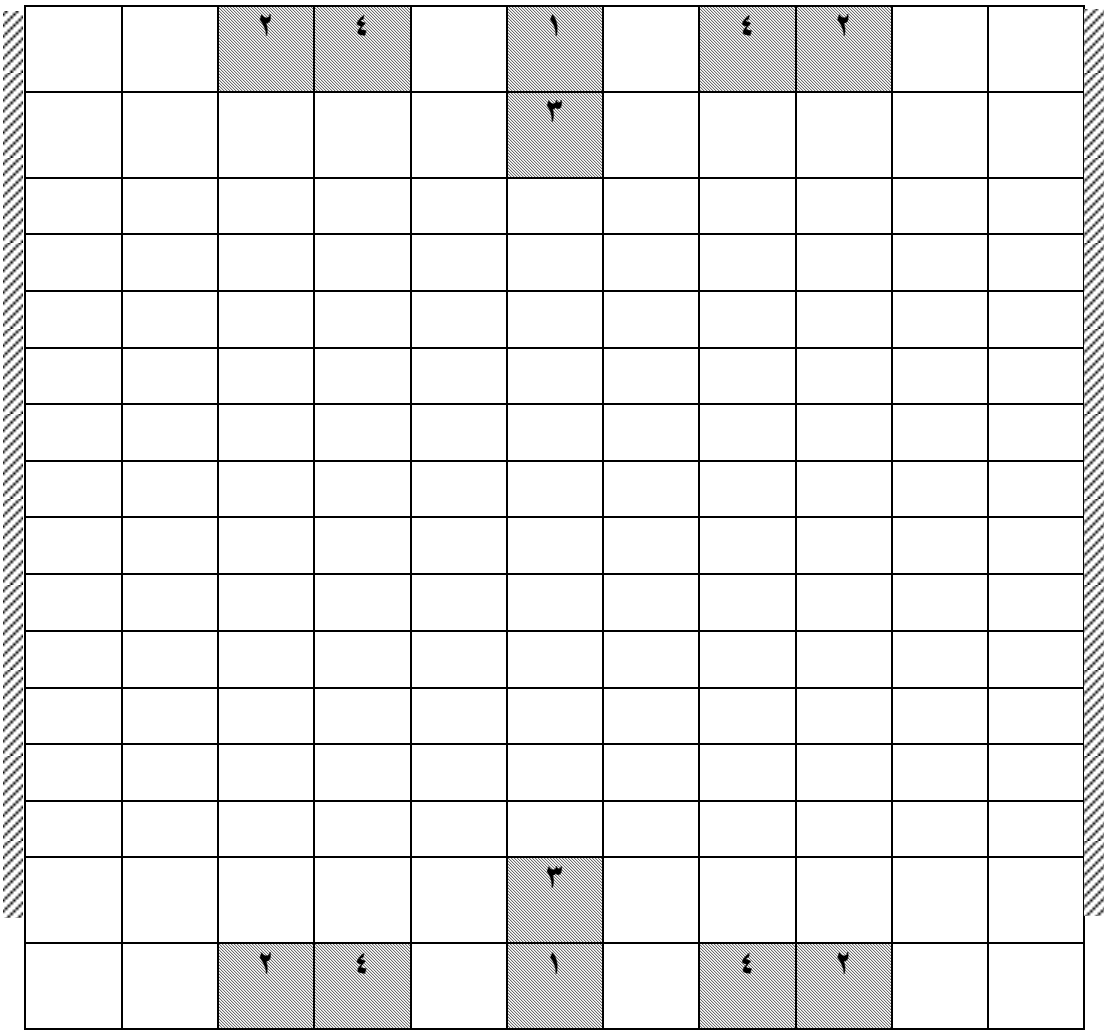

Figure (٦-١): Theoretical sequence of crack propagation for two end restrained reinforced concrete slab.

Table (٦-٢): Theoretical crack data for two end restrained of reinforced concrete slab.

Element No.	Date of cracking (days)	Strain in concrete ⊗ * ١٠-٦	Spacing (mm)	Crack width (mm)
١	٢٠.٢٥٠	٦٨٤.٨٩١	٤٠٩.١٠	٠.١٤٠١
٢	٢٦.٨٥٧	٥٣٩.٥٩٢	٣٥٧.٩٦٣	٠.١١٠٤
٣	٢٨.٥٤٨	٢٦٣.٦٦٧	١١٢٥.٠	٠.٠٥٤
٤	٣١.٦٧٢	٥٥٥.٨٨	٣٠٦.٨٢٥	٠.١١٣٧

⊗ **At (٦٠) days after curing duration.**

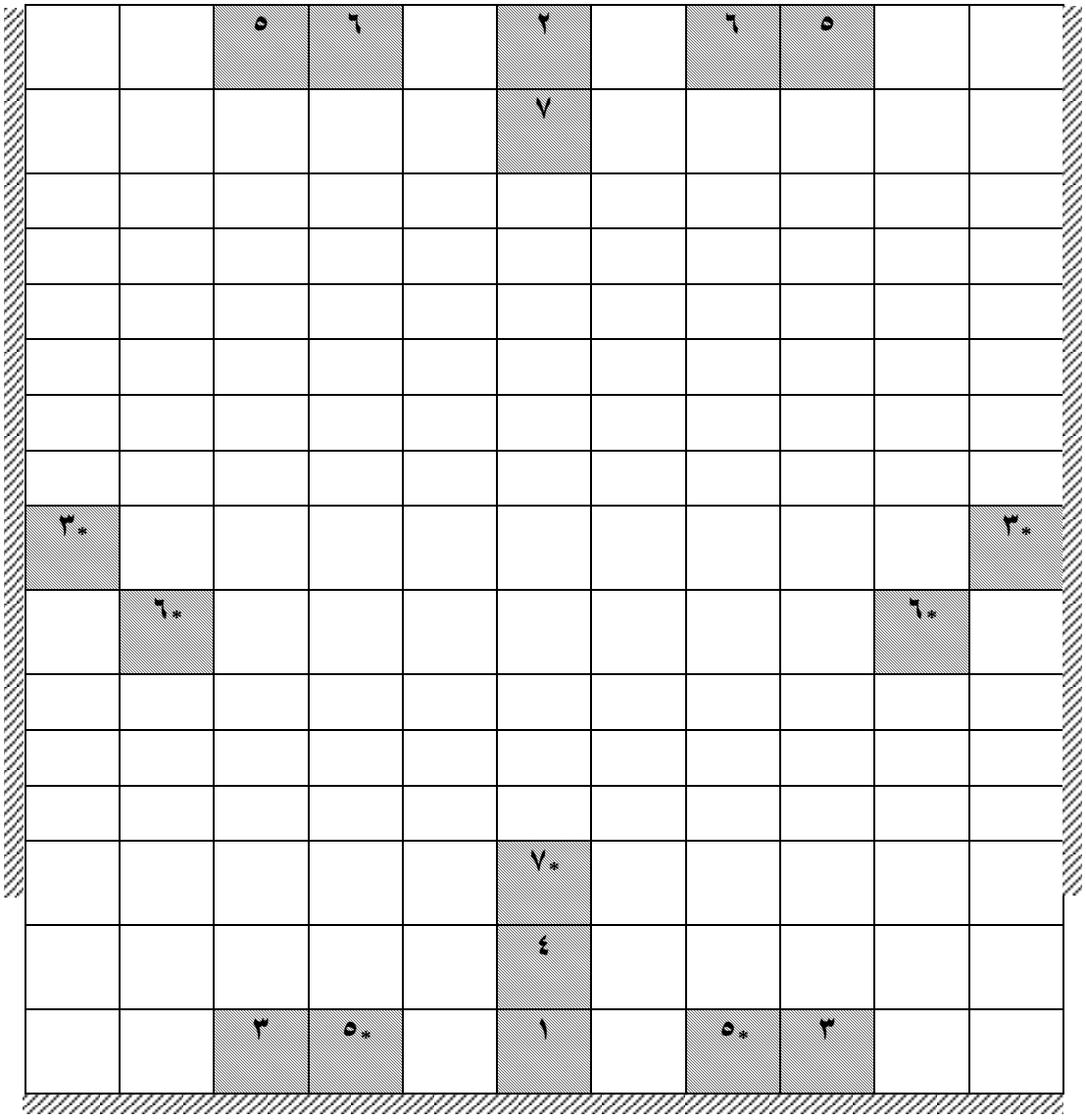

Figure (٦-٢): Theoretical sequence of crack propagation for three end restrained reinforced concrete slab.

Table (٦-٣): Theoretical crack data for three end restrained of reinforced concrete slab.

Element No.	Date of cracking (days)	Strain in concrete $\otimes$ * ١٠$^{-٦}$	Spacing (mm)	Crack width (mm)
١	١٧.٧٢٥	٣١٤.٩٨٥	٤٠٩.١٠	٠.٠٧٥٦
٢	٢١.٨٤٢	٦٣٥.٧٦٢	٤٠٩.١٠	٠.١٣٠
٣	٢٣.٢٥٥	٢٩٢.٨١٥	٣٥٧.٩٦٣	٠.٠٥٩٩
٣*	٢٣.٢٥٥	٢٧٥.٩٤٠	١١٢٥.٠	٠.٠٣٨٨

٤	٢٤.٦٩٠	٧٣٨.٧٨٨	١١٢٥.٠	٠.١٥٥٢
٥	٣١.٤٧٥	٥٨٩.٨٦١	٣٥٧.٩٦٣	٠.١٢٠٧
٥*	٣١.٤٧٥	٢٦١.١٥٥	٣٠٦.٨٢٥	٠.٠٥٤٤
٦	٣٣.١٢٦	٥٧٧.٩٥٢	٣٠٦.٨٢٥	٠.١١٨٣
٦*	٣٣.١٢٦	٤٤٠.٦٤٠	١١٢٥.٠	٠.٠٦٢
٧	٣٦.٧٦١	٢٧٩.٤٤٩	١١٢٥.٠	٠.٠٥٧٢
٧*	٣٦.٧٦١	١٩٢.٦٤٨	١١٢٥.٠	٠.٠٣٩٤

⊗ At (٦٠) days after curing duration.

Table (٦-٢) and (٦-٣) show the average distance between cracked elements at the end of the drying duration studied. Figures (٦-٣) and (٦-٤) give the minimum spacing between cracks at the end of drying duration for two and three end restrained reinforced concrete slabs respectively. It is obvious from these figures that the minimum spacing between cracks increases with its distance from the edge. It can also be seen that the minimum crack spacing using finite element analysis is greater than calculated using Eq.(٥-٣) and (٥-٥) and experimental work.

It can be seen from Figure (٦-٣) that the theoretical results of minimum crack spacing for two end restrained using Eq.(٥-٣) is closer to the experimental results than theoretical using finite element analysis. Whereas, in three end restrained Figure (٦-٤), it can be seen that the minimum crack spacing at the restrained edge using Eq.(٥-٥) is closer to the experimental results at the first stage of distance from the restrained edge, while that of finite element analysis closes better to the experimental results at the second stage.

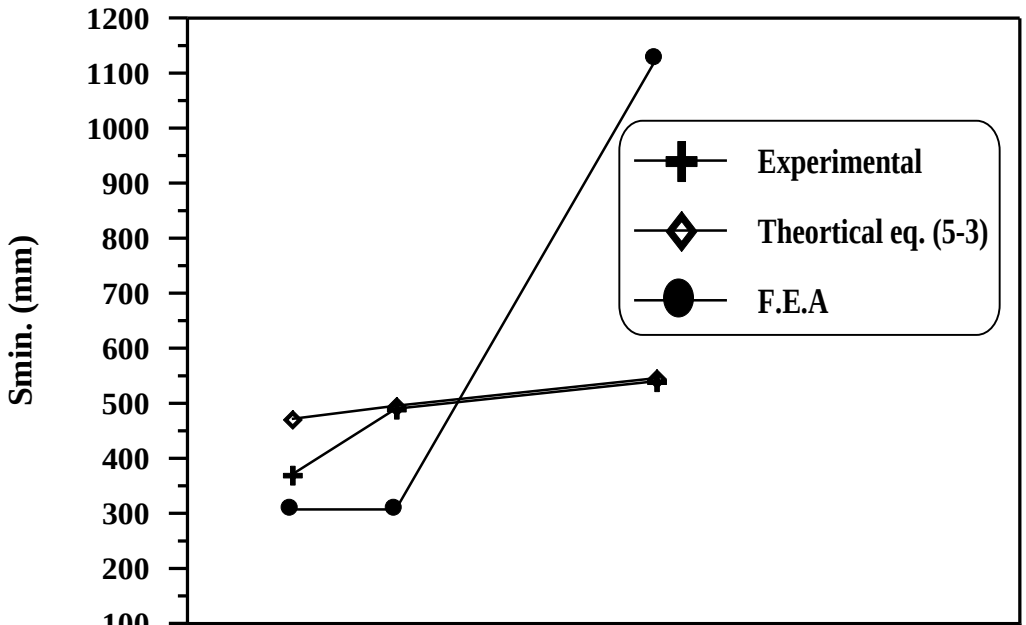

Figure (٦-٣): Experimental ,theoretical and finite element analysis(F.E.A),(Smin) with distance from free edge for two end restrained of reinforced concrete slab.

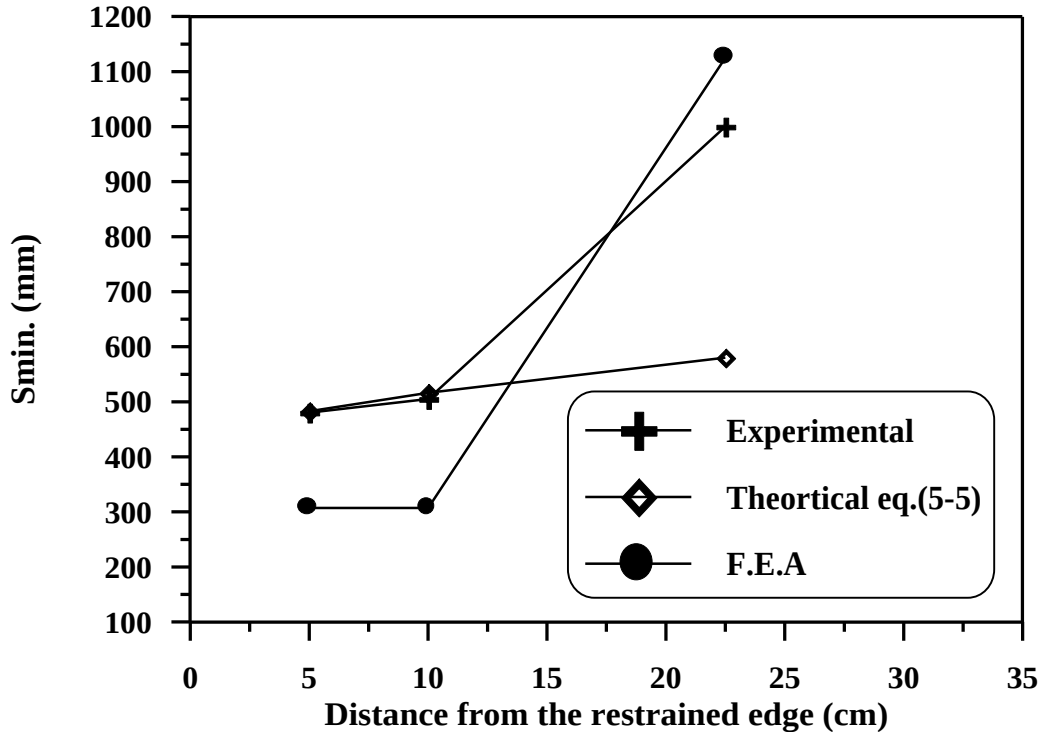

Figure (٦-٤): Experimental theoretical and finite element analysis (F.EA),(Smin) with distance from the restrained edge for three end restrained of reinforced concrete slab.

٦.٣ Crack Width

Tables (٦-٢) and (٦-٣) show the cracking data for two and three end restrained of reinforced concrete slabs respectively. These tables show the average distance between cracked elements at the end of the drying duration studied. Also, the values of crack width given in these tables are calculated by multiplying the element width by the strain which is calculated in the center of the cracked element.

The crack width at any level in the slab is simply a function of the amount of the tensile strain formerly carried by concrete and relieved by the process of cracking. In other words, the crack width at any level of the slab is proportional to the difference between the restrained shrinkage strain and the tensile strain capacity of concrete.

Figure (٦-٥) shows the development of crack length with time. From this figure, it is obvious that the (increasing the end restraint) increases the propagation of any crack which permits other cracks to initiate on both sides of that crack. It can be seen that the increase in restraint will cause to increase the length of cracks at the end of the drying period.

Figure (٦-٦) shows the variation in the width of the middle crack with its relative length and for different restrained cases. It can be seen from this figure that there is a decrease in the middle crack width with decreasing of the number of restrained edges.

Table (٦-٤) gives the crack widths calculated according to the present finite element procedure and the results obtained from the present experimental work. From comparing the values of crack width at a certain level from the edge, it can be seen that there is a reasonable agreement between the experimental results and the theoretical results.

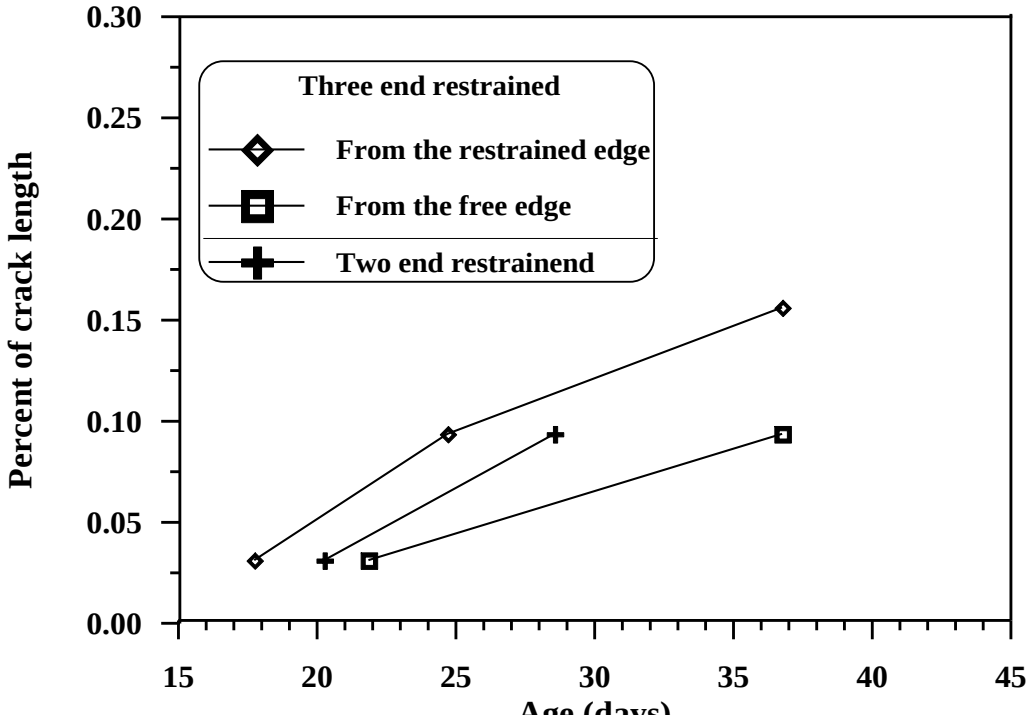

Figure (٦-٥): Middle crack propagation for different restrained cases of reinforced concrete slabs.

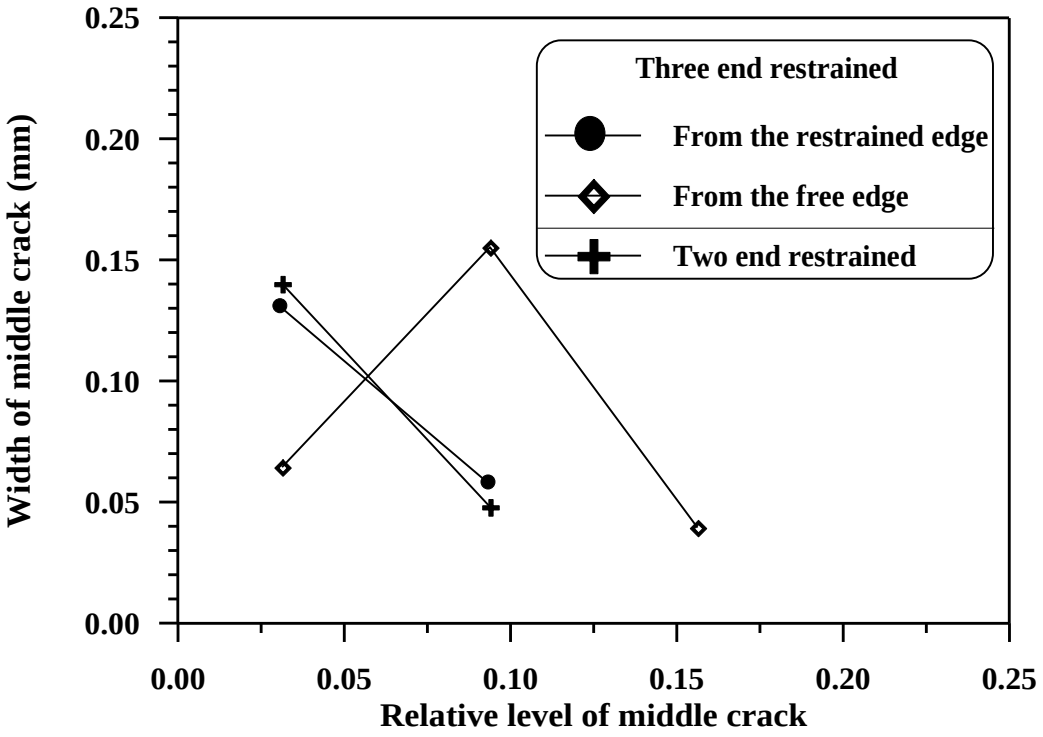

Figure (٦-٦): Width of middle crack versus its relative level with different restrained cases of reinforced concrete slabs.

Table (٦-٤): Calculated crack width at different level for different restrained cases of reinforced concrete slabs.

Slabs		Level %	Crack width (mm)	
			Experimental	Theoretical
Two end restrained		٠.٠٣١٢٥	٠.١٧٠	٠.١٤٠
		٠.٠٩٣٧٥	٠.٠٦	٠.٠٥٤٣
Three end restrained	From the restrained edge	٠.٠٣١٢٥	٠.١٢٠	٠.٠٧٥٦

		٠.٠٩٣٧٥	٠.١٤٥	٠.١٥٥٢
		٠.١٥٦٢٥	٠	٠.٠١١
	From free edge	٠.٠٣١٢٥	٠.١٢	٠.١٣٠
		٠.٠٩٣٧٥	٠.٠٤٥	٠.٠٥٧٢

CHAPTER SEVEN

CONCLUSIONS AND FUTURE WORKS

٧.١ Introduction

Based on the test results and theoretical analysis of the present work, the following conclusions can be drawn: -

١ Cracks in end restrained slabs have a certain width at the restrained edge before and after burning. As the distance from the restrained edge increases, the crack width increases up to (٢٠٪-٥٠٪) and (١٥٪-٣٨٪) of the crack length before and after exposure to fire flame respectively, then the width decreases to zero at the tip of the crack. But, the cracks which appeared from the free edge have a maximum crack width at the edge and decreases to zero towards the center of the slab before and after exposure to fire flame.

٢ The crack width in end restrained members is variable with its length, and its variation depends on the degree of restraint in the slab before and after cracking.

٣ Experimental and theoretical results show that the shrinkage cracks in end restrained slabs are numerous in the proximity of the edge and decrease away from the edge. It appears that the minimum crack spacing for shrinkage cracks decreases linearly with the distance (D) from the edge.

٤ Based on experimental results, an equation to estimate crack width in slabs after burning was suggested as follows:

$$W_{\max} = (T_d - T_b)\alpha_c L K$$

This equation gave a good agreement with the observed crack width in the experimental work.

٥ The predicted values of maximum crack width using the present method and those proposed by various previous researchers and bodies were compared with experimental and site observed data on reinforced concrete slabs. This comparison shows that the present method gives the closest results to the observed crack widths in both experimental and actual size slabs.

٦ The cracking tendency of concrete was seen to be affected by the restraint. Cracking time decreases with increased restraint, since cracking time (١٦, ٢١) days for four and two end restrained reinforced concrete slabs respectively.

٧ The limit of shrinkage crack width in reinforced concrete slabs is associated with the reduction in maximum crack length (L_c), and delaying in cracking age.

٨ The unexposed surface temperature increases as the exposure time increases. The unexposed surface temperature reaches a limit of (١٢١^{o}C) at which the slab is considered to have failed as specified in ASTM-E١١٩. It was noticed in the experimental work that this limit of temperature could be raised to ١٣٣^{o}C.

٩ The temperature distribution through the thickness of slab that was found in this investigation is similar for all the slabs, which have the same thickness and exposed period to fire flame. The results obtained show a good agreement with ASTM-E١١٩ specifications.

١٠ It was noticed that the fire endurance of the reinforced concrete slab increases when the slab restraint is more.

١١ Fire endurance of four end restrained slab is larger by (٤٣٪) than that of free end slab for the same temperature and slab thickness.

١٢ Based on the results obtained, it was found that the mid-span slab deflection was highly sensitive to the restraint under exposure to fire flame. The increase in restraint causes a decrease in deflection of reinforced concrete slabs, where the deflection of free end slab was larger by (٥٧٪) than that of four end restrained slab for the same exposure conditions such as temperature (٦٠٠^{o}C) and duration (١.٥ hr).

١٣ The experimental results clearly indicate that the cracks are developed

in reinforced concrete slabs during (١.٥ hr) period of exposure to fire flame temperature (٦٠٠^{o}C), and these cracks remain open even after cooling, i.e. the contraction of concrete and steel are insufficient to close the cracks. From observation of the experimental work, some cracks may close due to contraction of concrete and steel this phenomena occurs especially in the free slab.

١٤ The sequence of cracking, crack spacing and crack width show a resonable agreement with the test results, finite element analysis and theoretical results.

٧.٢ Recommendations and Further Works

To extend and complete the present investigation, the following recommendations are made for further work:

- Research is required to studying the combination effect of the fire flame and load on the behavior of reinforced concrete slabs with different restrained cases.
- Studying the effect of rainy-weather (wetting and drying) on the cracks behavior of reinforced concrete slabs with different restrained cases before and after exposure to fire flame.
- Considering thermal strains in the analysis.
- The two – dimensional finite element analysis can be developed to three dimensional finite element analysis.
- Using ٨-node element in the computer program.

APPENDIX A

EXPERIMENTAL DATA

Table (A-١) : Physical properties of the cement.

Physical properties	Test results	I.O.S. ٥ :١٩٨٤[٦٨]: Limits
Fineness , Blain, cm^2/gm	٣٠٩٠	≥ ٢٣٠٠
Setting time, Vicat's method		
Initial hrs : min.	١:٥٧	≥ ١:٠
Final hrs : min.	٣:٢٠	≤ ١٠:٠
Compressive strength of ٧٠.٧ mm cube, MPa		
٣ days	٢٠	≥ ١٥
٧ days	٢٧.٥	≥ ٢٣

Table (A-٢) : Chemical composition of the cement.

Oxide	(%)	I.O.S. ٥: ١٩٨٤[٦٨] Limits
CaO	٦١.٢٦	ـــــ
SiO_2	٢٠.٨٠	ـــــ
Fe_2O_3	٣.٢٠	ـــــ
Al_2O_3	٦.١٢	ـــــ
MgO	٤.٤٠	≤ ٥.٠
SO_3	٢.٣٣	≤ ٢.٨
Free lime	٠.٧٦	ـــــ
L.O.I	١.٧٥	≤ ٤.٠
I.R.	٠.٦١	≤ ١.٥
Compound composition	**(%)**	**I.O.S.٥: ١٩٨٤[٦٨] Limits**
C_3S	٣٨.٧٤	ـــــ
C_2S	٣٠.٥٢	ـــــ
C_3A	٩.٣٢	ـــــ
C_4AF	٩.٧٣	ـــــ
L.S.F	٠.٨٨	٠.٦٦-١.٠٢

Table (A-٣): Properties of the sand

Sieve size (mm)	Percent passing	I.O.S. ٤٥: ١٩٨٤[٦٩] Limits Zone ٣
٩.٥	١٠٠	١٠٠
٤.٧٥	٩٦	٩٠-١٠٠
٢.٣٦	٩٢	٨٥-١٠٠
١.١٨	٨١	٧٥-١٠٠
٠.٦	٥٦	٦٠-٧٩
٠.٣	٢٧	١٢-٤٠
٠.١٥	٠	٠-١٠
Properties	**Test results**	**I.O.S.٤٥ : ١٩٨٤[٦٩] Limits**
Sulphate content, SO_3	٠.٢٦	≤ ٠.٥
Specific gravity	٢.٦٠	____
Absorption (%)	١.٦٠	____

Table (A-٤): Properties of the gravel

Sieve size (mm)	**Percent passing**	**I.O.S. ٤٥: ١٩٨٤[٦٩] Limits**
٣٧.٥	١٠٠	١٠٠
٢٠	١٠٠	٩٥-١٠٠
٩.٥	٥٤	٣٠-٦٠
٤.٧٥	٣	٠-١٠
Properties	**Test results**	**I.O.S.٤٥ : ١٩٨٤[٦٩] Limits**
Sulphate content, SO_3	٠.٠٧	≤ ٠.١
Specific gravity	٢.٦٣	____
Absorption (%)	٠.٨	____

(A)Two end restrained

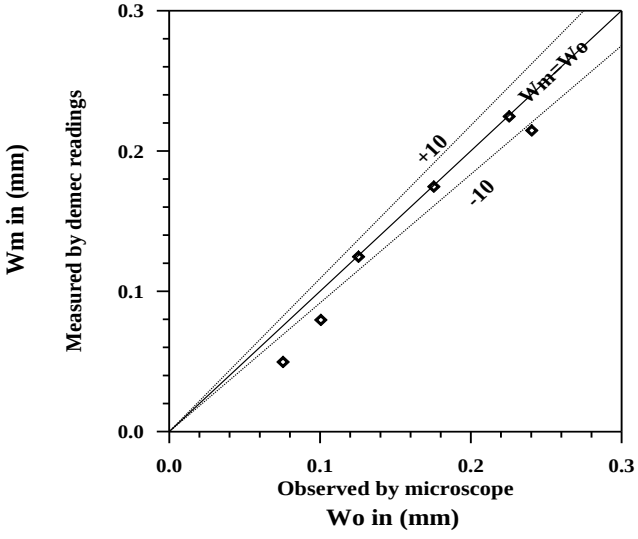

(A) Two end restrained

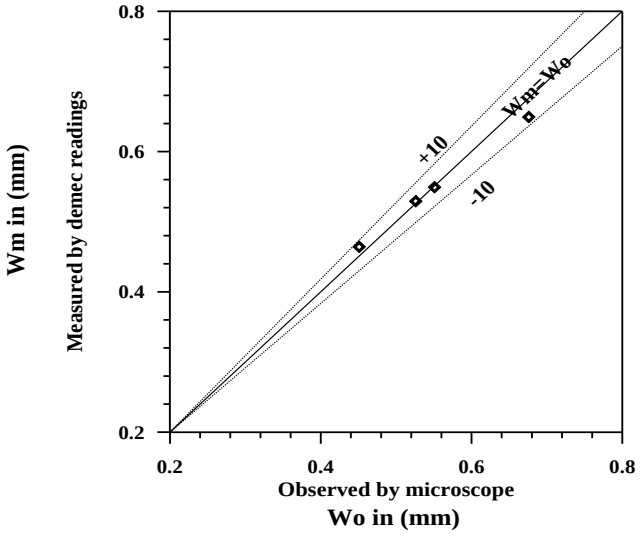

(B) Three end restrained

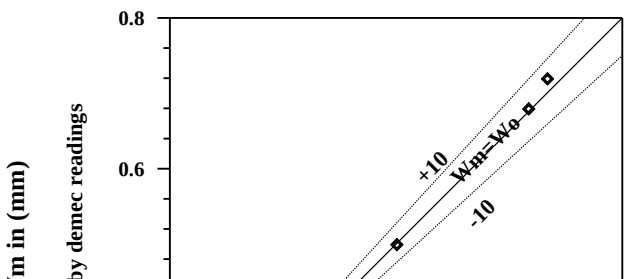

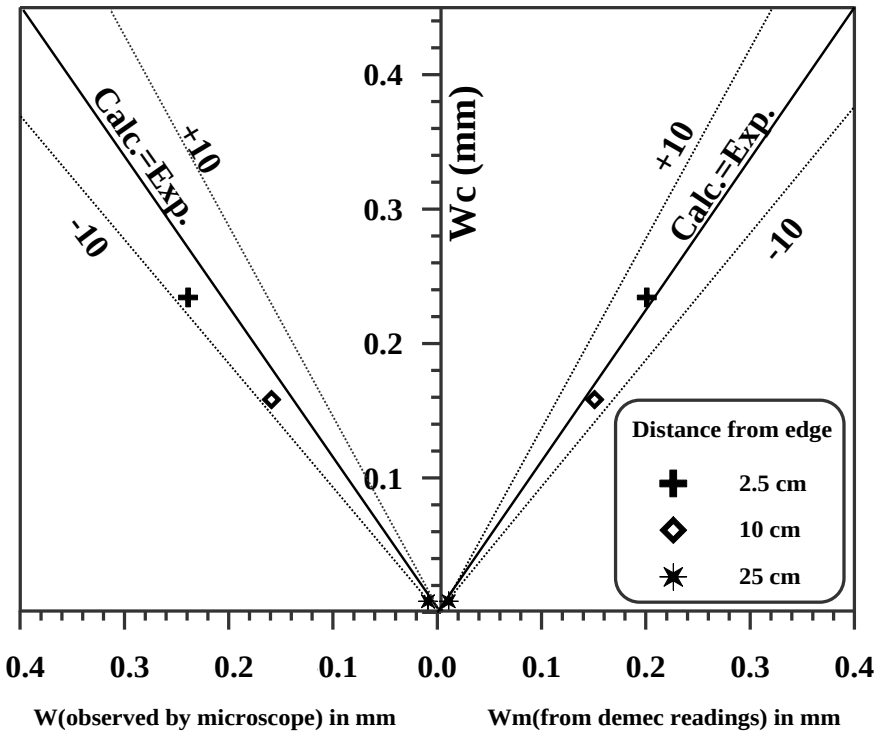

Figure (A-١٠): Comparison between calculated (Wc), observed (Wo) and measured (Wm) crack widths at different levels from the free edge of two end restrained slab.

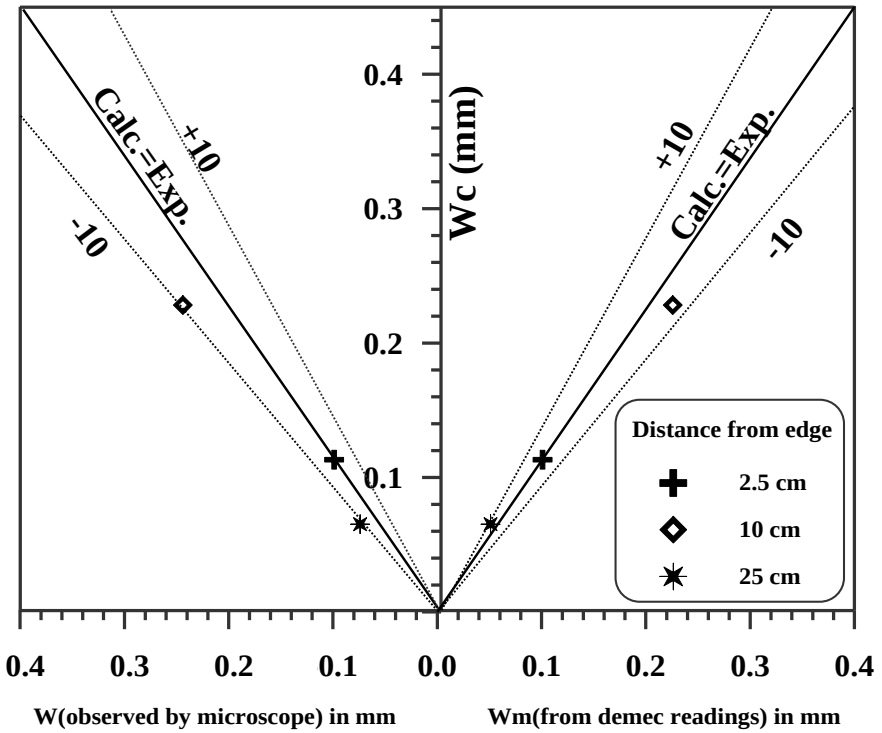

Figure (A-١١): Comparison between calculated (Wc), observed (Wo) and measured (Wm) crack widths at different levels from the restrained edge of three end restrained slab.

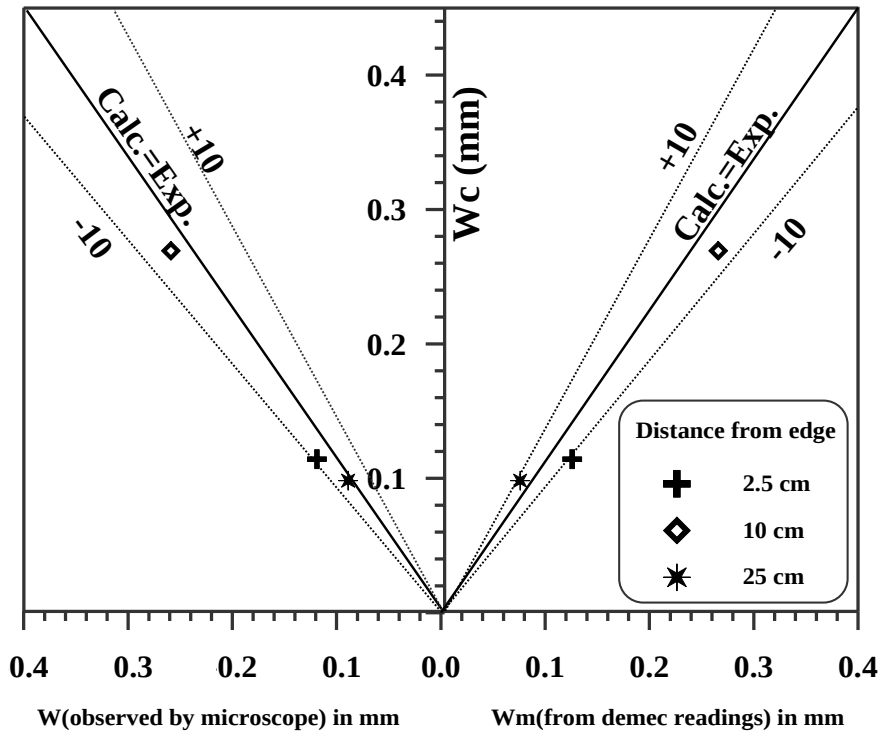

Figure (A-١٢): Comparison between calculated (Wc), observed (Wo) and measured (Wm) crack widths at different levels from the restrained edge of four end restrained slab.

APPENDIX B

The representation models of shrinkage and creep include correction factors other than standard conditions.

CORRECTION FACTORS FOR SHRINKAGE AND CREEP

B-١ Correction factors of shrinkage are:

١- Humidity

$$F_H^s = 1.4 - 0.01H \qquad ٤٠٪ \le H \le ٨٠٪$$

$$= 3.0 - 0.03H \qquad ٨٠٪ \le H \le ١٠٠٪$$

٢- Minimum member thickness (T=mm)

$$F_T^s = 1.23 - 0.0015T \qquad \text{for} \le ١ \text{ year loading}$$

$$= 1.17 - 0.00114T \qquad \text{for ultimate loading}$$

٣- Slump

$$F_S^s = 0.89 + 0.00264S \quad ; \quad (S=mm)$$

٤- Number of ٥٠ kg sacks/١m^3 concrete

$$F_B^s = 0.75 + 0.00061B$$

٥- Fine aggregate

$$F_F^s = 0.3 + 0.014F \qquad F \le ٥٠٪$$

$$= 0.9 + 0.002F \qquad F \ge ٥٠٪$$

٦- Air content

$$F_A^s = 0.95 + 0.008\,A$$

B-٢ Correction factors of creep are:

١- Loading age

$$F_\tau^c = 1.25 \times \tau^{-0.118} \qquad \text{for moist curing}$$

$$= 1.13 \times \tau^{-0.094} \qquad \text{for steam curing}$$

٢- Humidity

$$F_H^c = 1.27 - 0.0067\,H \qquad H \geq ٤٠٪$$

٣- Minimum member thickness (T=mm)

$$F_T^c = 1.14 - 0.00092\,T \qquad \text{for} \leq ١ \text{ year loading}$$

$$= 1.1 - 0.00067T \qquad \text{for ultimate loading}$$

٤- Slump

$$F_S^c = 0.82 + 0.00264\,S \quad ; \quad (S=mm)$$

٥- Percent fines

$$F_F^c = 0.88 + 0.0024\,F$$

٦- Air content

$$F_A^c = 1 \qquad \text{for A} \leq ٦٪$$

$$= 0.46 + 0.09A \qquad \text{for A} > ٦٪$$

APPENDIX C

Saenz Formulation

١٩٦٤, Saenz proposed a mathematical model for the uniaxial compression stress – strain relation for concrete. This formula is easy to apply and it shows good fit with experimental results for both ascending and descending parts of the σ, ε curve because it incorporates several parameters, namely, E, $f_{c'}$, strain at $f_{c'}$ (ε_o),the ultimate stress (σ_u), and the ultimate crushing strain ε_f , Saenz equation has the form

$$\sigma = \frac{E_c \cdot \varepsilon}{A + B + C\varepsilon^2 + D\varepsilon^3} \qquad \text{---------- C-١}$$

where A, B, C, D are coefficient. The conditions to be fulfilled are:

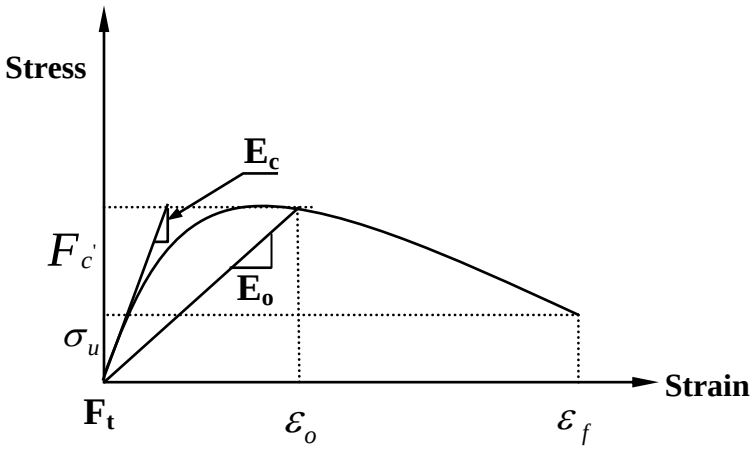

Figure(C-١): Typical $(\sigma - \varepsilon)$ curve for concrete under uniaxial compression.

١- @ $\varepsilon = 0 \Rightarrow \frac{\partial \sigma}{\partial \varepsilon} = E_c$ (value of young modulus)

٢- @ $\varepsilon = \varepsilon_o \Rightarrow \sigma =$ fc' (point of maximum stress)

٣- @ $\varepsilon = \varepsilon_o \Rightarrow \frac{\partial \sigma}{\partial \varepsilon} = 0$ (maximum of the curve)

٤-@ $\varepsilon = \varepsilon_f \Rightarrow \sigma = \sigma_u$ (point of maximum strain)

Fulfilling these conditions, the following coefficients are easily obtained

A=١, $B = \frac{\left(R_E + R - 2\right) E_c}{R_E \ f_c'}$, $C = \frac{-\left(2R - 1\right)}{R_E \ f_c' \varepsilon_o}$, $D = \frac{R E_c}{R_E \ f_c' \varepsilon_o}$ ----------C.(٢-٥)

Where:

$R = \frac{R_E \left(R_\sigma - 1\right)}{\left(R_\varepsilon - 1\right)^2} - \frac{1}{R_\varepsilon}$ (Ratio relation) ---------- C-٦

$R_E = \frac{E_c}{E_o}$ (Modulus ratio) ---------- C-٧

$R_\sigma = \frac{f_{c'}}{\sigma_u}$ (Stress ratio) ---------- C-٨

$R_\varepsilon = \frac{\varepsilon_f}{\varepsilon_o}$ (Strain ratio) ---------- C-٩

$E_o = \frac{f_{c'}}{\varepsilon_o}$ (Secant modulus at $f_{c'}$) ---------- C-١٠

APPENDIX

EXAMPLES

Example -١-

Calculation of maximum crack width at ١٠cm from the free edge of experimental two end restrained reinforced concrete slab: -

By using the information given in the experimental work, these parameters can be written

$-S_{\max}$: Maximum crack spacing, $S_{Max} = 2 \times S_{Min} = 2 \times 0.85 \times K \times \dfrac{d}{(\rho + \rho_R)}$

Where: $\rho_R = 0.9 - 1.1\left(\dfrac{l}{L}\right)^{0.6}$

$$= 0.9 - 1.1\left(\frac{10}{225}\right)^{0.6} = 0.73\%$$

$$\therefore \left(S_{\max} = 2 \times 0.85 \times 0.67 \times \frac{10}{(0.42 + 0.73)\%} = 990mm \right)$$

$-e_{sh}$: Shrinkage strain, $e_{sh} = 700 \times 10^{-6}$ (Figure ٥-١).

$-L.O.R$: Loss of restraint due to ends contraction before cracking.

$L.O.R = 60 \times 10^{-6}$ (Table ٥-١)

$-e_{ult}$: Elastic tensile strain capacity $e_{ult} = 140 \times 10^{-6}$ (Table ٥-١).

The calculated parameters are :

$-e_{shn}$: Net shrinkage strain,

$$e_{shn} = e_{sh} - L.O.R = 700 \times 10^{-6} - 60 \times 10^{-6} = 640 \times 10^{-6}$$

$-\ c_f$ Final creep strain,

$$c_f = 0.6 \times e_{shn} = 0.6 \times 640 \times 10^{-6} = 385 \times 10^{-6}$$

Therefore, the calculated maximum crack width using equation (٥-٧) is:

$$Wc = S_{\max}\left[a \times e_{shn} - b \times c_f - c \times \tfrac{1}{2} \times e_{ult}\right]$$

Where:

$a = -10.06$

$b = -26.92$

$c = 50.22$

$$Wc = 990\left[-10.06 \times 640 \times 10^{-6} + 26.92 \times 385 \times 10^{-6} - 50.22 \times \tfrac{1}{2} \times 150 \times 10^{-6}\right]$$

$$Wc = 0.159mm$$

Whereas the maximum observed crack width, Wo is ٠.١٦mm.

Example -٢-

Calculation of maximum crack width at ٣٥cm from the restrained edge for site observed four end restrained reinforced concrete slab: -

The calculated parameters are:

$-\ S_{\max}$: Maximum crack spacing, $S_{\max} = 2 \times S_{\min} = 2 \times 0.85 \times K \times \dfrac{d}{(\rho + 0.8K_R)}$

$$\left(S_{\max} = 2 \times 0.85 \times 0.67 \times \frac{12}{(0.323\% + 0.8 \times 0.7)} = 1550mm\right)$$

$-\ Rb$: Degree of restraint before cracking at center line of slab

$\left(\dfrac{l}{L} = 1\right)$ at a level of $\left(\dfrac{l}{L} = 0.7\%L\right)$ from the restrained edge,

$Rb = 0.7$ (Figure ٥-٩)

The other parameters can be assumed as flows:

$-\ e_{ult}$: Elastic tensile strain capacity = ١٤٠×١٠$^{-٦}$

$-\ e_{sh}$: Shrinkage strain plus strain due to loss of heat of hydration,

$$e_{sh} = 500\times10^{-6} + 200\times10^{-6} = 700\times10^{-6}$$

$-L.O.R$: Loss of restraint, $L.O.R = 60\times10^{-6}$

$-e_{shn}$: Net shrinkage strain = e_{sh}-L.O.R=٦٤٠×١٠$^{-٦}$

$-c_f$: Final creep strain, ($c_f = 0.6\times e_{shn} = 0.6\times640\times10^{-6} = 385\times10^{-6}$)

Therefore, the calculated maximum crack width using equation (٥-٨) is:

$$Wc = S_{\max}\left[a\times(Rb - 0.7Ra)e_{shn} - b\times c_f - c\times \tfrac{1}{2}\times e_{ult}\right]$$

Where:

$a = 0.83$

$b = 3.9$

$c = 23.46$

$$Wc = 1550\left[0.83(0.7 + 0.7\times0.05)640\times10^{-6} + 3.9\times385\times10^{-6} - 23.46\times \tfrac{1}{2}\times140\times10^{-6}\right]$$

$$Wc = 0.387mm$$

Whereas the maximum observed crack width, Wo is ٠.٤mm

Example -٣-

Calculation of maximum crack width at ٢٥cm from the free edge for site observed three end restrained reinforced concrete slab.

The calculated parameter is:

$-S_{\max}$: Maximum crack spacing, $S_{\max} = 2\times S_{\min} = 2\times0.85\times K\times\dfrac{d}{(\rho + 0.8\rho_R)}$

$$\rho_R = 0.9 - 1.1\left(\frac{l}{L}\right)^{0.6},\quad \rho_R = 0.9 - 1.1\left(\frac{25}{500}\right)^{0.6} = 0.717$$

$$\therefore S_{\max} = 2\times0.85\times0.67\times\frac{12}{(0.323 + 0.717)\%}$$

The other parameters can be assumed as flows:

-e_{ult} : Elastic tensile strain capacity =١٤٥×١٠$^{-٦}$

-e_{sh} : Shrinkage strain plus strain due to loss of heat of hydration,

$$e_{sh} = 500\times10^{-6} + 200\times10^{-6} = 700\times10^{-6}$$

- $L.O.R$: Loss of restraint, $L.O.R$ =٦٠×١٠$^{-٦}$

$\therefore e_{shn}$: Net shrinkage strain, $\left(e_{shn} = e_{sh} - L.O.R = 640\times10^{-6}\right)$.

$-\ c_f$ Final creep strain, $c_f = 0.6\times e_{shn} = 0.6\times640\times10^{-6} = 385\times10^{-6}$

Therefore, the calculated maximum crack width using equation (٥-٧) is:

$$Wc = S_{\max}\left[a\times e_{shn} - b\times c_f - c\times \tfrac{1}{2}\times e_{ult}\right]$$

Where:

$a = -10.06$

$b = -26.92$

$c = 50.22$

$$Wc = 1315\left[-10.06\times640\times10^{-6} + 26.92\times385\times10^{-6} - 50.22\times\tfrac{1}{2}\times145\times10^{-6}\right]$$

$$Wc = 0.375mm$$

Whereas the maximum observed crack width, W_o is ٠.٣٢٥mm

CERTIFICATE

We certify that the thesis titled **"*Shrinkage Cracking of Reinforced Concrete Slabs Exposed to Fire*",** was prepared by **"*Mohammed Mansour Kadhum*",** under our supervision at Babylon University in fulfillment of partial requirements for the degree of Master of Science in Civil Engineering.

Signature:

Name**: Assist Prof. Dr.Mahdi S. Essa**

Date: / / ٢٠٠٣

Signature:

Name: **Assist Prof. Mr. Samir A. AL-Mashhedi**

Date: / /٢٠٠٣

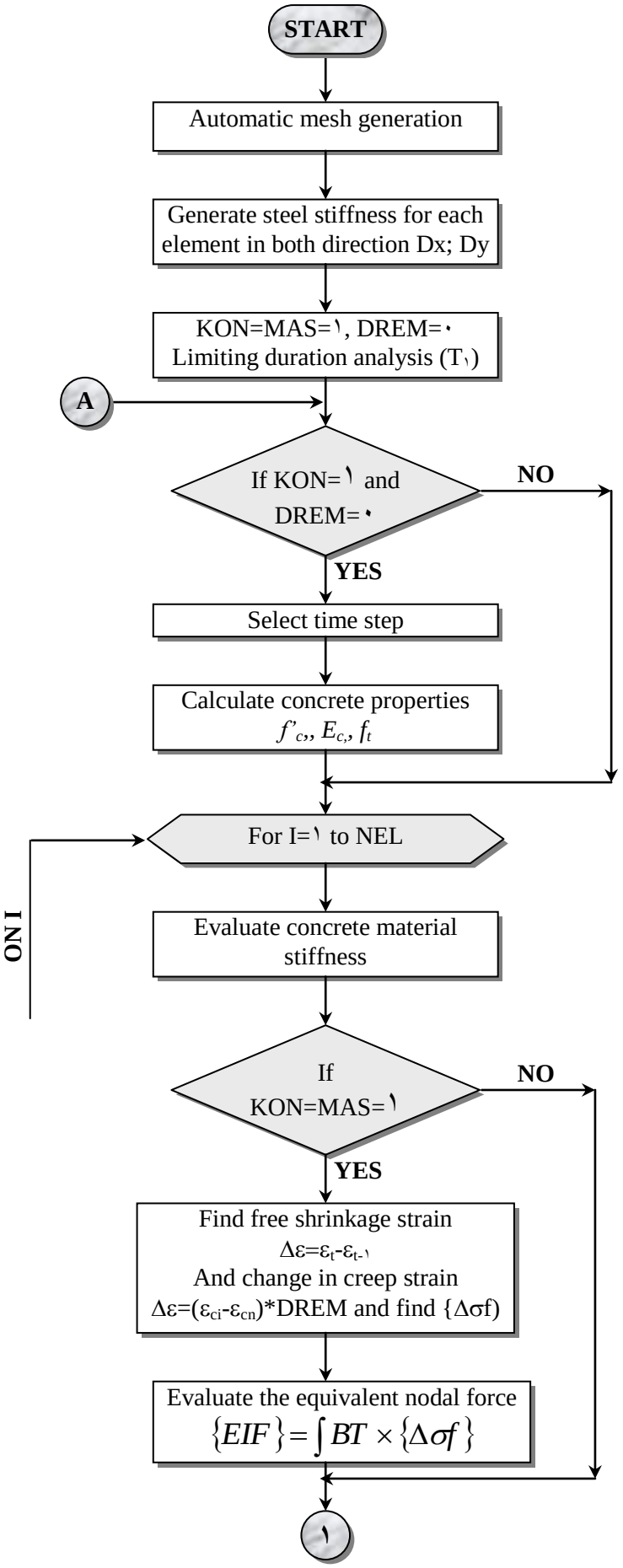

Figure (٤-١١): Flow chart of the computer program.

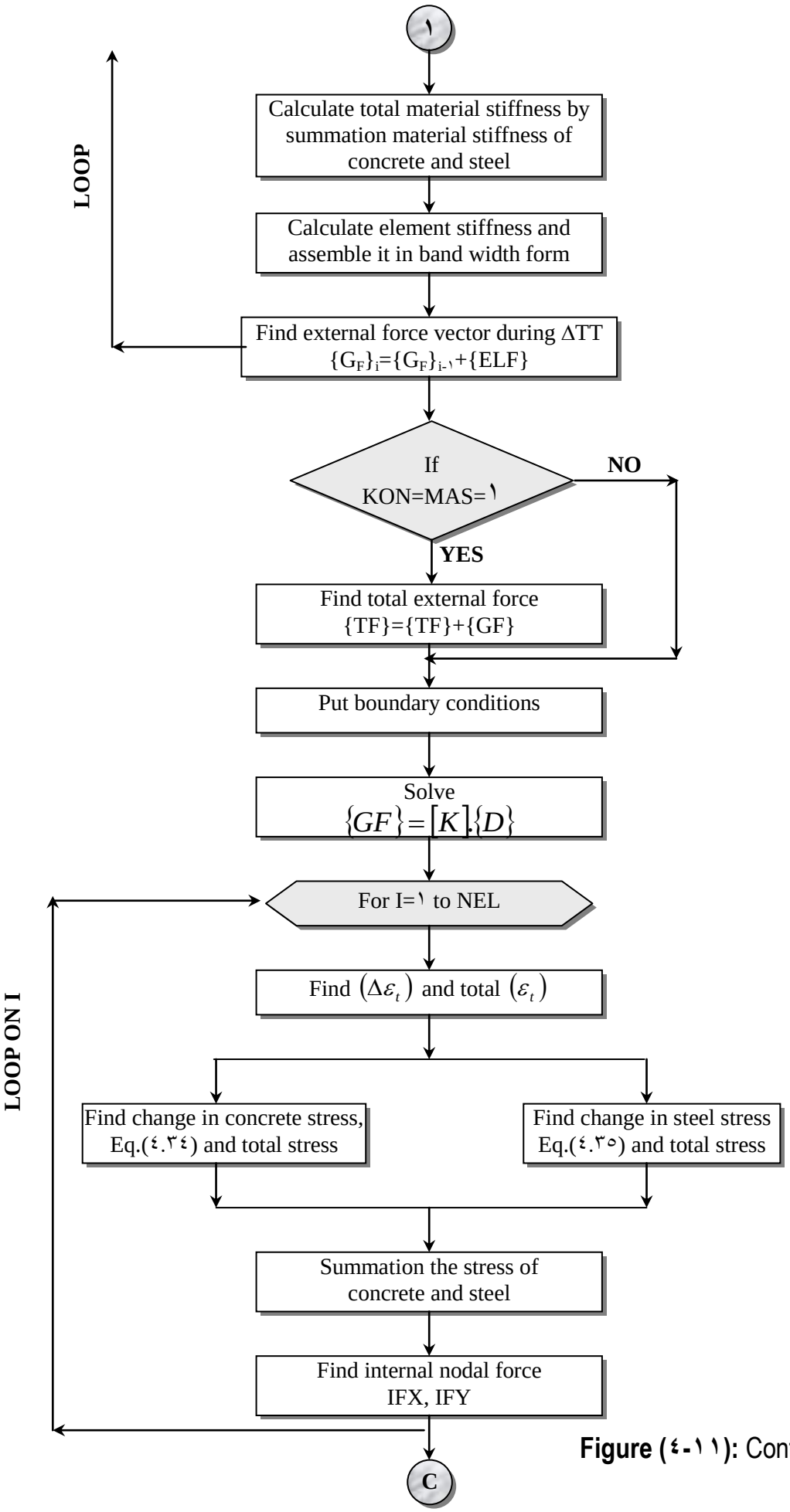

Figure (٤-١١): Continue.

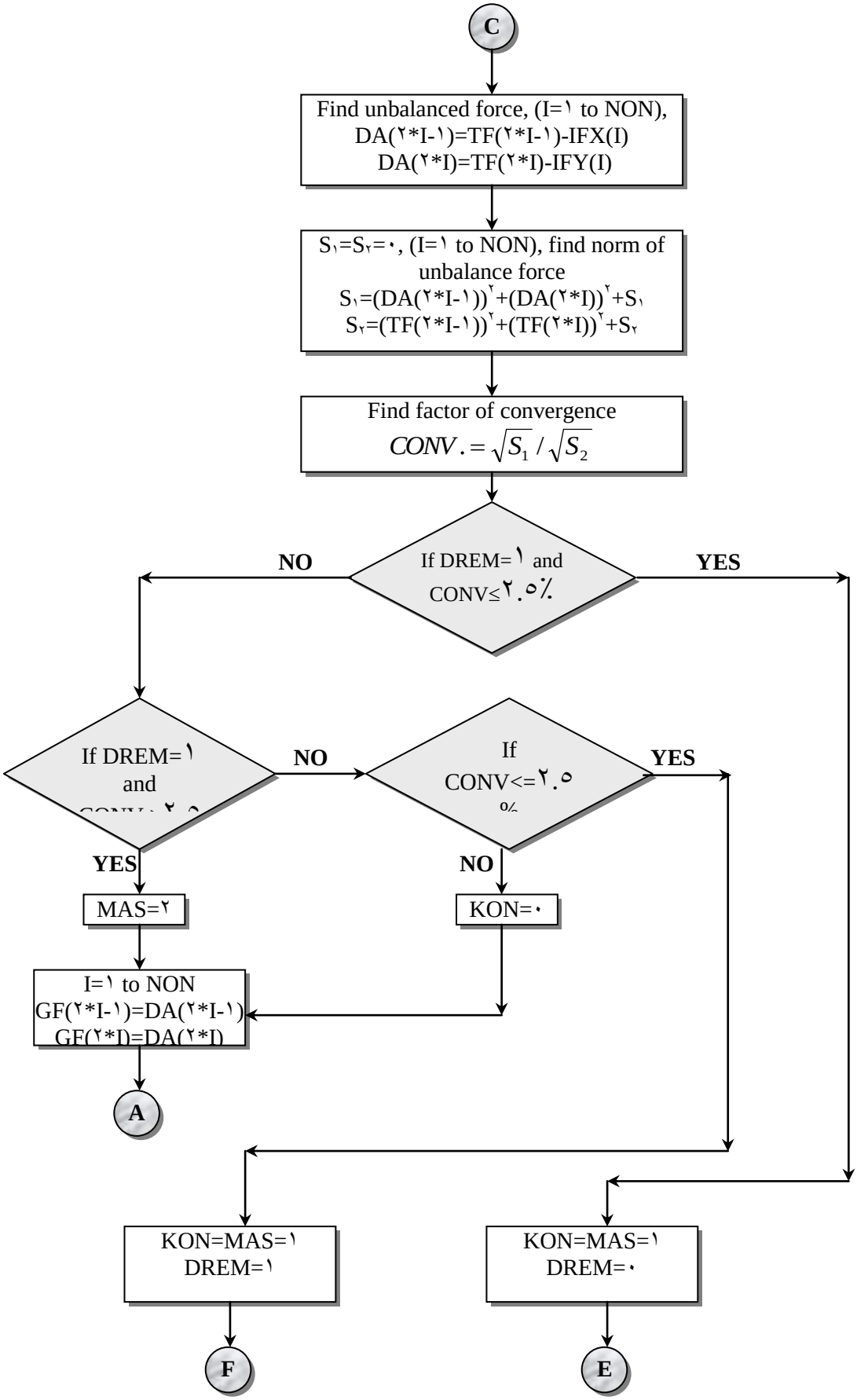

Figure (٤-١١): Continue.

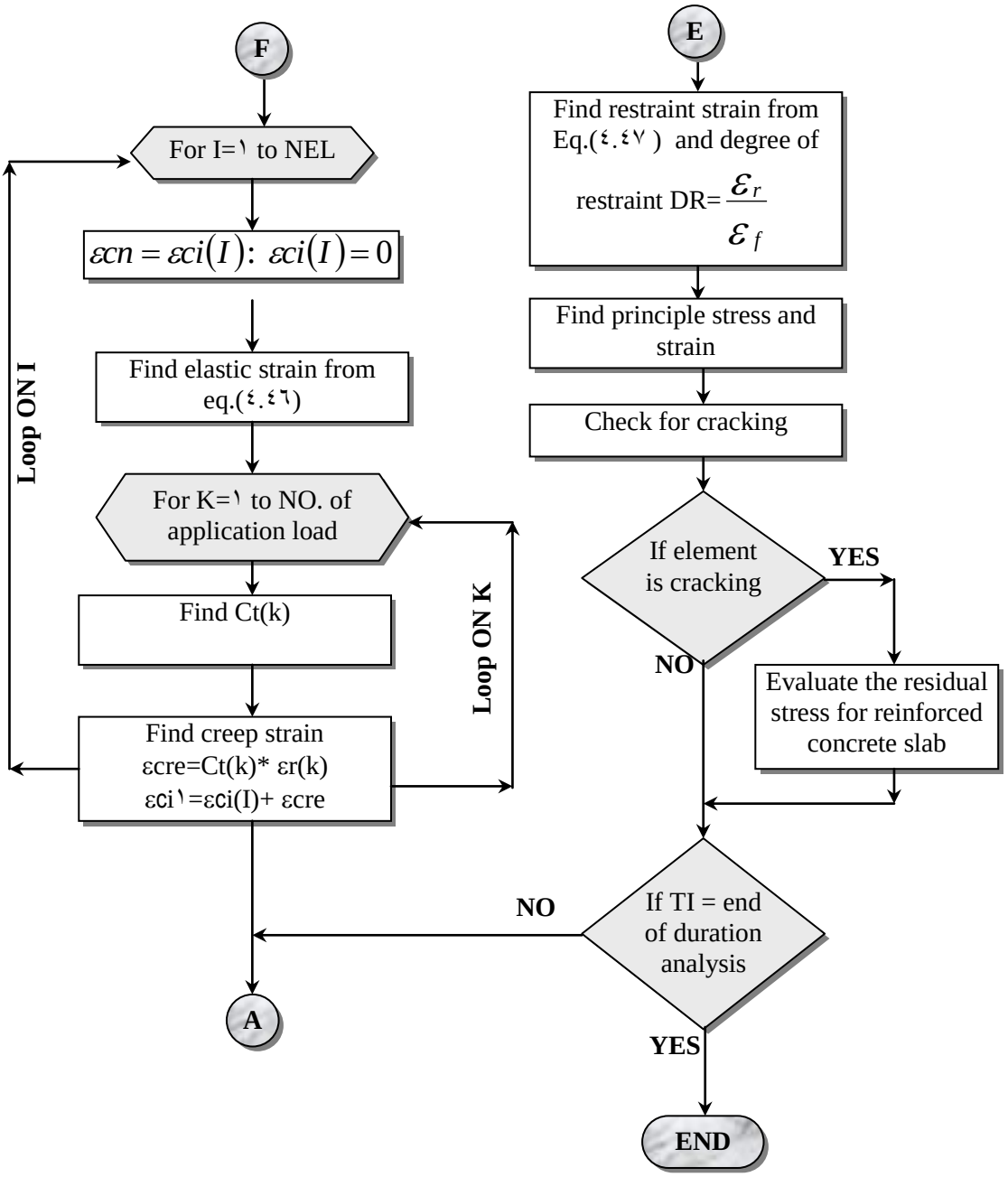

Figure (٤-١١): Continue.

LIST OF CONTENTS

NOTATIONS

Most commonly used symbols are listed below, these and others are defined where they appear in the research.

Symbol	Description
A, B, C, D	Coefficients of Saenz equation.
a, b	Constant depends on cement type and curing method.
$B_s(t_1)$	Factors to account for the rate at which shrinkage develops.
$[B]^T$	Conventional nodal displacement strain matrix.
$\overline{C}$	Constant of total net shrinkage.
C_a	Creep strain after cracking.
C_b	Creep strain before cracking.
C_t	Creep coefficient at time (*t*).
COV	Convergence factor.
C_u	Ultimate creep coefficient.
CON	Number of node in one column.
d	Bar diameter.
[D]	Total stiffness material for reinforce concrete .
$[D]_c$	Material stiffness for concrete element.
$[D_i]$	Material stiffness for (i)th steel layer.
DR, KR	Degree of restraint.
{DA}	Vector of residual unbalanced nodal force.
{d}	Vector of displacement.
E_c	Modulus of elasticity of concrete.
E_s	Modulus of elasticity of steel.
E_o	Secant modulus of elasticity at *fc'* for concrete.
Et	Tangent modulus of elasticity of concrete parallel to the crack direction.
{Elf}	Vector of change in equivalent external force during (ΔTT) for element.
e_{sh}	Free shrinkage strain.
e_{shn}	Net shrinkage strain.
e_{th}	Thermal strain.
e_{ult}	Elastic tensile strain capacity of concrete.
{F}	Vector of external force.
fb	Average bon strength between concrete and steel.
fc'(*t*)	Compressive strength at time (t) (MPa).
fc'	Maximum compressive strength of concrete.
Ft	Average tensile stress normal to the crack direction.
Fcm	Degraded maximum compressive strength.

Symbol	Description
f_{cf}, σ_u	Stress corresponding to (εf) on the uniaxial stress strain curve.
f_{tu}	Tensile strength of concrete.
G,G_o	Shear modulus of cracked and uncracked concrete respectively.
{Gf}	Vector of total external equivalent force during (ΔTT) for all elements.
H	Height of wall.
I_1, I_2, I_3, I_4	Nodes related to each element.
{I}	Nodal internal force vector.
{If_x}, {I_{fy}}	Vectors of internal nodal force in the (x) and (y) direction respectively.
K	Constant.
[K]	Band width matrix of total elements.
[K_G]	Stiffness matrix.
[K_{ele}]	Element stiffness matrix.
n	Number of equivalent load application.
NEQ	Number of equation.
NEL	Number of element in mesh.
NON	Number of node in mesh.
{P}	Vector of residual stress after cracking.
r	Correlation coefficient.
R	Ratio relation.
R_a	Degree of restraint after cracking.
R_b	Degree of restraint before cracking.
RE	Number of element in one row.
RN	Number of node in one row.
R_E	Modulur ratio.
R_σ	Stress ratio.
R_ε	Strain ratio.
S_1, S_2	Norm of internal and external nodal force respectively.
S_{max}	Maximum crack spacing.
S_{min}	Minimum crack spacing.
T	Temperature.
T_o	Initial temperature.
T_f	Fire temperature.
TIC	Age of concrete including duration of curing.
TI	Analysis duration.
{TF}	Vector of total external equivalent force.
t	Time.
t_o	Curing duration.
U	Displacement in (x) direction.
V	Displacement in (y) direction.
V/S	Volume / surface ratio.
W_i	Initial crack width.
W_{max}	Maximum crack width.
W_c	Calculated maximum crack width.

Symbol	Description
W_o	Observed crack width (by microscope).
X, Y	Node coordinates.
α_c	Coefficient of expansion of concrete.
α_s	Coefficient of expansion of steel.
$\alpha_1, \alpha_2,...,\alpha_7,\alpha_\lambda$	Coefficient of displacement field.
β, μ	Reducing and shear retention factor respectively.
$(\varepsilon_{sh})u$	Ultimate shrinkage strain.
ε_t	Average tensile strain normal to the crack direction after cracking or tensile strain in concrte.
ε_o	Strain corresponding to the maximum concrete compressive strength (*fc'*).
ε_f	Maximum compressive strain on the uniaxial stress-strain curve.
ε_{ci}	Free creep strain at time t=n١.
ε_{cn}	Free creep strain at time t=n١-ΔTT
ε_{cre}	Free creep strain for changes in elastic strain.
ε_{tc}	Total strain including creep stain at (t).
ε_{nc}	Total strain including creep strain at (tn).
$\{\varepsilon_f^s\}$	Vector of free shrinkage strain.
$\{\varepsilon_f^c\}$	Vector of free creep strain.
$\{\varepsilon_r\}$	Vector of total restraint strain.
ν	Poission's ratio.
ρ	Steel ratio.
σ_x, ε_x	Stress and strain in x-direction respectively.
σ_y, ε_y	Stress and strain y-direction respectively.
$\{\sigma\}$	Vector of residual stress.
$\{\sigma_c\}, \{\varepsilon_t\}$	Vectors of total stress and strain respectively.
$\{\sigma_c\}$	Vector of stress in concrete.
$\sigma_{o١}, \varepsilon_{o١}$	Initial stress and strain respectively.
$\Delta\sigma_i$, $\Delta\varepsilon_i$	Increased stress and strain change respectively.
T_{xy} , γ_{xy}	Shear stress and strain respectively.
ϕ	The angle between steel direction and crack direction counter clockwise in degree.
$\{\Delta\varepsilon_r\}$	Vector of change in restrained strain during (ΔTT).
ΔTT	Time step.
$\Delta\sigma_x$	Stress change in (x) direction.
$\Delta\sigma_y$	Stress change in (y) direction.
ΔT_{xy}	Shear stress change.
$\{\Delta\varepsilon_t\}, \{\Delta\sigma_t\}$	Vectors of change in strain and stress due to equivalent external force during (ΔTT).
$\{\Delta G_f\}$	Vector of change in total external equivalent force during (ΔTT).
$\{\Delta f\}$	Vector of residual unbalanced nodal force.

Symbol	Description
$\{\Delta d\}$	Vector of change in displacement.

REFERENCES

١. **Salse, E. and Lin, T.D.,** "Structural Fire Resistance of Concrete", ASCE, Journal of the Structural Division, V.١٠٢, No.ST١, Jan.١٩٧٥, p.٥١.

٢. **Shettey, M. S.,** "Concrete Technology Theory and Practice", Third Edition, ١٩٨٨, pp.٣٦١.

٣. **Troxell, G.E., Davis, H.E. and Kelly, J.W.**, "Composition and Properties of Concrete", McGraw-Hill, ٢nd Edition, ١٩٦٨, pp.٥٢٩.

٤. **ACI-Committee ٣٠٥,** "Hot Weather Concreting", American Concrete Institute, ١٩٩١.

٥. **Powers, T.C. and Brownyard, T.L.** "Studies of the physical properties of Hardened Portland Cement Paste", Proceeding of the ACI, V.٤٣, October-December, ١٩٤٦.

٦. **Hobbs, D.W. and Parrot, L.J.,** "Prediction of Drying Shrinkage", Concrete, Feb., ١٩٧٩, pp.١٠٥-١٨٠.

٧. **ACI Committee ٢٠٩,** "Prediction of Creep, Shrinkage and Temperature Effect in Concrete Structures", ACI Manual of Concrete Practice, Part١, ١٩٨٩,pp.١٩٣-٣٠٠.

٨. **Houk, I.E., Borge, O.E. and Houghton, D.L.** "Studies of Autogenous Volume Change in Concrete for Dworshak Dam", J. Amer. Concr. Inst, ٦٦, (July ١٩٦٩), p.٥٦٠.

٩. **Carlson, R.W., Houghton, D.L. and Polivka, M.,** "Causes and Control of Cracking in Unreinforced Mass Concrete", ACI Journal, V.٧٦, No.٧, July ١٩٧٩, pp.٨٢١-٨٣٧.

١٠. **ACI Committee ٢٢٤,** "Control of Cracking in Concrete Structures", ACI ٢٢٤R-٨٠, ACI Manual of Concrete Practice, ١٩٨٥, Part ٣.

١١. "New Technical Methods for Control Thermal Cracks in Mass Concrete", Paper Submitted to the International Convention on Temperature Effects on Concrete by **R.T. Torrent, Translated by Dr. Moufuk Al-Harbi,** Oct. ١٩٩٩, pp. ٥-٣٦.

٢. **Troxel, G.E., Raphael, J.M. and Davis, H.E.,** "Long Time Creep and Shrinkage Tests in Plain and Reinforced Concrete", ASTM, V.٥٨, ١٩٥٨.

٣. **Carlson, R.W.** "Drying Shrinkage of Concrete as Affected by Many Factors", Proceedings ASTM, V.٣٥, Part II, (١٩٣٥), pp.٣٧٠.

٤. **Brooks J.J and Neville, A.** "Creep and Shrinkage of Concrete as Affected by Admixture and Cement Replacement Materials and Environmental", ACI SP-١٣٥, (Detroit, Michigan, ١٩٩٢), pp.١٩-٣٦.

٥. **Hanson, J.A.,** "Effects of Curing and Drying Environments on Splitting Tensile Strength of Concrete", ACI Journal, July ١٩٦٨, pp.٥٣٥-٥٤٣.

٦. **Neville, A.M.,** "Properties of Concrete", Fourth and Final Edition, Wiley, New York and Longman, London, ١٩٩٥.

٧. **Campbell-Allen, M.A.** "The Prediction of Shrinkage for Australian Concrete", Civil Engineering Transactions, V.CE١٥, No.٢, Institution of Engineering (Australia), ١٩٧٣, pp.٥٣-٥٧.

٨. **Hansen, T.C. and Mattock, A.H.,** "Influence of size and Shape of Member on the Shrinkage and Creep of Concrete", Journal of the ACI, No.٦٣-١٠, February, ١٩٦٦.

٩. **Al-Rawi, R.S. and Kheder, G.F.,** "Control of Cracking due to Volume Change in Base-Restrained Concrete Members", ACI-Structural Journal, July-August ١٩٩٠, pp.٣٩٧-٤٠٥.

٠. **ACI ٣٠٥R-٩١** "Hot Weather Concreting", ACI Manual of Concrete Practice Part ٢, Construction Practices and Inspection Pavements, Detroit, Michigan ١٩٩٤, p.٢٠.

١. **Lerch, W.,** "Plastic Shrinkage", J. Amer. Concr. Inst. ٥٣, (Feb.١٩٥٧). pp.٧٩٧-٨٠٢.

٢. **Al-Rawi, R.S.,** "Determination of Tensile Strain Capacity and Related Properties of Concrete Subjected to Restrained Shrinkage", ACI Symp. Singapore, Aug. ١٩٨٥, Our world in Concrete and Structure, ١٨.pp.

٣. **ACI Committee ٢٠٧,** "Effect of Restraint, Volume Change and Reinforcement on Cracking of Massive Concrete", ACI ٢٠٧. ٢R-٧٣, ACI Manual of Concrete Practice, ١٩٨٥, Part١.

٤. **Gilbert, R.I.** "Shrinkage, Cracking and Deflection the Serviceability of Concrete Strucutures", Electronic Journal of Structural Engineering, Vol.١, No.١, ٢٠٠١, pp.٢-١٤.

٥. **Al-Mashhedi, S.A.,** "Control of Secondary Shrinkage Cracks in Reinforced Concrete Walls", M.Sc Thesis, University of Baghdad, College of Engineering, Sep. ١٩٨٩.

٦. **Al-Rawi, R.S.** "Laboratory Tests on Small Beams to Study Shrinkage Cracking in Continuously Reinforced Concrete Pavement", Transportation Research Board, Annual Meeting, Washington, D.C., U.S.A. January ١٩٨٦, ٢٤pp.

٧. **Beeby , A. W.,**"The Prediction of Crack Widths in Hardened Concrete", The Structural Engineer ,V.٥٧A.No.١,Jan.١٩٧٩,PP.٩-١٧.

٨. **Evans, E.P and Hughes, B.P.,** "Shrinkage and Thermal Cracking in a Reinforced Concrete Retaining Wall", Proceedings The Institution of Civil Engineers (London), V.٣٩, Jan., ١٩٦٨, pp.١١١-١٢٥.

٩. **B.S. Code ٥٣٣٧ ١٩٨٢ (Amendment ٢).**

٠. **Harrison, T.A. ,** "Early Age Thermal Crack Control in Concrete",CIRIA Report No.٩١, Construction Industry Research and Information Association, London, ١٩٨١, ٤٨pp.

١. **Mann,** "Designing for Effects of Creep, Shrinkage and Temperature in Concrete Structures", ACI Publication SP.٢٧, American Concrete Institute, ١٩٧١.

٢. **Hughes B.P. and Ghunaim, F.,** "An Experimental Study of Early Thermal Cracking in Concrete", Magazine of Concrete Research, V.٣٤, No.١١٨, England, March ١٩٨٢, pp.١٨-٢٤.

٣. **Hobbs, D.W.,** "Influence of Aggregate Restraint on the Shrinkage of Concrete", ACI Journal, Title No.٧١-٣٠, September ١٩٧٤.

٤. **Harada, T., Takeda, J., Vamane, S., and Furumura, F.,** "Strength, Elasticity and Thermal Properties of Concrete Subjected to Elevated Temperatures", ACI Special Publication, SP-٣٤, V.١, ١٩٧٢, pp.٣٧٧-٤٠١.

٥. **RILEM-Committee ٤٤-PHT,** "Behavior of Concrete at High Temperature" Edited by U. Schneider, Dept. of Civil Engineering Gesamtho-Chschulc, Kassel University, Kassil, Germany, ١٩٨٥, ١٢٢p.

٦. **Mohamadbhai, G.T.G.,** "Effect of Exposure Time and Rates of Heating and Cooling on Residual Strength of Heated Concrete", Magazine of Concrete Research, V.١٣٦, September ١٩٨٦, pp.١٥١-١٥٨.

٧. **Dias, W.P., Khoury, G.A., and Sulilivon, P.J.,** "Shrinkage of Hardened Cement Paste at Temperature up to ٦٧٠^{o}C (١٢٣٨ F)", ACI Materials Journal, V.٨٧, No.٣, May-June ١٩٩٠, pp.٢٠٤-٢٠٩.

٨. **Piasta, J., Sawicz, Z. and Rudzinski, L.,** "Changes in the Structure of Hardened Cement Paste Due to High Temperature", RILEM, Materials and Struct., V.١٧, No.١٠٠, ١٩٨٤, pp.٢٩١-٢٩٦.

٩. **Umran, M.K.,** "Fire Flame Exposure Effect on Some Mechanical Properties of Concrete", M.Sc. Thesis, College of Engineering, Department of Civil Engineering, University of Babylon, October, ٢٠٠٢, ١٠٣ pp.

٠. **Edwards, W.T., and Gamble, W.L.,** "Strength of Grade ٦٠ Reinforcing Bars After Exposure to Fire Temperatures", Concrete International, Oct., ١٩٨٦, p.١.

١. **Holmes, M., and Anchor, R.D.,** "The Effects of Elevated Temperatures on the strength Properties of Reinforcing and Prestressing Steels", Structural Engineering, V.٦٠, No.١, March ١٩٨٢, pp.٧-١٣.

٢. **J. Hannant and P.S. Pell,** "Thermal Stresses in Reinforced Concrete Slabs", Magazine of Concrete Research, V.١٤, July ١٩٦٢, pp.٩١-٩٩.

٣. **Salse, E., and Lin, T.D.,** "Structural Fire Resistance of Concrete", Journal of Structural Division, ASCE, V.١٠٢, No.ST١, Jan ١٩٧٦, pp.٥١-٦٣.

٤. **Shirly, S.T., Burg, R.G., and Fiorato, A.E.,** "Fire Endurance of High Strength Concrete Slabs", ACI Material Journal march-April ١٩٨٨, pp.١٠٢-١٠٨.

٥. **Gustaferro, A.H., and Carlson, C.C.** "An Interpretation of Results of Fire Tests of Prestressed Concrete Building Components", Journal of Prestressed Concrete Institute, V.٧, No.٥, ١٩٦٢, pp.١٤-٢٢.

٦. **"Standard Method of Fire Tests of Building Construction and Materials"**, ASTM E١١٩-٨٨, American Society for Testing and Materials, Philadelphia, Pennsylrania, ١٩٨٨.

٧. **Lie, T., T., and Leir, G., W.,** "Factors Affecting Temperature of Fire Exposed Concrete Slabs", Fires and Materials, V.٣, No.٢, ١٩٧٩, pp.٧٤-٧٩.

٨. **Hidayat, A.,** "Influence of High Temperature on the Behavior of Reinforced Concrete Slabs', MSc. Thesis, University of Technology, ١٩٩٤.

٩. **Lie, T.T. and Irwin, R.J.,** "Method to Calculate the Fire Resistance of Reinforced Concrete Columns with Rectangular Cross Section", ACI Struct., Jou., V.٩٠, No.١, ١٩٩٣, pp.٥٢-٦٠.

٠. **Nizamuddin, Z.,** "Thermal and Structural Analysis of Reinforced Concrete Slabs in Fire Environments", Thesis Presented to the University of California at Berkeley, California in ١٩٧٦, in Partial Fulfillment of the Requirements for the degree of Doctor of Philosophy.

١. **Cruz, Carlos, R.,** "Elastic Properties of Concrete at High Temperatures", Journal, PCA Research and Development Laboratories, V.٨, No.١, Jan. ١٩٦٦, pp.٣٧-٤٥, Also, Research Department Bulletin, No.١٩١, PCA, land.

٢. **Haramathy, T.Z., and Allen, L.W.,** "Thermal Properties of Selected Masonry Unit Concrete", ACI Journal, Proceeding, V.٧٠, No.٢, Feb. ١٩٧٣, pp.١٣٢-١٤٢.

٣. **Dettling, Heinz,** "The Thermal Expansion of Hardened Cement Past, Aggregates, and Concrete (Die Warmedhung des Zementsteines, Der Gesteine and der Betone)", Bulletin No.١٦٤, Deutscher Ausschuss Fur Stanlbeton Berlin, ١٩٦٤, Part٢, pp.١-٦٤, Also, English Translation, Foreign Literature Study No.٤٥٨, Portland Cement Association.

٤. **Zoldners, N.G.,** "Thermal Properties of Concrete Under Sustained Elevated Temperatures", ACI Publ. SP-٢٥, Temperature and Concrete, ١٩٦٩, pp.١-١١.

٥. **Khoury, G.A., Grainger, B.N. and Sullivan, P.J.E.,** "Transient Thermal Strain of Concrete: Literature Review, Conditions Within Specimen and Behavior of Individual Constituents", Magazine of Concrete Research, V.٣٧, No.١٣٢, ١٩٨٥a, pp.١٣١-١٤٤.

٦. **Malhotra, H.L.,** "Properties of Materials at High Temperatures", RILEM, Materials and Structures, V.١٥, No.٨٦, ١٩٨١, pp.١٦١-١٧٠.

٧. **Takeuchi, M., Hiramoto, M., Kumagai, N., Yamazaki, N., Kodaira, A. and Sugiyama, K.,** "Material Properties of Concrete and Steel Bars at Elevated Temperatures", Trans. of the ١٢th Int. Conf. on SMIRT, V.H, pp.١٣٣-١٣٨.

٨. **Nasser, K.W.,** "Creep of Concrete at Low Stress-Strength Ratios and Elevated Temperatures", ACI Publ. SP-٢٥, Temperature and Concrete, ١٩٦٩, pp.١٣٧-١٤٧.

٩. **Khoury, G.A., Grainger, B.N. and Sullivan, P.J.E.,** "Strain of Concrete During First Cooling from ٦٠٠°C Under Load", Magazine of Concrete Research, V.٣٨, No.١٣٤, ١٩٨٦, pp.٣-١٢.

٠. **Attiyah, A.N.,** "Elevated Temperature Response of Reinforced Concrete Slabs", Ph.D. Thesis, College of Engineering, Department of Civil Engineering, University of Baghdad, February ٢٠٠٠, ٢١٥ pp.

١. **Khoury, G.A.,** "Separation and Prediction of Irrecoverable Strain Components of Concrete During the First Thermal Cycle", Trans. of the ١٢th Int. Conf. on SMIRT, V.H, ١٩٩٣, pp.٣٥١-٣٦٢.

٢. **Habeeb, G.M.,** "Residual Mechanical Properties of High Strength Concrete Subjected to Elevated Temperature", Ph.D. Thesis, College of Engineering, Department of Civil Engineering, Al-Mustansiriyah University, Baghdad, Iraq, November, ٢٠٠٠, ١٦٤, pp.

٣. **Gustaferro, A.H., and Selvaggio, S.L.,** "Fire Endurance of Simply-Supported Prestressed Concrete Slabs", Journal, Prestressed Concrete Institute, V.١٢, No.١, Feb., ١٩٦٧, pp.٣٧-٥٢. Also, Research Department Bulletin No.٢١٢, Portland Cement Association.

٤. **Ehm, H., and Von Postel, R.,** "Tests of Continuous Reinforced Beams and Slabs under Fire", Proceedings, Symposium of Fire Resistance of Prestressed Concrete, English Translation, SLA Translation Center, John Crerar Library, Chicago.

٥. **Gustaferro, A.H.,** "Temperature Criteria at Failure", Fire Test Performance, STP-٤٦٤, American Society for Testing and Materials, Philadeiphia, ١٩٧٠, pp.١٩٧٠, pp.٦٨-٨٤.

٦. **British Standards Institution,** "Method for Specifying Concrete Mixes", BS ٥٣٢٨: Part٢: ١٩٩١.

٧. **ACI Committee ٣١٨,** "Building Code Requirement for Structural Concrete (٣١٨-٩٩)", American Concrete Institute, Michigan, pp.٦٣.

٨. **Iraqi Organization of Standards, IOS ٥: ١٩٨٤**, for Portland Cement.

٩. **Iraqi Organization of Standards,** IOS ٤٥: ١٩٨٤; for Aggregate.

٠. **American Society for Testing and Materials,** C١٤٣-٨٩a, "Standard Test Method for Slump of Hydraulic Cement Concrete", Annual Book of ASTM Standards, V.٠٤.٠٢, ١٩٨٩, pp.٨٥-٨٦.

١. **British Standard Institution,** "Method for Determination of Compressive Strength of Concrete Cubes", B.S. ١٨٨١: Part ١١٦: ١٩٨٣: ٣ pp.

٢. **American Society for Testing and Materials, C٢٩٣-٧٩,** "Standard Test Method for Flexural Strength of Concrete (Using Simple Beam with Center-point Loading)", Annual Book of ASTM Standards, V.٠٤.٠٢, ١٩٨٩, pp.١٦٥-١٦٦.

٣. **Metha, P.K.** "Concrete : Structure Properties and Materials, Prentice-Hall; pp.٤٥٠, ١٩٨٦.

٤. **Abrams, M.S.,** "Compressive Strength of Concrete at Temperatures to ١٦٠٠F" Temperature and Concrete, SP-٢٥, American Concrete Institute, Detroti, ١٩٧٠, pp.٣٣-٥٨.

٥. **Felicetti, R., and Gambarova, P.G.,** "Effect of High Temperature on the Residual Compressive Strength of High-Strength Siliceous Concrete", ACI Material Journal, V.٩٥, No.٤, Jully-August ١٩٩٨, pp.٣٩٥-٤٠٦.

٦. **Phan, L.T., and Carino, N.J.** "Review of Mechanical Properties of High Strength Concrete at Elevated Temperature" Journal of Materials in Civil Engineering, February, ١٩٩٨, ٥٨-٦٤.

٧. **Castillo, C., and Durrani, A.J.,** "Effect of Transient High Temperature on High-Strength Concrete", ACI Mat. J. V.٨٧, No.١, Jan-Feb.١٩٩٠, pp.٤٧-٥٣.

٨. **Al-Saadi, A.U.,** "Shrinkage Cracks in Base Restrained Plain and Reinforced Concrete Walls", MSc. Thesis, College of Engineering, Department of Civil Engineering, University of Babylon, August ٢٠٠٠, ٨٠pp.

٩. **Athman, K.** "Lectures Stated in ١٩٩٦ for Graduated Studies in Structures".

٠. **Nilson, A.H.,** "Nonlinear Analysis of Reinforced Concrete by the Finite Element Method", American Concrete Institute Journal, Vol.٦٥, No.٩,Sept., ١٩٦٨.

١. **Scanlon, A. and Murry, D.W.,** "Time-Dependent Reinforced Concrete Slab Deflection", ASCE J. of Structure Divisions, V.١٠٠, ST٩, ١٩٧٤, pp.١٩١١-١٩٢٤.

٢. **Christian Meyer and Bathe K.J.,** "Nonlinear Analysis of R/C Structures in Practice", J. of Strut. Div. ASCE, V.١٠٨, No.ST٧, ١٩٨٢.

٣. **Hu, H.T. and Schnobrich, W.C.** "Nonlinear Analysis of Cracked Reinforced Concrete", ACI Struct. J., V.٨٧, No.٢ March-April, ١٩٩٠, pp.١٩٩-٢٠٧.

٤. **Selna, L.G.,** "Creep Cracking and Shrinkage in Concrete Frame Structures", J. of Struct. Eng. Div., ASCE, V.٩٥, No.ST١٢, December, ١٩٦٩.

٥. **Zienkiewicz, O.C.,** "The Finite Element Method", McGraw Hill Co., ٣rd, Edition, ١٩٧٧.

٦. **Aldstedt, E. and Bergan, P.G.,** "Nonlinear: Time-Dependent Concrete-Frame Analysis", Journal of the Structural Division, ASCE, V.١٠٤, No.ST٧, July ١٩٧٨, pp.١٠٧٧-١٠٩٢.

٧. **Kang., Y.J. and Scordelis, A.C.,** "Nonlinear Analysis of Prestressed Concrete Frames", ASCE, J. of Struct. Eng. Div. V.١٠٦, No.ST٢, Feb, ١٩٨٠.

٨. **Chow, C.O.** "The Finite Element Analysis of Creep and Shrinkage Effects in Reinforcing Concrete Beams" M.Sc, Thesis, Dept. of Civil Engineering, Univer. Coll of Swansea, ١٩٨٤.

٩. **Branson, D.E.,** "Deformation of Concrete Structures", McGraw-Hill Inc., ١٩٧٧.

٠. **Bazant, Z.P., and Witlman, F.H.,** "Creep and Shrinkage in Concrete Structures", ١٩٧٨.

١. **Challal, O., Benmokrane, B. and Ballivey, G.** "Drying Shrinkage Strains: Experimental Versus Codes", ACI Materials J., V.٨٩, No.٣, May-June, ١٩٩٢, pp.٢٣٦-٢٦٦.

٢. **"Some Factors in the Investigation of Long Term Behavior of R.C. Struct.**" Report of Road Research Laboratory. Harmonds Worth, Middle Sex, February-March-١٩٦٢.

٣. **Chen, F.W.** "Plasticity in Reinforced Concrete", McGraw-Hill Book Company, ١٩٨٢.

٤. **Ngo, D. Scordelis, A.C.,** "Finite Element Analysis of Reinforced Concrete Beams", ACI Journal, V.٦٤, No.٣, March ١٩٦٧.

٥. **Schnobrich, W.C.** "Behavior of Reinforced Concrete Structures Predicted by the Finite Element Method", Computer and Structures, V.٧, ١٩٧٧, pp.٣٦٥-٣٧٦.

٦. **Al-Naimi, H.A.,** "٣-Dimensional Dynamic and Static Time Depended Finite Element Analysis of Reinforced Concrete Member", Ph.D Thesis, University of Baghdad, College of Engineering, Feb. ١٩٩٦.

٧. **Rockey, K.C., Evans, H.R., Griffths, D.W., and Nethercot D.A.** "The Finite Element A Basic Introduction of Engineering", ١٩٧٥.

٨. **Taan, S.A. and Ali, T.Q.M.,** "Nonlinear Finite Element Analysis of Fibrous Concrete Deep Beams", Eng. And Technology, V.١٧, No.٩, ١٩٩٨, pp.٨٦٢-٨٧٧.

٩. **Mercer, J.G. and Palazatto, A.N.,** "Elastic – Plastic Non-Linearties Considering Fracture Mechanics" Comp. And Struct. J., V.٢٥, No.٦, ١٩٨٧, pp.٩١٩-٩٣٥.

١٠. **ACI Committee ٢٠٧,** "Mass Concrete for Dams and Other Structures", ACI Manual of Concrete Practice, Part ١, ١٩٧٨.

١١. **Lee, C.R., and Lamb, W.** "Effects of Various Factors on the Extensibility of Concrete", Building Research Establishment, London, England, Jan.١٩٧٩, ٧٦pp.

١٢. **Nizomuddin, Z. and Bresler, B.** "Fire Response of Reinforced Concrete Slabs", ASCE, J. of Stru. Div., V.١٠٥, No.ST٨, August ١٩٧٩, pp.١٦٥٣-١٦٦٩.

١٣. **Hughes, B.P.,** "Controlling Shrinkage, and Thermal Cracking", Concrete, V.٦, No.٥, May ١٩٧٢, pp.٣٩-٤٢.

١٤. **Al-Rawi, R.S.,** "Control of Shrinkage Crack Spacing in Reinforced Concrete", T.R.B., Annual Meeting Jan, ١٩٨٦, Washington, D.C., U.S.A.

١٥. **Campbell-Allen, D. and Hughes, G.W.,** "Reinforcement to Control Thermal and Shrinkage Cracking", The Institution of Engineers, Australia, CET, V.CE ٢٣, No.٥, August ١٩٨١, pp.١٥٨-١٦٥.

٠٦. **Popovics, S.,** "Model for the Quantitative Description of the Kinetics of hardening of Portland Cement", Cement and Concrete Research, No.٥, ١٩٨٧,pp.٨٢١-٨٣١.

٠٧. "السلوك المعتمد على الزمن للاعمدة الخرسانية المسلحة"، **الدكتور هاني محمد فهمي والمهندس نمير نجيب عمسو**، المؤتمر العلمي الرابع لمجلس البحث العلمي، بغداد، العراق، ١٩٨٦.

٠٨. **Dhahir, K.N.,** "Fire Endurance of Concrete joist Floors", MSc. Thesis College of Engineering ,Department of Civil Engineering ,University of Al-Nahrain, October ١٩٩٩, ٨٨pp.

٠٩. **Abrams, M.S., and Gustaferro, A.H.,** "Fire Endurance of Concrete Slabs as Influenced by Thickness, Aggregate Type and Moisture" PCA Research Department Bulletin ٢٢٣.

١٠. **ACI Committee ٤٣٥,** "Deflection of Reinforced Concrete Flexural Member", ACI Journal, Proc., V.٦٣, No.٦, June ١٩٦٦, pp.٦٣٧-٦٧٤.

١١. **Nuri, D.,** "The Effect of Temperature on Some Properties of Concrete", MSc. Thesis, Submitted to the Building and Construction Department, University of Technology, September ١٩٨٣.

Table (٥-١٥): Strain before, during and after exposure to fire flame of reinforced concrete free slab.

Age		Temperature °C	Strain in (millionths) at		
			٢.٥ cm from the edge	٢٢.٥ cm from the edge	The center
Days	٠	(٢٣) before burning	٠	٠	٠
	١		١٥٥	١٣٥	١١٥
	٣		٢٨٠	٢٥٠	٢٠٥
	٧		٣٤٠	٣٢٠	٢٩٥
	١٥		٤١٥	٤٠٠	٣٧٥
	٣٠		٤٩٥	٤٧٠	٤٤٠
	٤٥		٥٧٠	٥٥٠	٥٣٠
	٦٠		٦١٥	٦٠٠	٥٦٠
Minutes	٠	(٢٣-٦٠٠) during burning	٦١٥	٦٠٠	٥٦٠
	١٥		٥٣٥	٥٠٥	٤٧٠
	٣٠		٣٨٥	٣٧٠	٣٤٥
	٤٥		١٩٠	١٨٠	١٦٥
	٦٠		١٠٥	١٠٠	٩٠
	٧٥		٨٠	٨٠	٧٠
	٩٠		٧٥	٦٥	٥٠
Days	٦٠	(٢٣) after burning	٧٥	٦٥	٥٠
	٦١		٢٧٠	٢٣٥	٢١٥
	٦٣		٣٨٥	٣٧٠	٣٥٠
	٦٧		٤٧٠	٤٥٥	٤٣٥
	٧٥		٥١٠	٤٩٥	٤٧٥
	٩٠		٥٥٥	٥٤٠	٥١٥
	١٠٥		٥٦٥	٥٥٠	٥٣٠
	١٢٠		٥٦٥	٥٥٠	٥٣٥

Table (٥-٦): Maximum crack widths measured for cracks in each slab before, during and after burning.

Age		Temperature °C	Maximum crack width in (mm)			
			Free end	**Two end restrained**	**Three end restrained**	**Four end restrained**
Days	٠	(٢٣) before burning	–	–	–	٠.٠٧٥
	١		–	–	٠.٠٦	–
	٣		–	–	٠.٠٦	٠.٠٨٥
	٧		–	٠.٠٥	–	–
	١٥		–	٠.١٢٥	٠.١٣٥	٠.١٧٥
	٣٠		–	٠.٢	٠.٢١	٠.٢٥
	٤٥		–	٠.٢٣	٠.٢٤٥	٠.٢٧٥
	٦٠		–	٠.٢٤	٠.٢٥٥	٠.٢٧٥
Minutes	٠	(٢٣-٦٠٠) during burning	٠	٠.٢٤	٠.٢٥٥	٠.٢٧٥
	٢٠		٠.١	٠.٤	٠.٣٥	٠.٣
	٤٠		٠.١٧٥	٠.٥٧٥	٠.٤٧٥	٠.٤٢٥
	٦٠		٠.٢٢٥	٠.٦٨٥	٠.٦	٠.٥٧٥
	٧٥		٠.٢٥	٠.٧٣٥	٠.٦٩	٠.٦٧٥
	٩٠		٠.٢٥	٠.٧٥	٠. ٧٢٥	٠.٧١
Days	٦١	(٢٣) after burning	٠.١٢٥	٠.٥	٠.٥	٠.٥٢٥
	٧٠		٠.١	٠.٥٥	٠.٥٥	٠.٦
	٨٠		٠.٠٨٥	٠.٦	٠.٦٢٥	٠.٦٧٥
	٩٠		٠.٠٨	٠.٦٥	٠.٦٧٥	٠.٧١٢٥
	١٠٠		٠.٠٧٥	٠.٦٦٥	٠.٦٨٥	٠.٧٣٥
	١١٠		٠.٠٧٥	٠.٦٧٥	٠.٧	٠.٧٥
	١٢٠		٠.٠٧	٠.٦٧٥	٠.٧	٠.٧٥

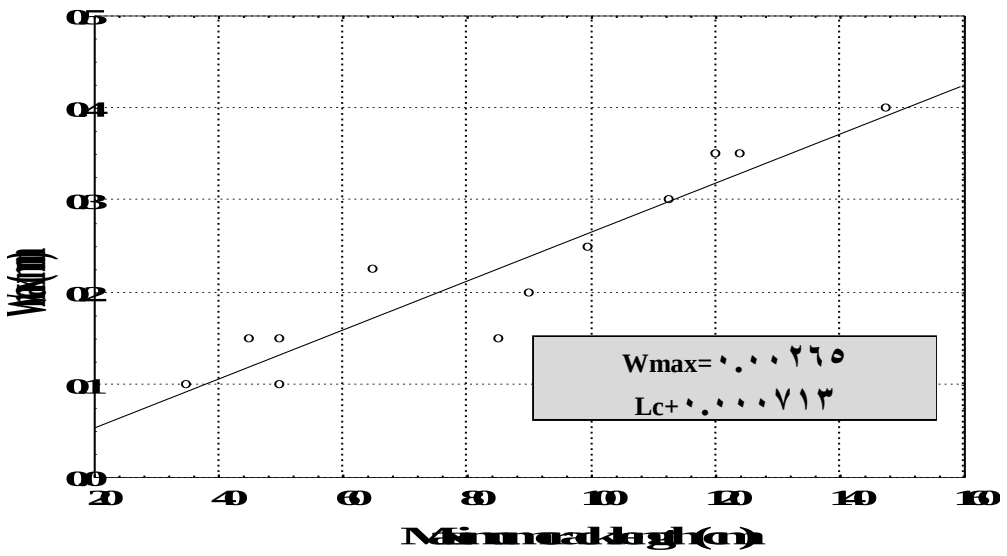

Figure (٥-١٢): Relation between maximum crack width and maximum crack length for site observation of three and four end restrained slabs.

٥.٤.٤ Crack Width

Crack widths were measured to the slabs investigated at regular intervals. The crack width was measured at levels spaced (٠, ٢٥, ٥٠, ١٠٠, ١٥٠, ٢٠٠, ٢٥٠, ٣٠٠, ٣٥٠, ٤٠٠, ٥٠٠, ٦٠٠, ٧٠٠, ٨٠٠, ٩٠٠, ١٠٠٠, and ١١٢٥ mm) from the edge. The crack width was obtained by two different ways. The first way is by the use of a portable micrometer-microscope with an accuracy of (٢٥ micro-m), and ٤٠ x magnification as illustrated in Article (٣-٣-٦). The second way is from the demec readings across the crack. A comparison between the final crack width after a period of ٢ months of drying shrinkage before and after exposure to fire flame of these slabs as obtained by the two different ways as can be seen in Appendix (A-٨ and A-٩) for different restrained cases of reinforced concrete slabs. For the site observed slabs the measurement levels were spaced ٢٥٠ mm along the slab

dimensions, and the crack width was obtained by a portable microscope only.

Figure (٥-١٣) shows the development of maximum crack width with different ages for the slabs investigated. These cracks widened progressively until a certain nearly constant width in about ٦٠ days occurred. The first crack in each slab was observed at an age which is indicated by the first point in the corresponding curve. There are many factors affecting cracking age, i.e.; the high roughness of the rigid beams surface (interaction between the rigid beams and edge beams for slabs) may be the most important factor governing earlier cracking age. Whereas, the low early rate of shrinkage and low temperature variation for reinforced concrete slabs are the most important factors which lead to delay cracking age. For the investigated slabs, the maximum crack width in each slab was that of the earliest crack.

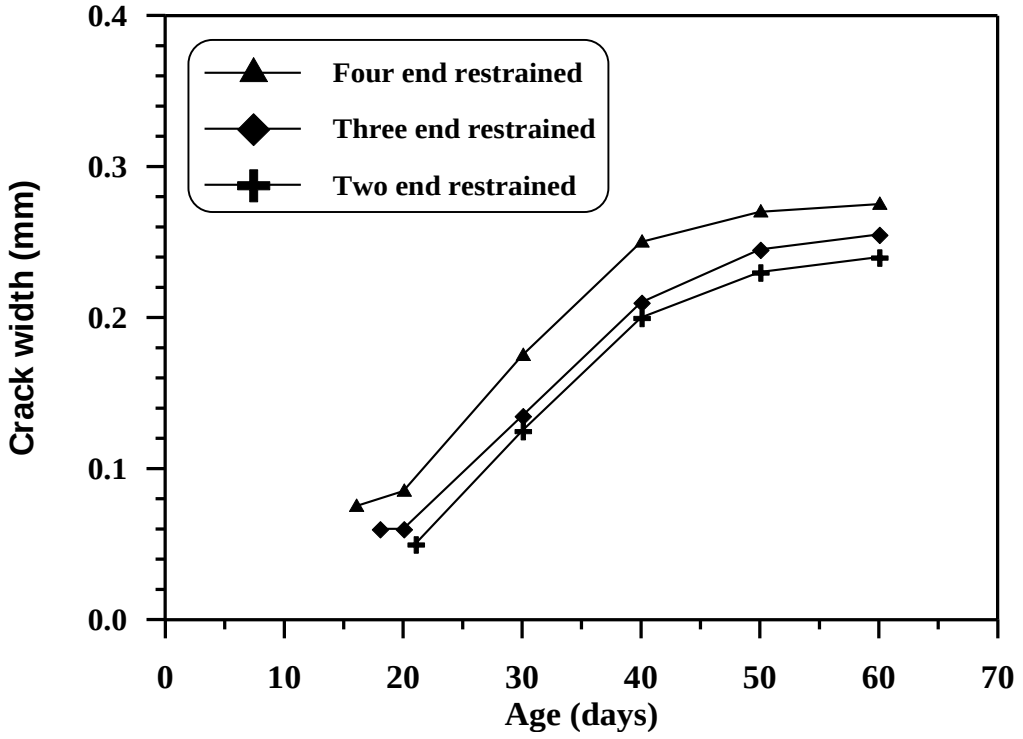

Figure (٥-١٣): Development of maximum crack width with age of reinforced concrete slabs for different restrained cases before exposure to fire flame.

Figures (٥-١٤ and ٥-١٥) show the development of maximum crack width with age during and after exposure to fire flame. The crack width increases during burning for (١.٥ hour) at a temperature of (٦٠٠^{o}C). The maximum crack width reached was (٠.٢٥, ٠.٧٥, ٠.٧٢٥ and ٠.٧١ mm) for (free, two, three and four end restrained slabs respectively). After one day from exposure date the maximum crack width became (٠.١٢٥, ٠.٥, ٠.٥ and ٠.٥٢٥ mm). Then these cracks developed with age for a period of ٢ months from exposure date to fire flame to become (٠.٠٧٥, ٠.٦٧٥, ٠.٧ and ٠.٧٥ mm) for (free, two, three and four end restrained respectively).

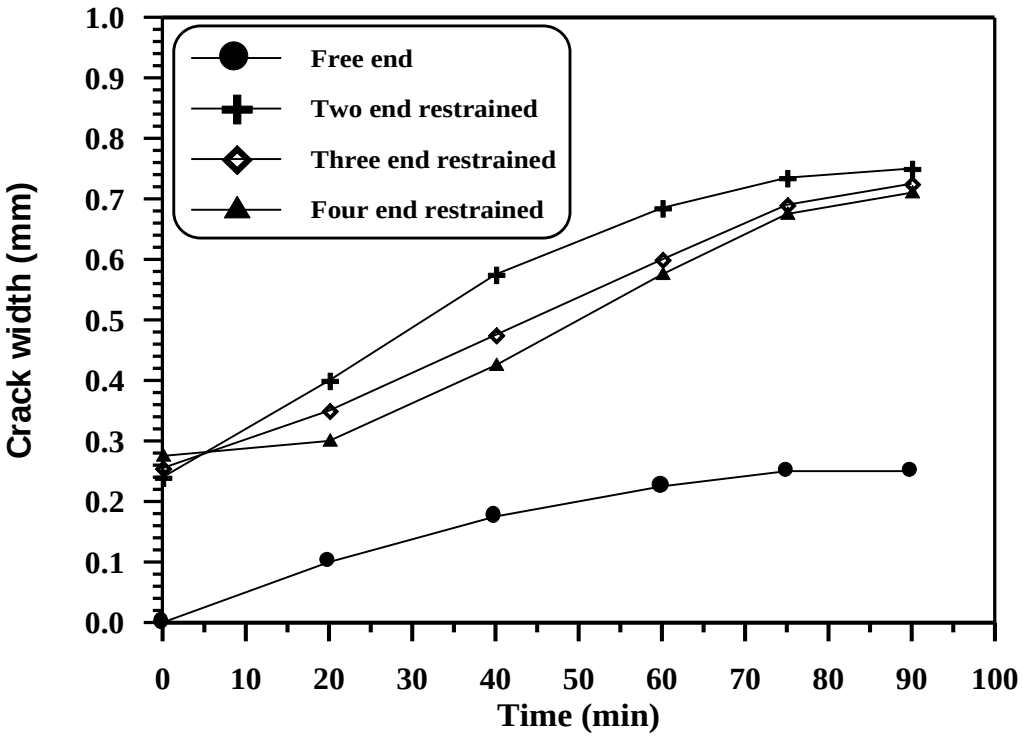

Figure (٥-١٤): Development of maximum crack width with time of reinforced concrete slabs for different restrained cases during exposure to fire flame.

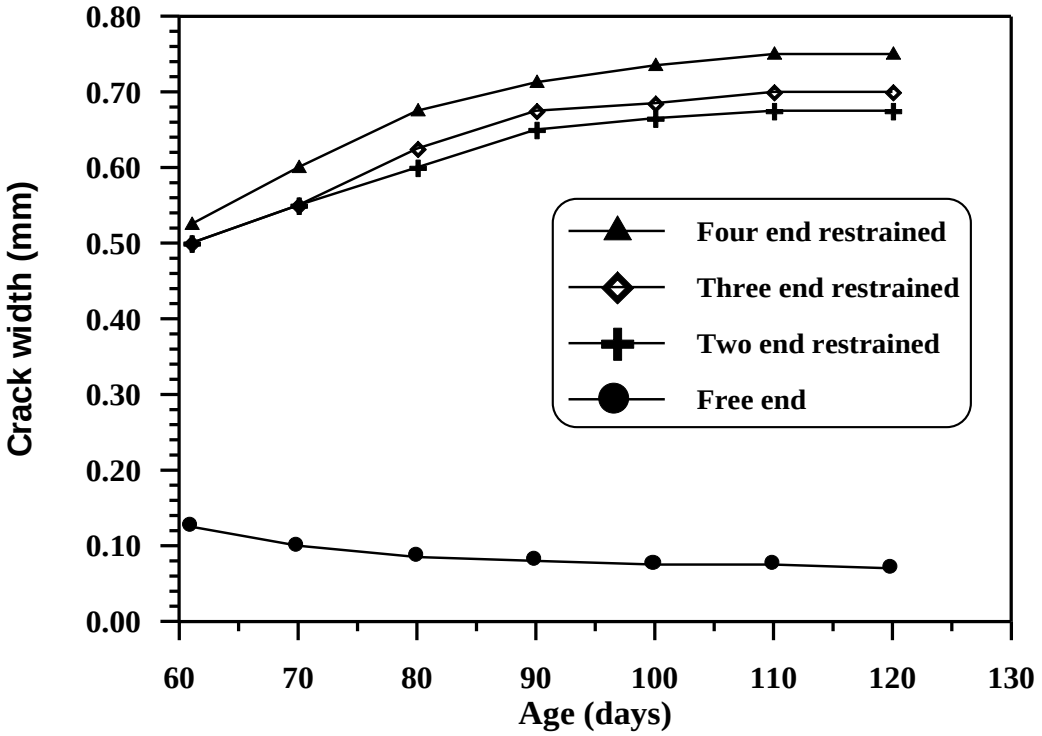

Figure (٥-١٥): Development of maximum crack width with age of reinforced concrete slabs for different restrained cases after exposure to fire flame.

From the above figures, it can be concluded that the rate of crack widening, however, tended to decrease with age for all slabs investigated before and after exposure to fire flame. This notice is expected as a higher percentage of shrinkage would be consumed for the later age cracks, and consequently less crack widening would be experienced in this case.

According to the experimental results, it was found that the range of crack widths measured in the present study varies between (٠.٠٥-٠.٢٧٥ and ٠.٠١-٠.٧٥ mm) for slabs before and after exposure to fire flame respectively.

Table (٥-٦) summarizes the final crack widths measured for cracks in each slab before, during and after burning.

The cracks which have been observed for the crack widths measurement were selected and plotted in Figures (٥-١٦ to ٥-١٨). From these figures it is clearly seen that the crack width initiated at a certain value at the restrained edge and , therefore, increased towards the center of the slab up to a certain level beyond which it decreased to zero at the tip of the crack, while at the free edge the crack width was the maximum and gradually decreases towards the center of the slab, and diminishes at the end of the crack. Also, it was obvious from Figures (٥-١٧ and ٥-١٨) that the same trend was also observed in walls for the variation of maximum crack width with wall height by *Al-Rawi* [١٩], *ACI-Committee* [٢٣] and *Al-Mashhedi* [٢٥].

From Figures (٥-١٧ and ٥-١٨), it can be seen that the variation of crack width with its length for cracks which appeared from the restrained edge could be explained according to the theory of change of restraint, where in edge restrained members there will be a residual restraint after cracking. Due to the effect of the edge beam, the variation of the crack width will depend on the (length/width) ratios of the newly formed slabs after cracking. Thus, the crack width will depend on the difference between the restrained movement before and after cracking or in other words it will be a function of change in restraint along the member length. This trend was found by *Al-Rawi* [١٩], *ACI-Committee* – ٢٠٧[٢٣] and *Al-Mashhedi* [٢٥] in walls.

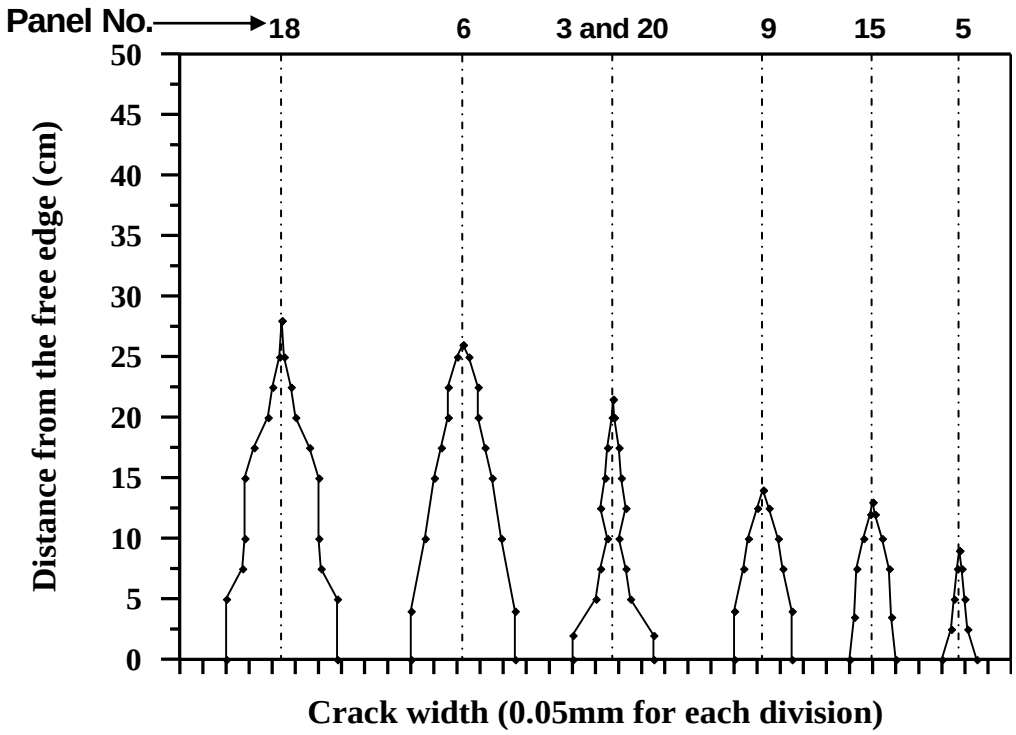

Figure (٥-١٦): Variation of final crack width with distance from the free edge for two end restrained reinforced concrete slab.

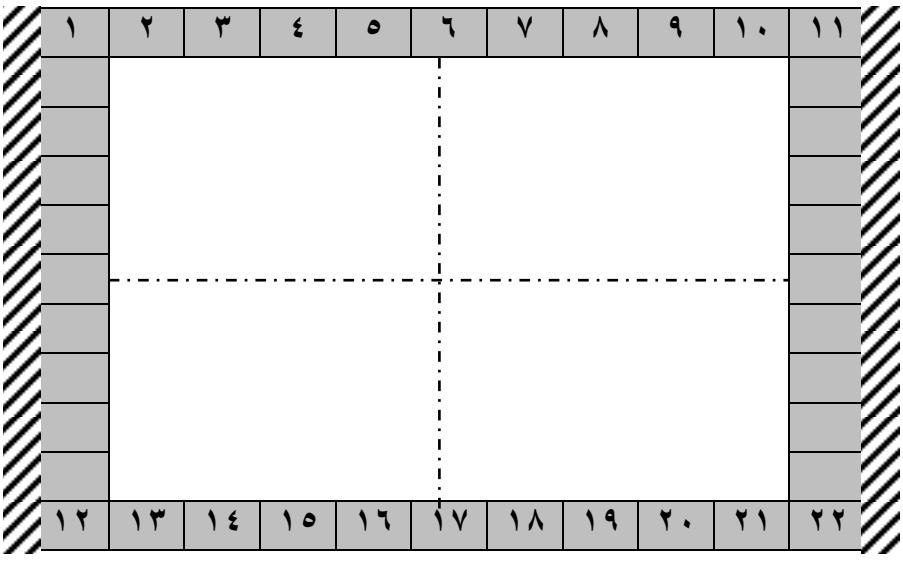

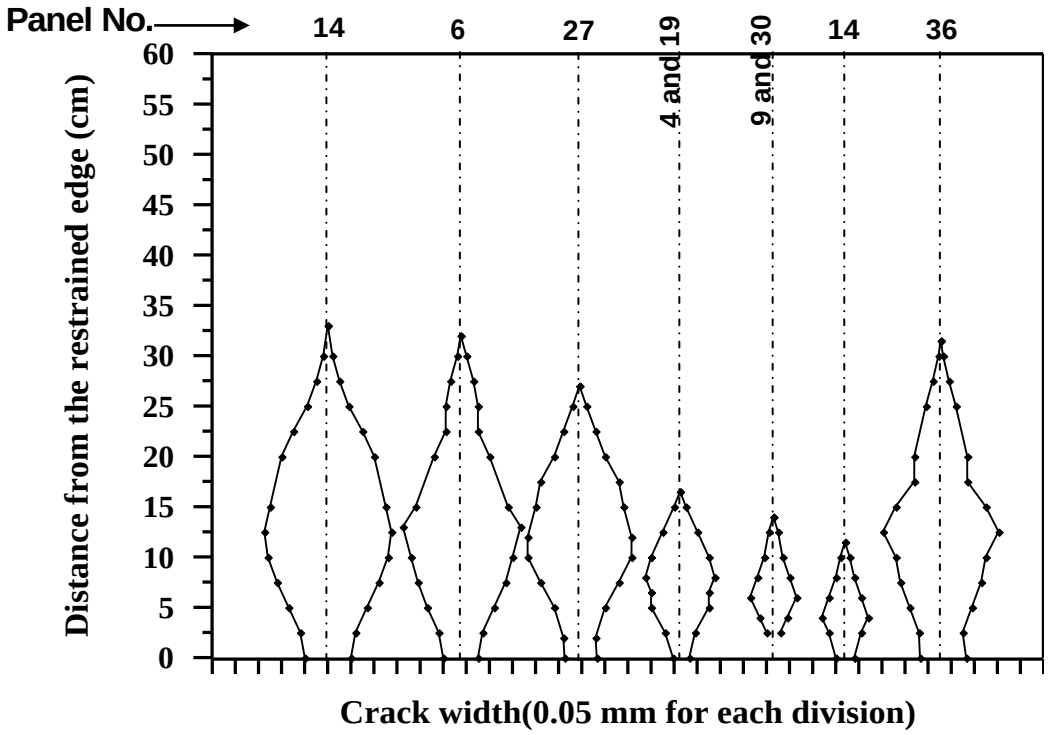

Figure (٥-١٧): Variation of final crack width with distance from the restrained edge of four end restrained reinforced concrete slab.

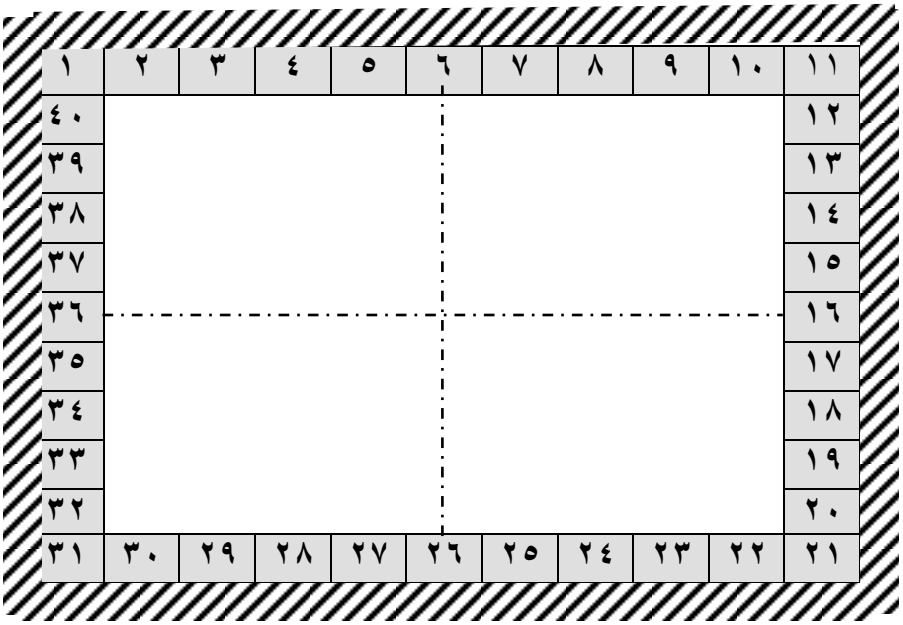

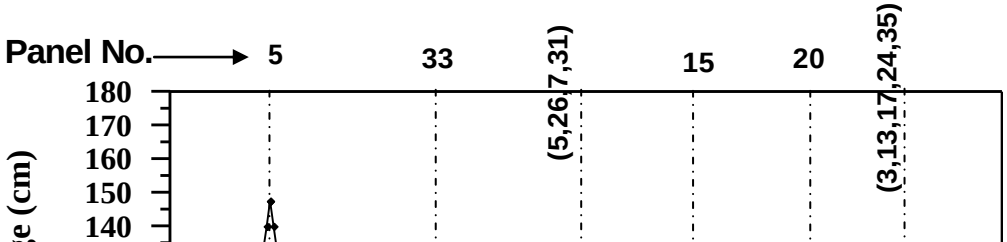

Figure (٥-١٨): Variation of crack width with distance from the restrained edge for selected cracks in site observed four end restrained slab.